TELEOPERATION OF A BIOMIMETIC SQUID ROBOT'S ARMS VIA MULTIPLE HAPTIC INTERFACES

A Thesis Submitted to the
Graduate School of Engineering and Sciences of
İzmir Institute of Technology
in Partial Fulfillment of the Requirements
for the Degree of

MASTER OF SCIENCE

in Mechanical Engineering

by
Hazal EMET

March 2022
İZMİR

ACKNOWLEDGMENTS

I am sincerely grateful to my supervisor Dr. Mehmet İsmet Can Dede, most of all for his faith in me in the times I did not have faith in myself, by giving me a chance to be a part of the team. Furthermore, I am thankful for the guidance, support, and in particular, patience through this 3-year period.

I would like to thank the rest of my thesis committee: Dr. Berke Gür and Dr. Tolga Ayav, for their insightful comments and encouragement.

I would like to thank the advisor of my second project, Dr. Ünver Özkol, for bearing with me through all the ups and downs on the work and for his guidance and support on the road.

I would like to express my sincere gratitude to my family, whose names would take pages to write one by one, for making me feel their unlimited and unconditional support, love, and in particular, pride through all my successes and failures without discriminating.

I am indebted to all my friends, in no particular order, Ceylin Yavuzkurt, Yunus Can Genç, Ege Naz Altın, Ceyda Başaran, Begüm Gürbay, Erkan Paksoy, Aslı Demir, and Pelin Ölçer for making me who I am right now. Without them it would not be possible to even begin and then complete this thesis.

I wish to thank the members of IRL, MPL, HURL, RAML, in no particular order, for their contributions on my dead alleys and simply being there for me: Emre Uzunoğlu, Osman Nuri Şahin, Orhan Ayıt, İbrahimcan Görgülü, Furkan Küçükoğlu, Mehmet Görkem Karabulut, Uğur Nalbant, Tarık Büyüköztekin, Egecan Türk, Kaan Erol Kurt, Merve Özkahya, Murat Demirel, Cevahir Karagöz, Emir Mobedi, Çağhan Kirişçi, Mert Yılmaz, Talha Erez, Fırat Kara, Ataol Behram Aldanmaz, Yunus Cebeci, Tuğrul Yılmaz, Rüstem Can Öztürk, and Gökhan Arslan.

This study is funded by *The Scientific and Technological Research Council of Turkey (TÜBİTAK)* with the project name *Robotic Squid for Underwater Manipulation and Intervention* and grant number *216M219*.

ABSTRACT

TELEOPERATION OF A BIOMIMETIC SQUID ROBOT'S ARMS VIA MULTIPLE HAPTIC INTERFACES

Biomimetic robot systems have captured the attention of researchers for the past two decades. Along with biomimetic systems, the implementation of soft robotic arms has emerged and studied. Teleoperation of such biomimetic soft robots, i.e., a biomimetic squid robot, is still an open area of research.

This study aims to initiate the development of a teleoperation system, which has multi-master multi-slave with dissimilar master-slave kinematics, to be adapted for the operation of an underwater biomimetic squid robot. The communication between the slave robot, which is the biomimetic squid robot's soft arms, and the master system on the ground is estimated to have limited bandwidth. To overcome this problem, the model-mediation technique is selected to be adapted. The abstract information received from the slave side is used for regenerating the slave environment on the master side. The human operator uses two haptic devices to manipulate the four soft arms of this biomimetic robot via interacting with this regenerated model on the master side. The models of the biomimetic robot's soft arms are developed by using the constant-curvature approach.

While this study is limited in the sense that the slave side regeneration is previously completed on an ideally received signal even before the teleoperation is initiated, the teleoperation of 4 soft arms with two haptic devices is investigated. 4 different control strategies are formulated and evaluated on test subjects. The performances of the test subjects are evaluated based on their task completion duration, accuracy, and feedback received from their questionnaire answers. The primary investigation conducted is for the ergonomic use of teleoperation systems. Another evaluation is carried out to understand the influence of haptic feedback in telepresence. The evaluation results clearly indicate that the haptic feedback has improved the telepresence. The position-to-position mapping produced shorter task completion durations with worse accuracy relative to the position-to-velocity mapping.

ÖZET

BİOMİMETİK MÜREKKEPBALIĞI ROBOTUNUN KOLLARININ ÇOKLU HAPTİK ARAYÜZLERLE TELEOPERASYONU

Biyomimetik robot sistemleri, son yirmi yıldır araştırmacıların dikkatini çekmektedir. Biyomimetik sistemlerle birlikte yumuşak robot kollarının uygulaması ortaya çıkmıştır ve incelenmektir. Bu tür biyomimetik yumuşak robotların, bir biyomimetik kalamar robotunun teleoperasyonu hala açık bir araştırma alanıdır.

Bu çalışma, bir sualtı biyomimetik kalamar robotunun operasyonu için uyarlanacak, farklı ana sistem-bağımlı sistem kinematiğine ve çoklu ana sistem ve çoklu bağımlı sistem özelliğine sahip bir teleoperasyon sisteminin geliştirilmesine ilk adım oluşturmayı amaçlamaktadır. Biyomimetik kalamar robotunun yumuşak kolları olan bağımlı robot ile karada bulunan ana sistem arasındaki iletişimin sınırlı bant genişliğine sahip olduğu tahmin edilmektedir. Bu sorunun üstesinden gelmek için model-aracılı teleoperasyon tekniği uyarlanmak üzere seçilmiştir. Bağımlı sistem tarafından alınan yalın bilgi, ana sistem tarafında bağımlı sistem ortamını yeniden oluşturmak için kullanılmaktadır. İnsan operatör, bu biyomimetik robotun 4 yumuşak kolunu ana sistem tarafındaki bu yenilenen modelle etkileşime girerek manipüle etmek için iki haptik cihaz kullanmaktadır. Biyomimetik robotun yumuşak kollarının modelleri, sabit eğrilik yaklaşımı kullanılarak geliştirilmiştir.

Bu çalışma, teleoperasyon başlatılmadan önce ideal olarak alınan sinyal ile bağımlı sistem tarafının yenilenmesinin önceden tamamlanmış olması anlamında sınırlı olmakla birlikte, iki haptik cihazla 4 yumuşak kolun teleoperasyonu araştırılmıştır. Denekler üzerinde 4 farklı kontrol stratejisi formüle edilmiş ve değerlendirilmiştir. Deneklerin performansları, görev tamamlama süreleri, doğrulukları ve anket cevaplarından alınan geri bildirimlere göre değerlendirilmiştir. Yapılan temel araştırma, teleoperasyon sistemlerinin ergonomik kullanımına yöneliktir. Haptik geribildirimin telebulunma üzerindeki etkisini anlamak için ikincil bir değerlendirme yapılmıştır. Değerlendirme sonuçları, dokunsal geribildirimin telebulunmayı iyileştirdiğini açıkça göstermektedir. Konumdan konuma eşleme, konumdan hıza eşlemeye göre daha kötü doğrulukla daha kısa görev tamamlama süreleri üretmiştir.

This thesis is dedicated to my beloved grandparents Bahar and Kamuran TEKELİ.

TABLE OF CONTENTS

LIST OF FIGURES

Figure **Page**

Figure **Page**

Figure **Page**

LIST OF TABLES

CHAPTER 1

INTRODUCTION

The word “tele” means at a distance in its Greek origin. Teleoperation indicates operating a system over some distance and provides the ability to extend the capability of manipulation over some range. Teleoperation systems, as seen in Figure 1.1, are consist of 2 ends: master and slave. The master contains a manipulator that supplies the operator the capability to interfere with the remote environment by transmitting motion commands to the slave. On the other hand, the slave performs the actual tasks and mimics the movement received from the master. The necessity of teleoperation arises when the operation is unacceptably hazardous for humans to interfere or expensive with human labor. The most common application fields are underwater and space applications, where the tasks are considered both dangerous and costly.

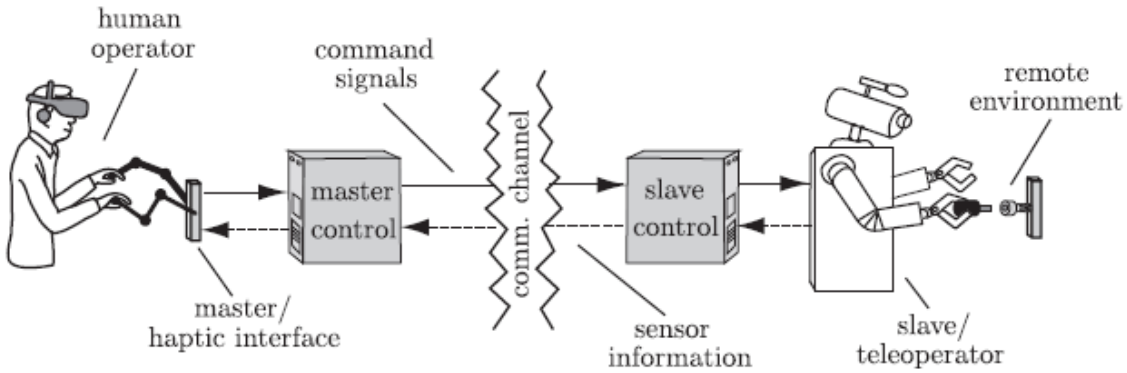

Figure 1.1 Teleoperation system.
(Source: Passenberg, Peer & Buss, 2010)

1.1. Background on Teleoperation System Architecture

Teleoperation systems are categorized according to the information transmission between master and slave as unilateral and bilateral teleoperation, illustrated in Figure 1.2. In unilateral teleoperation, data is transmitted only one way, from master to slave, with the purpose of transmitting motion commands constituted on the master side by the operator. The slave end does not transfer any sensory feedback data to the master end.

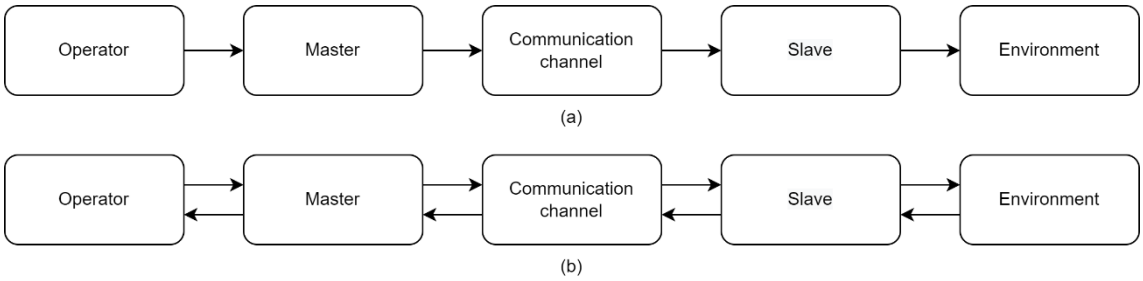

Figure 1.2 Teleoperation types (a) Unilateral teleoperation (b) Bilateral teleoperation.

However, in bilateral teleoperation, data is transmitted in both ways, from master to slave and also slave to master. Unlike unilateral teleoperation, the slave end collects sensory data and uses this to transfer haptic or audio force and/or position feedback to the master. The feedback of the performed task by the slave is transferred to the master side as input to inform the teleoperator in order to control bilaterally. Thus, the operator can rely on the tasks they performed in the sense of presence in the slave environment.

There are two primary objectives for teleoperation systems as stability and telepresence from a control-theoretic point of view. Stability means overcoming the uncertainties of the different components, such as unknown remote environments or varying operator behavior. Telepresence is the feeling of presence in the remote environment provided to the operator, which can be quantitatively measured by the system's transparency, which is described as the unfelt medium between the operator and the remote environment.

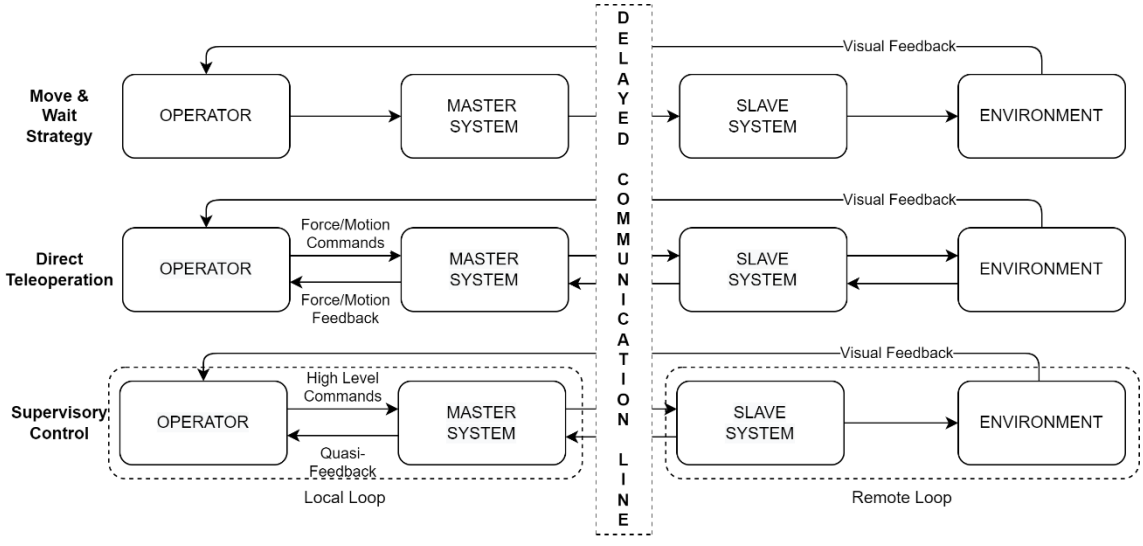

Figure 1.3 Move & Wait Strategy, Direct Teleoperation, and Supervisory Control.

In order to decide on the type of teleoperation to implement, certain variables such as the communicational or environmental conditions should be considered. When the time delay on the system is negligible, the aforementioned bilateral teleoperation ensures the stability of the system and the telepresence of the operator. Although, if a considerable amount of time delay is present in the system, actions on the master side and the reactions on the slave side appear out of phase, different methods are investigated to eliminate this problem, some illustrated in Figure 1.3. The high road to eliminate the handicaps of time delay is simply designating unilateral teleoperation. Though in unilateral teleoperation, telepresence is lost, and the operator can only rely on the visual feedback from the remote environment. Ferrell (1965) revealed that the operator adopts a move-and-wait strategy with unilateral teleoperation, which increases the task completion time significantly with respect to the amount of delay. Ferrell and Sheridan (1967) proposed another method to decrease the task completion time as supervisory control. The idea behind this method is to reduce the workload of the operator by giving particular autonomy with the predefined tasks to the slave.

When the time delay in the system is not negligible, and telepresence is required, the sole and exclusive remedy is bilateral teleoperation. Anderson and Spong (1988) developed a control strategy to overcome the drawbacks of time delay, based on maintaining the passivity of the system to keep it stable independent of the time delay. A system is said to be passive if the power input to the system is not greater than the absorbed power. The main aspect of this model is to convert the signals constituted on both sides as scattering variables before transmitting them to the other side across the communication line with time delay. Niemeyer and Slotine (1991) presented another approach based on scattering theory as the wave variable method. The idea behind this method aims to overcome the difficulties of time delay while maintaining the transparency of the system by using wave transformations on both sides.

Model mediated teleoperation was firstly proposed by Mitra and Niemeyer (2008) as a new approach to teleoperation systems with time delay and the necessity of telepresence. The following chapter explains this method in further depth.

1.2. Model Mediated Teleoperation

Bilateral telemanipulation allows to interact with a remote environment via the sense of presence at that location. However, non-negligible communication delays endamage the stability and the performance of the system. The model-mediated teleoperation approach presents a solution to bilateral telemanipulation under significant communication delays in both known and unknown environments.

In this model, rather than directly transmitting the parameters by the communication line, the data gets transformed to an abstract order and then gets transmitted with the intention of enhancing the operator's perception and manipulation capabilities. The environment model acquired from the slave sensory data gets haptically rendered on the master side without any lag, and the slave gets stably tracked by means of this method. The acquired model of the remote environment is used to generate a virtual world for the user to directly interact. Moreover, abstraction in the data transmission removes the need of slave intelligence as used in the supervisory control methods. The performance of the proposed method highly depends on the accuracy of the generated virtual model.

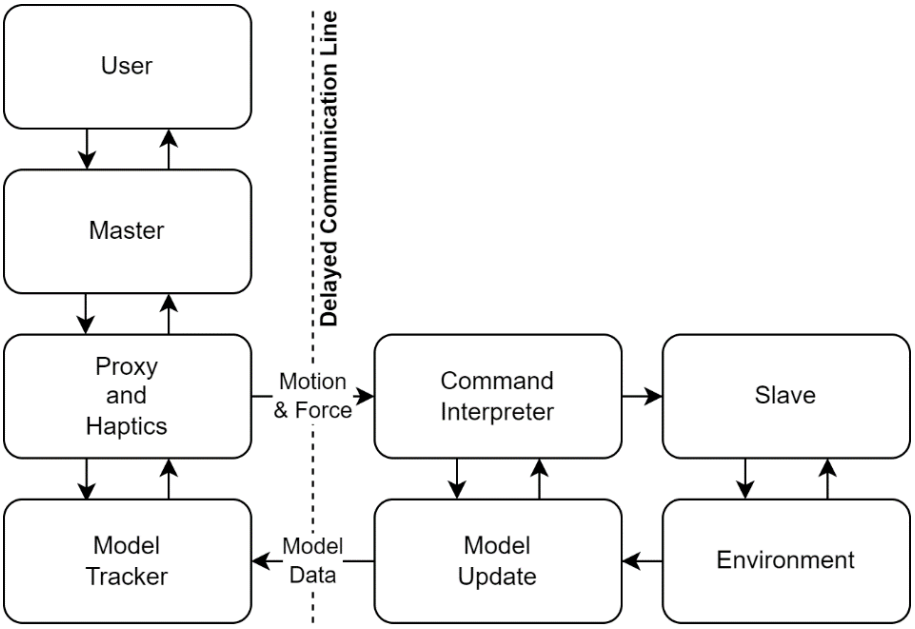

Figure 1.4 The proposed algorithm by Mitra and Niemeyer.

The proposed model-mediated teleoperation scheme is illustrated in Figure 1.4. The dotted line indicates the delayed communication line. The left side of this line represents the master system, while the right side represents the slave system. The proxy is the representation of the slave in the virtual model.

Mitra and Niemeyer (2008) demonstrated this approach on one degree of freedom (DoF) telerobotic system with two seconds of communication delay in each direction, a four second round delay, to prove the proposed method. This method states that the level of delay in the communication line must be linearly correlated with the level of abstraction in the data transmission. Model-mediated teleoperation offers a solution to systems with present time delay to prevent system instability, while supervisory control provides a high abstraction and low update rate, and direct teleoperation is limited to systems with negligible or non-delayed models.

Model mediated teleoperation approach provides a higher level of data abstraction compared to the traditional position or force-feedback loops. Instead of continuously feeding back the position or force measurements, it extracts and transmits an environment model based on these measurements and/or other sensor data. The user interacts with the locally rendered haptic model (Mitra and Niemeyer, 2008).

Implementation of MMT with the master, slave, and proxy telemanipulation is represented in Figure 1.5. The slave robot tracks the force/motion commands sent from the master and updates the environment model by obstacle detection. The proxy embodies a virtual representation of the slave that resides within the model and follows the motion of the master when in free space. If the master penetrates with the surface, the proxy stops at the object boundaries and hovers on the surface yet keep the distance with the master at minimum.

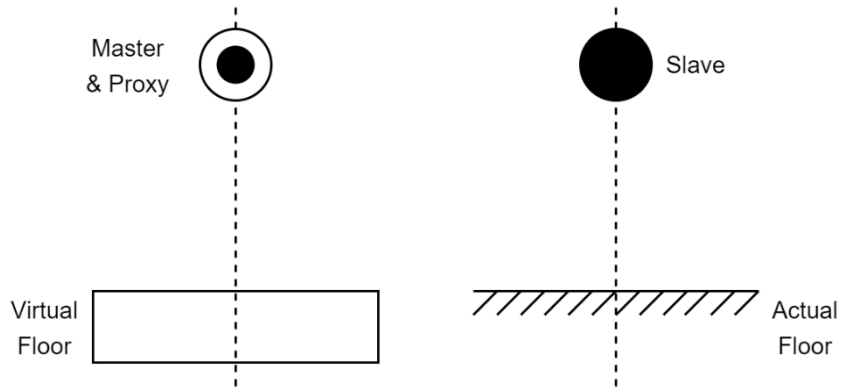

Figure 1.5 Representation of the MMT concept.

The updated environment model by obstacle location estimation of the slave robot enables the master to create a haptic virtual surface. The haptic feedback is only sent to the operator if the slave penetrates the virtually created surface. The feedback is directly sent to the operator by the master based on PD tracking of the proxy. The equation of exerted forces by the master is given in Equation 1.1.

$$F_m = k_{pm}\left(x_p - x_m\right) + k_{vm}\left(V_p - V_m\right) \tag{1.1}$$

The x_p, x_m, V_p, and V_m parameters are the proxy and master positions and velocities, respectively, where F_m is the exerted force by the master. The PD gains k_{pm} and k_{vm} represents the master position and velocity gains. In order to recreate a virtual environment based on reality, the parameters are tuned to produce a similar stiffness to the actual rigid obstacle.

In order to update the master model and reproduce the environment accurately, the location of the virtual surface must track the estimated location of the obstacle in the slave environment. The implementation is as follows

$$x_{mfloor} = x_{sfloor} \tag{1.2}$$

with the constraint of

$$x_{mfloor} \leq x_p \tag{1.3}$$

where x_{sfloor} is the slave estimation of the obstacle location and, x_{mfloor} is the location of the master's virtual surface. This constraint ensures to avoid abrupt forces being exerted on the user and the haptic interface's stability while restraining proxy penetration with the virtual surface. Figure 1.6 illustrates the relocation of the model tracking and the proxy until the correct location is reached.

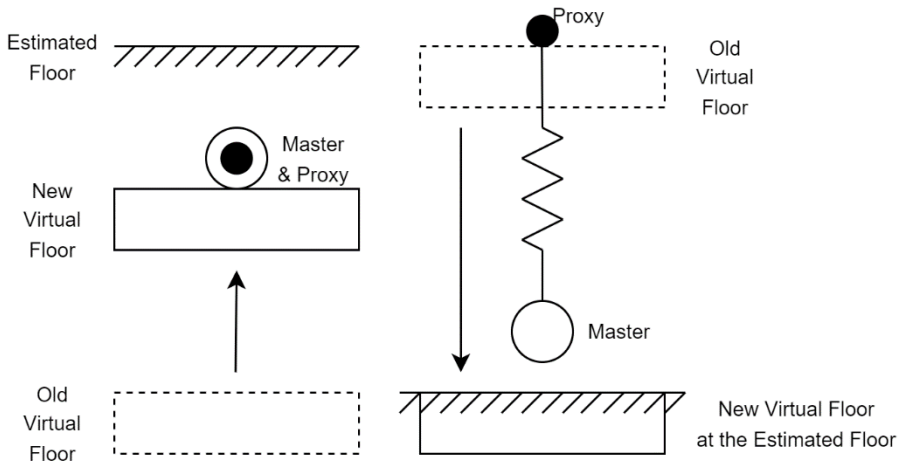

Figure 1.6 Force generation when floor location is updated.

1.3. Telepresence

Telepresence is the sensation of being physically present in a remote environment where the teleoperator is. The earliest models of telepresence are comprised of a camera and monitor duo, yet more sophisticated versions are constituted by adding more sensors to the system to mimic a real physical presence. In order to create absolute telepresence, all human senses should be generated by the book. Although forming a human from scratch might be too much to overcome, a humanoid version can be made. The typical ways of telepresence are the combinations of visual, acoustic, haptic, and tactile sensors in the remote-site and operator-site displays, as demonstrated in Figure 1.7.

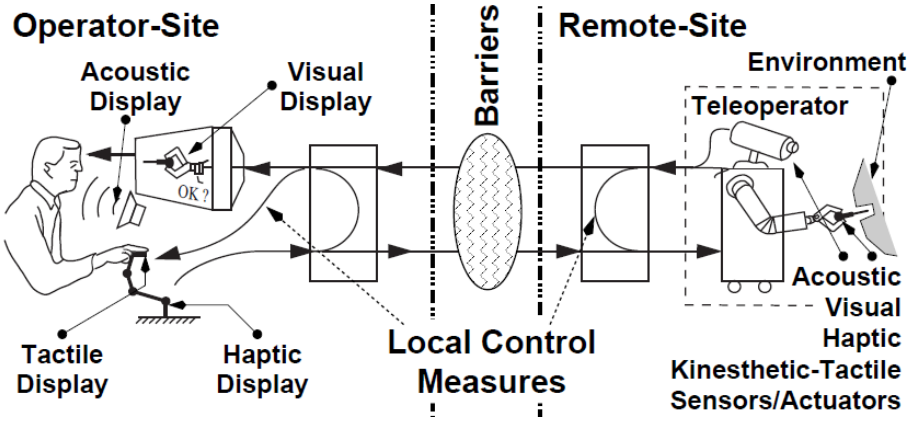

Figure 1.7 Telepresence system.
(Source: Hirche and Buss, 2006)

Visual telepresence systems are mostly constituted of a static camera on the environment and a display on the operator site. In order to advance the feeling of telepresence, the camera can be unfixed to mimic the operator's head or eye movements. In both cases, the created visual feedback cannot be compared to the real visual sense of a human due to the lack of depth and the reduced field of view caused by the monitor system.

In some cases, rather than the visual sense, acoustic telepresence is more confidential and convenient. By using a duo of a microphone and a speaker, an artificial perception of hearing can be created.

Haptic feedback creates an elevated amount of telepresence by utilizing both tactile and kinesthetic information. Tactile information refers to the sense of contact with an object, while kinesthetic information converges the sense of position and motions of the limbs along with the associated forces. Human touch sensors, mechanoreceptors, covers both tactile and kinesthetic information and are activated by external pressure. Kinesthetic information can be created artificially in the sense of telepresence as force feedback and fed back to the operator.

An evolved version of telepresence can be created by using virtual and augmented reality technology. Increased sense and perception of depth in virtual reality and the reliability and the sense of safety of augmented reality provide an elevated experience of telepresence to the operator by making them feel physically inside the remote environment (Kirişçi, 2019).

1.4. Application Fields of Teleoperation

The application area of teleoperation involves all kinds of operations that are considered hazardous or expensive with the operator on board. The first modern teleoperation technique was developed in the Argonne National Laboratory in 1949. The task included handling nuclear materials which were considered dangerous to be in contact with. Later, teleoperation techniques were utilized for underwater exploration to keep the barrier with its hostile environment. Another application field for teleoperation is space and military applications. In addition to the hostile environment, with an operator on board, the task is also much more expensive compared to teleoperation.

Figure 1.8 (a) Remotely Operated Vehicle (b) Autonomous Underwater Vehicle. (Copyright: Oceaneering & Teledyne Marine)

Underwater operations were one of the first mobile applications where teleoperation techniques were adopted. Unmanned underwater vehicles are classified into remotely operated vehicles (ROV) and autonomous underwater vehicles (AUV), illustrated in Figure 1.8. ROVs are designed with redundant actuation systems to have high maneuverability capability and controlled by an operator located on the surface with a tethered communication line. The upside of ROVs is that they can interfere with the environment with the help of a manipulator mounted on the body. By means of these features, ROVs are highly anticipated in the survey, inspection, maintenance, and simple manipulation tasks. On the other hand, AUVs are designed with deficient actuation systems with nontethered communication lines and are capable of reaching high speeds. AUVs do not have the ability to interfere with the environment, and their application field is scientific investigations, military, and construction mapping applications.

The physical presence of a human operator on a vehicle in outer space requires many resources or is impossible; therefore, it is considered that using teleoperated vehicles to perform human-robot interactive tasks is more efficient. Space applications gain a major place in the market through well-known robots, including the landing robot Curiosity, exploration probe Voyager, deep space observer Hubble Observatory, satellites, and outer space robot arms, shown in Figure 1.9.

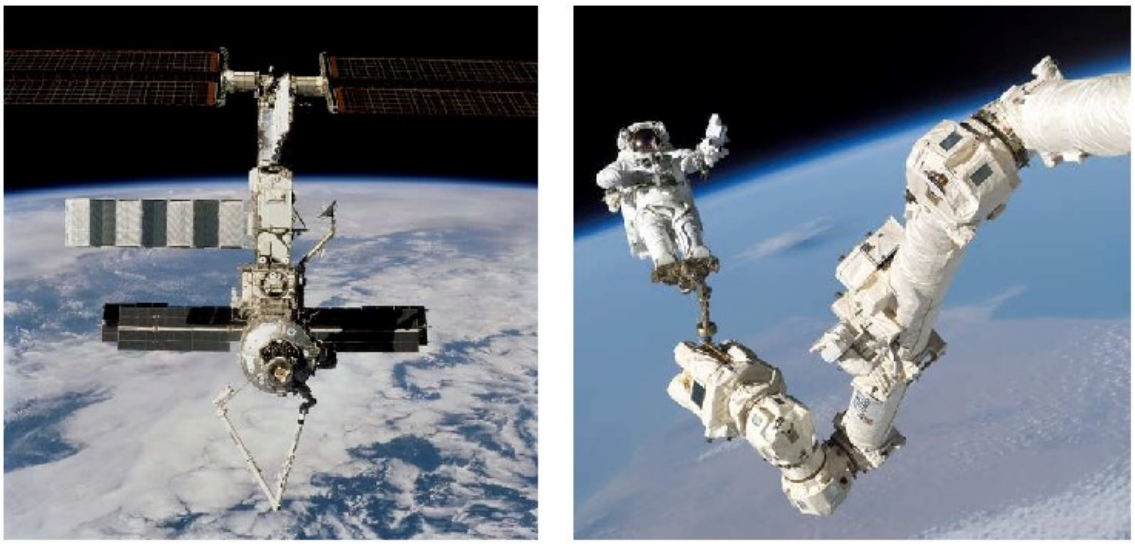

Figure 1.9 Canadarm2 robotic arm on ISS and EVA with Canadarm2.
(Copyright: NASA)

Military operations have a wide application field of teleoperation in order to avoid the probability of loss or harm of humans. Different kinds of environments require a variety of teleoperated machinery. Unmanned Air Vehicles (UAVs) are remotely piloted with the help of radio and satellite links or operate autonomously for the tasks of surveillance, inspection, and target annihilation. Unmanned Ground Vehicles (UGVs), an example shown in Figure 1.10, are favored for mine detection, route clearing, and reconnaissance.

Figure 1.10 Unmanned Ground Vehicle Harris T7, British Army.
(Copyright: HARRIS)

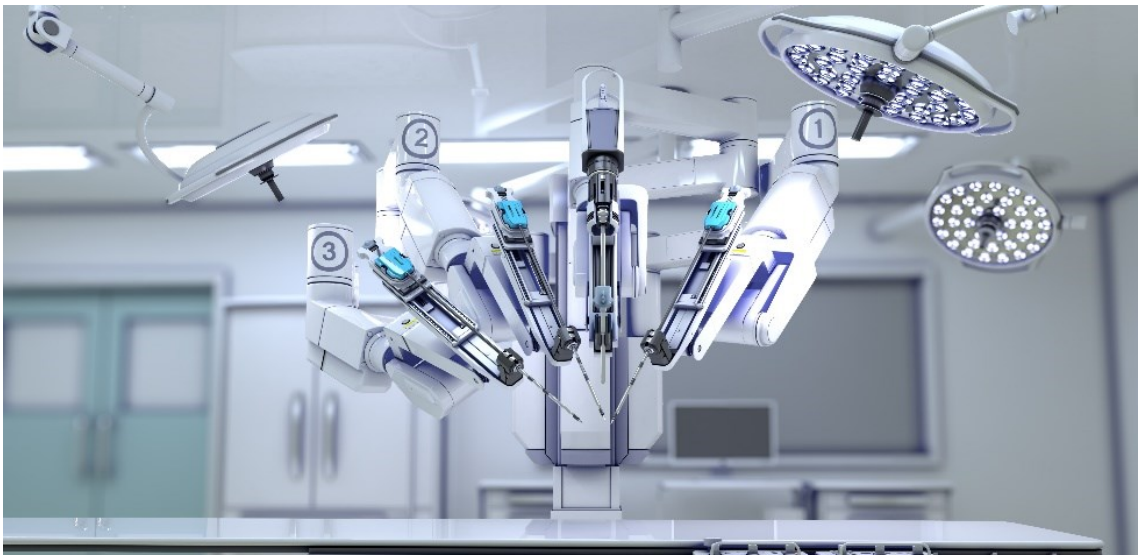

Figure 1.11 DaVinci surgery robot.
(Copyright: DaVinci)

The call into play of robotic devices in the medical field paved the way for teleoperated surgeries. Though a number of surgery robots play an active role today, it is not yet quite possible to replace the surgeon with the teleoperated robot due to cover the emergency situations that might occur both on the patient and mechanical side. Various numbers of teleoperation systems in the medical field are based on the collaborative work of a human operator and a robot; one of the most known surgery robots, DaVinci, can be seen in Figure 1.11.

1.5. Robotic Squid for Underwater Manipulation and Intervention Project

The proposed study consists of a biomimetic robot inspired by squids, a member of the cephalopod mollusk class. The aim of the slave design is the development of an underwater robot that can interact and intervene with the underwater environment much more effectively than existing systems. In this model, the streamlined and agile body is combined with very dexterous and versatile multitask tentacles capable of reaching, grabbing, pulling, and exploring. Similar to the squid tentacles, the robot arms are hyper-redundant links made of soft and very deformable materials. Thus, the robot is able to interact with the environment in tasks such as palping and grasping without the concern of possible deformation on contact.

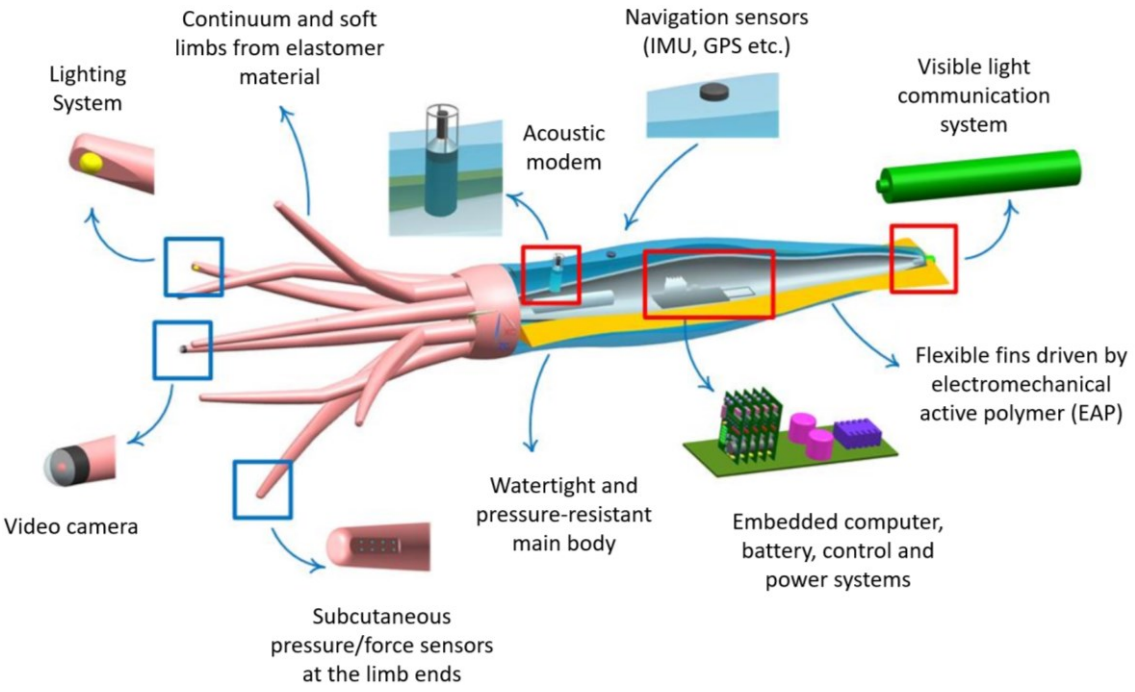

Figure 1.12 Slave robot.

Squid inspired propulsion techniques of jet pulses and undulating fins are also integrated into the model to eliminate the need of a propeller and for high maneuverability capability. The elimination of the propeller from the design has gained the robot the ability to navigate through dirty waters or close to seabed and structures. The model has an untethered communication system based on visible light-based optical communication, which eliminates the link with the surface, thus eliminates the limits of the workspace. The design of the slave robot with its components can be seen in Figure 1.12.

This study is consisted of multiple work packages including modeling and control of the robot, designing embedded systems, and developing a teleoperation system for the robot arms. The proposition of this thesis is a teleoperation approach for the study. In order to overcome the limitations of the communication system that transfers data from master to slave and vice versa, increase the telepresence of the operator, and create a virtual environment for the user to directly interact, model mediated teleoperation approach is adopted. The soft slave arms of the robot with different capabilities and/or end-effectors are controlled and manipulated with haptic devices. Considering the complexity of multi-master multi-slave systems, experiments were held with human subjects to evaluate their perception and performance on the proposed approach.

1.6. Aim of the Thesis

This thesis aims to develop an initial step of the model-mediated teleoperation approach for an underwater soft biomimetic squid robot and to investigate the utility and ease of use of the proposed method considering the capabilities of the human operators, and to evaluate the telepresence of the proposed method under data interruptions with low-bandwidth abstract data transmitted from the communication channel. The study consists of the investigation of multi-master multi-slave systems with dissimilar master-slave kinematics, adapting and implementing the teleoperation method to the slave robot, designing and carrying out experiments with user studies to validate the proposed methodology and to evaluate the ease of use of the user interface.

1.7. Contributions of the Study

This thesis contributes to the literature by collaborating two independent research fields: teleoperation of soft robots and teleoperation systems with dissimilar master-slave kinematics.

1.8. Outline

This study is presented in six chapters. In this chapter, the purpose of the thesis is stated with a brief prologue on the relevant studies. In Chapter 2, surveys related to the literature by means of teleoperation, model-mediated teleoperation, multi-master multi-slave teleoperation systems, and telepresence are investigated. Chapter 3 introduces the control methods, software, and hardware used to implement the teleoperation systems design. In Chapter 4, the procedure for the first set of user tests is defined, and the results to evaluate the validity of the proposed methods are presented. Chapter 5 includes the procedure for the second set of user tests for evaluating the performance difference between position to position and position to velocity mappings and their results. The thesis is concluded with Chapter 6, in which a summary of the study is given, and the outcomes of the thesis and possible future works for improvement are discussed.

CHAPTER 2

LITERATURE SURVEY

The earliest type of teleoperation in history was invented assumably due to the daily needs of humanity that includes using tools to perform different tasks. Once the fire has been set, the goal is to evaluate the intensity or burn time with external influence. The need for the reinvigorated fire was obvious yet hazardous that created the demand for remote manipulation. That is accepted as the earliest type of teleoperation of civilization. After the pre-historical times, the area of usage of teleoperation has been widely increased as the jeopardizing situations that wished to encounter also increased.

2.1. History of Teleoperation

The first modern teleoperation system, in Figure-1, was developed at the Argonne National Laboratory in 1949 with the need for the manipulation of radioactive materials carefully. R. Goertz and his team designed a mechanical pantograph accepted as the first master-slave teleoperator. Soon after that, in 1954, the first electromechanical manipulator that is consisted of a feedback servo controller has also been invented by the same team.

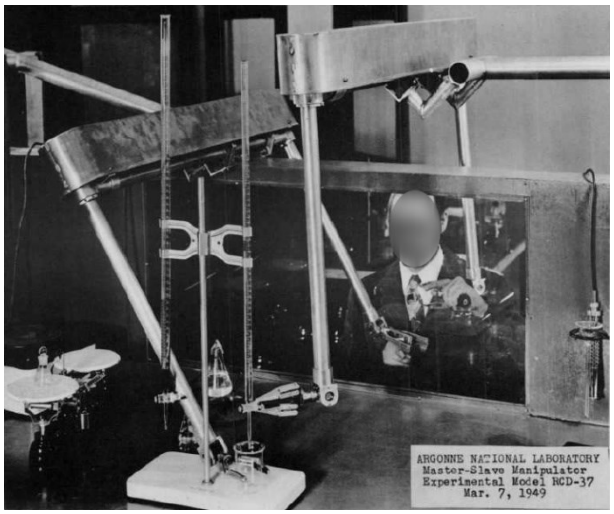

Figure 2.1 Master-slave manipulator in the Argonne National Laboratory.

(Source: Goertz, 1949)

The innovation of teleoperation with computer technology led to many more branches to utilize the advantages of this new technique. In today's idea of teleoperation, on the contrary of the designs of Goertz, there is no more direct visual contact with the slave system. In order to increase the dominance feeling of the operator without the visual control opportunity, different techniques of telepresence have been implemented. Among these, force reflection feedback was used to experiment on the effects of time delay between the slave and the operator. At the beginning of the 1960s, during the cold war era, the space race began between the Soviet Union and the United States. An apparent problem was the expected time delay between the earth and the moon. Ferrell (1965) revealed that the only way to avoid the instability caused by the time delay is to remove the closed-loop feedback control and make an open loop move then wait for confirmation before the next step. The "Move & Wait" strategy eliminated the instability yet increased the time to perform even the simplest tasks. Ferrell and Sheridan (1967) developed "Supervisory control" to undermine the effects of time delay by giving the slave more intelligence to overcome more straightforward tasks autonomously and paved the way for teleoperation-oriented software languages that aim reduced communication data between master and slave.

Beginning in the 1980s, position and force control techniques rapidly grew when advanced control methods started to appear. Hogan (1984) proposed the impedance control method to control the dynamic behavior of the manipulator in addition to modulating external disturbances to control dynamic interactions. Hannaford and Fiorini (1988) developed hybrid representation by defining master and slave parts of a teleoperation system as a two-port network that involves the estimation of dynamic behavior on both sides and transmitting that behavior to the opposite side of the network.

One of the major drawbacks of teleoperation in distant sites is the time delay experience in the communication line. This delay results in unstable behavior of the teleoperation system. Consequently, Anderson and Spong (1989) proposed scattering theory with passivity-based control to enhance the stability of control systems with time delays. The substantial part of this theory is to define a teleoperation system as a two-port network as Hannaford and Fiorini did, and then convert the signals transmitted as scattering variables to maintain the teleoperation system's stability by making the time delay element passive.

In the early 90s, it was uncovered that dissipating elements such as dampers ensured the passivity and stability of the system independent of time delays. Niemeyer and Slotine (1991) introduced the wave variable method by reformulating the scattering theory as generating a virtual master manipulator in the wave domain to make use of its passive nature and create the desired trajectory for the controllers to follow. Hence, most bilateral teleoperation control systems are designed within the passivity framework using concepts of scattering or wave variable techniques to provide robust stability against time delay in the communication line.

Various teleoperation techniques with solutions that address the time-delay problem have been proposed over the years. Many approaches are being designed from scratch, while some adapt currently available ones. Model-mediation technique is one that improved step by step after its creation in 2008 (Mitra and Niemeyer). Although the model-mediation technique is formulated for systems with time delays, this approach can be adapted to systems that have abstract information sent back from the slave to the master side. This abstract information can be used to regenerate the slave environment on the master side, where the human operator uses the master system to interact with this regenerated slave environment. The following sub-section reveals the formulation of the model-mediation technique.

2.2. Model Mediated Teleoperation

Model mediated teleoperation method, in Figure 2.2, was first proposed by Mitra and Niemeyer (2008). This method presents an approach to bilateral teleoperation with significant time delays. Rather than directly sending the data collected from the slave part of the system to the master, this method abstracts the data and forms a much simpler model to transmit. The operator interacts with a virtually created slave environment and receives the locally rendered haptic feedback. This approach was demonstrated on one DoF system with four seconds of round-trip time delay. The conclusion on the accuracy of the system is stated as dependent on the virtual model.

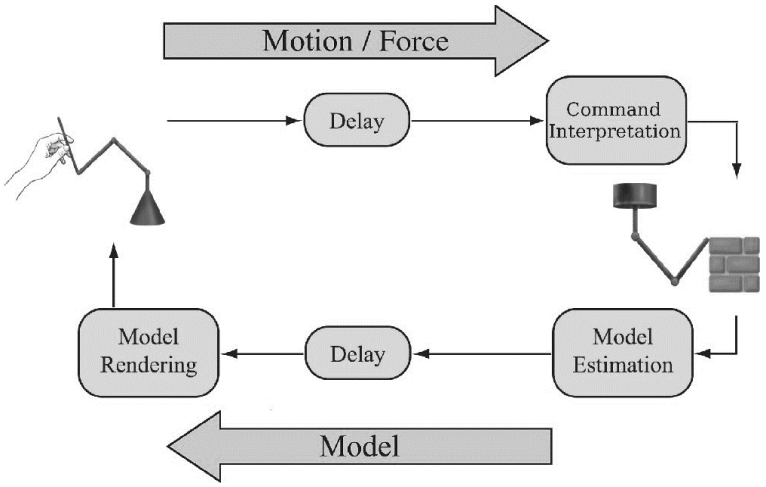

Figure 2.2 The proposed telemanipulation scheme by Mitra and Niemeyer.
(Source: Mitra and Niemeyer, 2008)

Passenberg et al. (2010) implemented model-mediated teleoperation on a multi-operator multi-robot system for the first time, using position-based admittance controllers on the master sides. The contribution of this technique to the literature is the allowance of cooperation of more than one master-slave subsystem.

Willaert et al. (2012) focused on the challenges that arise with multiple DoF by using multiple sensors as position, force, and vision to explore the environment in order to improve the accuracy of the virtual model. Furthermore, vision is also used to predict the possible contact points of the slave and the environment to create touch feedback before the contact occurs.

Xu (2013) extended the model-mediated teleoperation method to 6 DoF systems by using a time-of-flight (ToF) camera. Rather than the original model mediated teleoperation method, a point cloud model is used to approximate the remote environment, generate forces and directly produce haptic feedback.

Taner et al. (2015) applied the model-mediated teleoperation method to a virtual slave mobile robot with unlimited workspace and a haptic master device. Likewise, Taner proposed a new approach to haptic feedback for mobile robots with an unlimited workspace that avoids collision of the slave robot by considering the slave velocity and distance to the environment.

Uzunoğlu and Dede (2017) extended the model-mediated teleoperation method to 3 DoF by using two haptic devices as one master and one slave with impedance controller. The virtual surface model is created by using a grid-based system. The

results indicate that the investigated method ensured the passivity and stability of the system.

Liu et al. (2018) designed a model-mediated teleoperation method to be used in robot assisted surgery for real-world applications. The presented method is constituted of a nonlinear Hunt-Crossley (1975) scheme to enhance system transparency by using the recursive least squares (RLS) technique to estimate the environment.

Valenzuela-Urrutia et al. (2019) proposed a model-mediated teleoperation method with virtual reality, using a point cloud model obtained with an RGB-D camera. The operator commands the virtual slave robot with the master device; after the intended position of the virtual slave robot is finalized, the real slave robot relocates to that position while both the visualized and real slave robot is presented in the environment. Comparisional experiments between visuo-haptic feedback and non-haptic feedback were carried out to validate expected lower task completion times with more accuracy and less collision.

Kirişçi (2019) implemented augmented reality to model mediated teleoperation to enhance the telepresence of the operator. In this study, a mobile robot with unlimited workspace is constructed and implemented to the proposed method. The results disclose that the overall accuracy is improved with the implemented method as the telepresence is increased.

2.3. Multi-Master Multi-Slave Teleoperation Systems

The notion of teleoperation is extended to multi-master and multi-slave systems with integrated collaboration. Multi-slave robotic systems must simultaneously work remotely in complex environments, target hunting, and prevent errors with the human factor. Further, multi-slave teleoperation amplifies the effort of the operator. Multi-master systems, on the other hand, offer the opportunity of cooperative tasks between different operators on-board or two-handed master consoles.

Due to the inherent time delay between the master and slave robots, slave robot navigation necessitates a local formation control mechanism with obstacle avoidance when the received command is interrupted and/or corrupted. Balch and Arkin presented a behavior-based control theory for multi-slave systems to avoid collusion by a temporary distortion in a formation. Lalish et al. (2006) presented a virtual structure

approach in which the slave formation is considered as a single virtual rigid structure. By means of this method, the formation is maintained, and the behavior of all slave robots is predicted, yet results in more communication delays. Desai et al. (2001) proposed a leader-follower strategy. The designated leader or leaders are put in charge of guiding the formation of followers. The followers are guided by the leaders with predetermined clearances. This leader-follower approach improves the simplicity, modularity, and reliability of the system. However, the entire team of leaders and followers is potentially desperate to system malfunctions since the leader failure affects the whole follower system.

Dual-user teleoperation systems are one of the most prevalent amongst the multi-master systems, together with two-handed master methods. Moghimi et al. (2008) developed adaptive nonlinear control architectures for impedance and admittance dynamic simulations of multi-master systems compatible with haptic interactions, yet time delays are not addressed. Shahbazi et al. (2011) presented an adaptive impedance controller in the presence of constant time delays to stabilize a dual-user system, with stability analysis of the system. Khademian et al. (2011) investigated the influence of environmental factors on the performance of the operators in a dual-user system with cooperatively performed tasks in a virtual environment.

2.4. Teleoperation with Dissimilar Master-Slave Kinematics

For different teleoperation scenarios, the necessity to control various slave arms that have different kinematics with the same master device has emerged since there are general purpose haptic systems available commercially. This teleoperation setting with dissimilar master-slave kinematics is named as master-slave manipulation with different configurations (MSM-DC) in (Mathsuhira et al., 1993).

Apart from operations that utilize the replica of the slave arm as a master device, the ergonomics of the operator and the need of the operation are considered while MSM-DC is designed. One of the most benefited fields from MSM-DC is the teleoperation of soft robots with limited DoF master and infinite DoF slave arms.

Csencsits et al. (2005) proposed a new series of mappings from a joystick to a continuum robot to evaluate the intuitivism and effectiveness at both position and velocity levels and evaluated with a set of tests on human subjects. Fellmann et al.

(2015) compared different types of master devices, such as a 3D mouse, Novint Falcon haptic device, and gamepad, to control a concentric tube continuum robot to evaluate the performance on the same task by considering the task completion times and accuracy. Frazelle et al. (2016) used a 6 DoF master device to control a three-section, 9 DoF continuum robot with different master-slave mapping constrictions. The conducted tests contained different matches of master-slave joints to form a general knowledge about human operator ergonomics with MSM-DC. Sropppa et al. (2020) designed a wearable master around the wrist of the operator to control a continuum robot rather than using a traditional rigid-link master manipulator.

2.5. Telepresence

As a future application in teleoperation systems, in order to provide force reflection and reflect the remote environment, haptic master devices (Sansanayuth et al., 2012), haptic gloves (Zhou and Ben-Tzvi, 2014), virtual reality googles (Sun et al., 2020), and visuo-haptic displays (Yun et al., 2013) are used to expand the force-feedback capabilities that allow the operator to feel the environment naturally.

Geomagic Touch devices have a wide range of applications in systems with haptic force feedback requirements. Bejzay et al. (1990) extended the bilateral teleoperation theory for systems with time delay and implemented predictive displays to improve the task performance of the operator. Hwang et al. (2007) designed a single-master multi-slave system by utilizing this device. Valenzuela-Urrutia et al. (2019) used this device to reflect haptic feedback based on the use of point cloud data obtained with an RGB-D camera.

2.6. Conclusion on Literature Survey

The background on both teleoperation and model-mediated teleoperation is reviewed in this chapter. The earliest teleoperation methods and the improvements on the subject by considering the main encountered problems are summarized. Different techniques and enhancements on telepresence methods are introduced by considering the improvements in teleoperation. The conducted literature survey assisted the studies on this thesis.

In this thesis, the slave environment on the master side is regenerated with the received abstract data from the slave side. Model-mediation technique is aimed to be implemented to eliminate the drawbacks of abstract information exchange. Considering the complexity of multi-master and multi-slave systems and dissimilar master-slave kinematics, different mapping methods that investigates the user ergonomics and performance are investigated. In order to improve telepresence in the remote environment, haptic feedback is implemented to the system, which is shown to increase the accuracy and task performance. The proposed teleoperation method is constructed with the help of reviewed literature survey, explained in detail in the following chapter.

CHAPTER 3

METHODOLOGY

This chapter introduces the methods and components employed in this study. First, the experimental teleoperation setup with hardware and software components is introduced. Then, the proposed teleoperation method and then the implementation of the proposed teleoperation method are explained in detail. The components utilized in this study are illustrated in Figure 3.1. Master devices are two haptic devices denoted with 1 and 2, a foot switch to trigger a specified action is numbered as 3, and 4 denotes the master PC on which the teleoperation algorithm runs.

Figure 3.1 Teleoperation setup.

3.1. Proposed Teleoperation Setup

Bilateral teleoperation systems comprise master and slave systems, control hardware, and a communication system. In this study, the actual slave device is not present since it has not been manufactured during the thesis time interval. Therefore, there was no slave to be mediated on the master side. This study aimed to prepare the generated model of the slave on the master side so that when the actual slave is ready to be used, its regenerated model components will be ready to be mediated with the information received from the actual slave system. All hardware and software used in the experiments are listed in Table 3.1 below.

Table 3.1 Hardware and software.

Hardware	**Software**
Mater PC	SolidWorks© (CAD) Dassault Systèmes
2 Geomagic Touch™ haptic devices 3D Systems© Inc.	MATLAB© Simulink MathWorks Inc. Available toolboxes: • Control System • Robotics System • Simulink 3D Animation
Foot switch KF 1PW - 2m steute Technologies©	Quarc v2.0 Quanser©
Arduino® Mega 2560 Microcontroller Board	
Slave robot (virtual model)	

In this thesis, bilateral teleoperation for a multi-master multi-slave system with dissimilar master-slave kinematics is considered, and motion mappings on position and velocity levels are studied. The teleoperation test setup is composed of a master system and a virtual slave environment. The master system consists of a PC, a foot switch, an Arduino Mega board to receive inputs from the foot switch, and two haptic devices, Geomagic Touch, explained in sub-section 3.1.1. The slave environment includes a virtual replica of soft robot arms in an unlimited virtual environment as presented in sub-section 3.1.2.

The ideal operation of the system is sketched in Figure 3.2. However, since the actual slave robot could not be used in this thesis study, the virtual representation of the slave system is used in the test setup. This virtual slave represents the mediated slave system as if the feedback signals (force, vision-related, etc.) are available from the slave system, and the slave environment is regenerated on the master side. The test system is composed of two Geomagic Touch devices that operate four soft arms positioned on the slave robot. While the first haptic device controls the camera and light arms cooperatively, the second one controls the grasper and palpation arms, respectively. The second haptic device button or foot switch is used for switching between the control of the grasper and palpation arms, and the grasp or palp action is initiated by the click of a button on the second haptic device. The controller's performance and the system's employability considering user ergonomics are investigated with the aforementioned test setup.

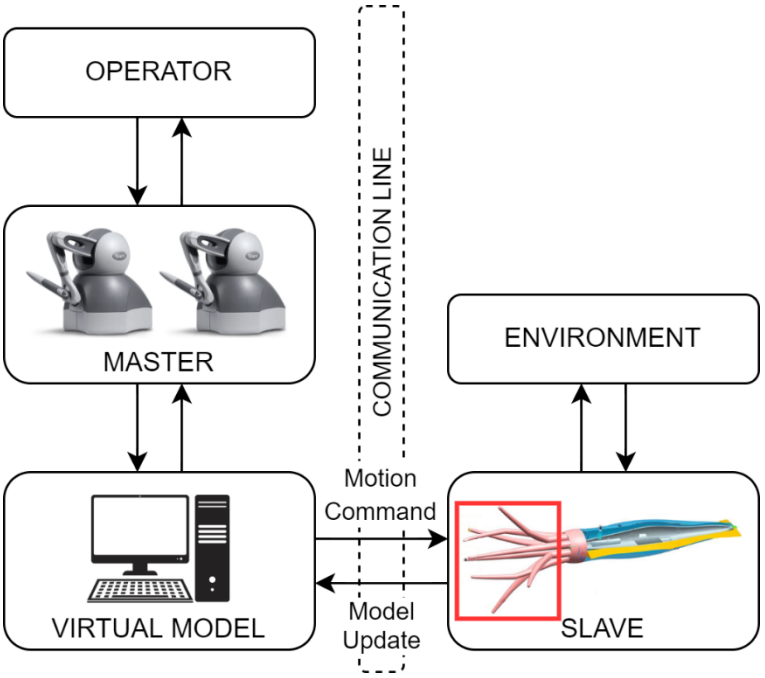

Figure 3.2 Operation of the system.

3.1.1. Master System

Centerpieces of the master system are two Geomagic Touch haptic devices, the product of 3D Systems, as shown in Figure 3.3. Geomagic Touch is a serial haptic device with 6 DoF. Built-in encoders in the robotic arm track the position and orientation of the stylus, which is used to send motion commands to the slave. Only the first three joints have actuators, and as a result, point-type of contact can be simulated; thus, only forces in 3 axes can be reflected back to the human operator. The haptic device is connected to the master PC through a USB interface, and commands from the master computer are transferred to the device by this interface and decoded by onboard firmware to supply actuation. In terms of feedback, sensor signals extracted from built-in encoders are transmitted back in the same manner to the controlling computer. Geomagic Touch provides an SDK that allows to develop control algorithms in MatLab Simulink via Quarc. Further technical specifications of the Phantom device are given in Appendix-A Table-1.

Figure 3.3 Geomagic Touch™ haptic device.

3.1.2. Slave System

The slave is a biomimetic soft robot inspired by squids. The aim of the slave design is the development of an underwater robot that can interact and intervene with the underwater environment much more effectively than existing systems. In this model, multitask tentacles are presented that are capable of reaching, grabbing, pulling, and exploring. Similar to the squid tentacles, the robot arms are hyper-redundant links made of soft and very deformable materials. Thus, the robot is able to interact with the environment in tasks such as palping and grasping without the concern of possible deformation on contact. The virtually created slave replicates the proposed design of the slave prototype, illustrated in Figure 3.4.

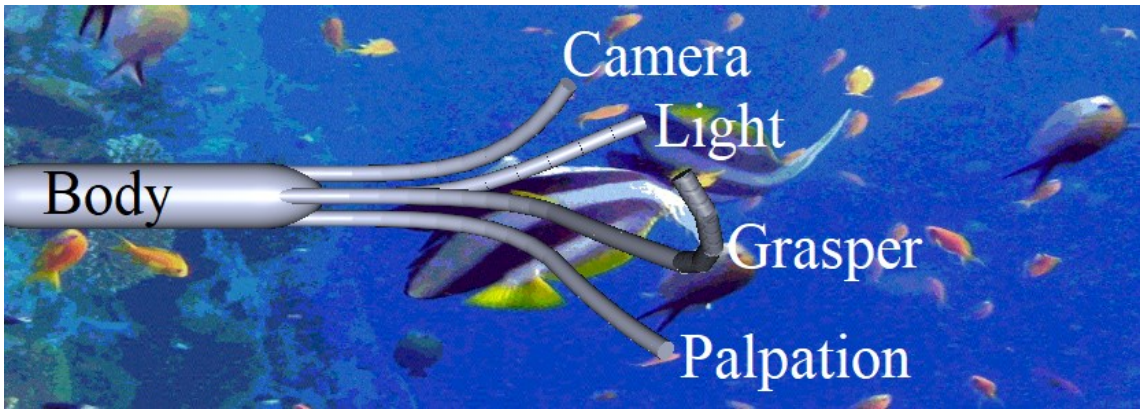

Figure 3.4 Slave system.

Two master devices manipulate the slave arms: 1) the first master device controls the camera and the light arms, (2) the second master device controls the grasper and palpation arms. The buttons located on the haptic devices and the foot switch are used for changing the controlled type of arm and the type of motion. The assigned joints and buttons of the master devices for the controls of the slave arms are defined in sub-sections 4.1 and 5.1.

The grasper arm is designed with two segments and an end-effector mounted on the tip point, providing the grasping motion. The segments of the arm are driven by the first and/or last three joints of the master device. The end-effector is designed with four sections having an RRR serial mechanism driven by the assigned joint motion of the haptic device. The capability of the arm provides interactions such as holding or picking an intervened object.

The palpation arm is also designed as two-segmented, and its task is assigned as palping motion. A force sensor is mounted on the end of the limb. The manipulation of the arm is designed similar to the grasper arm's. The palping motion is achieved by the elongation of the soft arm and operated by the assigned joint on the master device.

The camera arm is composed of only one segment and is driven by the motion demands acquired from the first three joints on the master device. A camera is mounted on the tip point of the arm to capture visuals of the environment and feedback visual data. The collected data from the camera is transformed into abstract information (location and sizes of the objects in the slave environment) and then transmitted to the master side by the communication channel. The virtual environment is generated and updated by the acquired data for the slave to directly interact. However, it should be noted that this operation of the camera arm is represented virtually as the actual slave does not exist.

The light arm is composed of one segment and operated relative to the camera arm to ease the job of the operator. The viewpoints of these arms constantly collide at some distance, which is adjusted by operating the assigned joint or buttons on the master device. In order to synchronize the motion of the light arm with the camera arm, the inverse kinematic model of the light arm is derived and obtained joint variables are used to operate the light arm autonomously.

The slave robot arms are actuated by tendons implanted inside the body of the soft arms. One actuator for each tendon and an additional actuator for the end-effector of the grasper arm to perform the grasping motion are used; thus, 25 actuators in total.

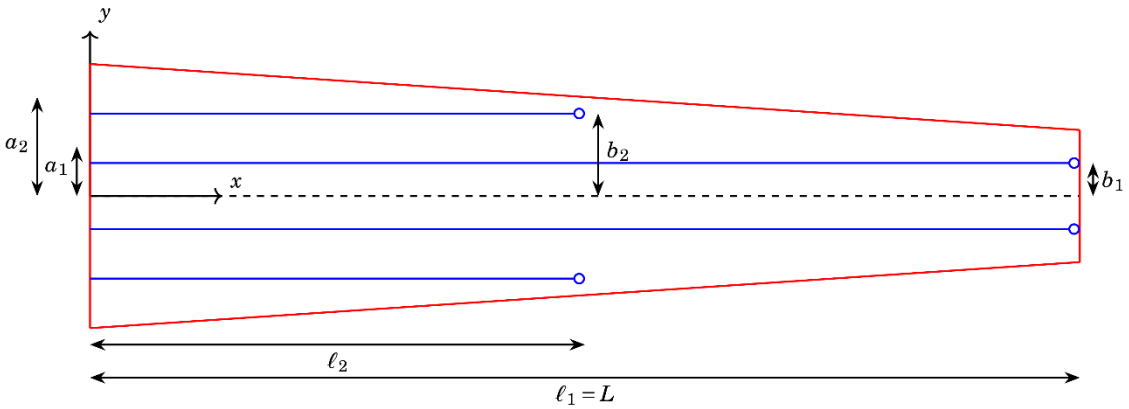

Figure 3.5 Tendon positions inside the robot arm.

The illustration of tendon insertions is shown in Figure 3.5. The blue lines represent the tendons, and the red frame is the robot arm. The a and b parameters represent the distance from the mid-point to tendon anchorage in the z- and x-axes, respectively. ℓ_1 and ℓ_2 parameters reflect the length of the tendons in the first and second segments, where ℓ_1 is equal to the total length of the arm. For the robot arms with one segment, the a_2, b_2, and ℓ_2 parameters are not used.

3.2. Teleoperation Control Algorithm

This sub-section explains the steps to create the virtual slave system, the background algorithm to actuate the slave robot arms, and the control methods employed. The method for creating a soft robot model in a simulation environment is described in the first sub-section. Ideally, when the forward and inverse kinematics models are available for a soft robot, the actuation of a teleoperated soft robot arm is presented below:

i. Map the variables of the master system to the slave arms.
ii. Acquire the simplified parameters by the piecewise constant curvature approach.
iii. Convert the acquired parameters to tensions by using the inverse kinematics of the model.
iv. Create the curved shape representation of the soft arm by using the obtained tension parameters in the forward kinematics model.

The inverse kinematic model to acquire tensions from the parameters as indicated in step 2 was not yet present when this thesis work is carried out. Therefore, a curve equation is used to represent the shape of the soft robot arm without the need of tension calculation appearing in forward or inverse kinematics. Sub-section 3.2.1 investigates and compares different types of mappings between systems that have dissimilar master-slave kinematics. Sub-section 3.2.2 explains the discretized model of the soft robot arms and the necessity of the approach. Sub-section 3.2.3 states the derivation of the forward and inverse kinematic model of the soft robotic arms. Lastly, sub-section 3.2.4 explains the implementation of the teleoperation system.

3.2.1. Mapping of Master-Slave Systems with Dissimilar Kinematics

From rigid-link arm to redundant continuum system mappings requires an intuitive relation that allows users to perform several tasks successfully. In order to adapt the slave design with its soft robot characteristics in the virtual model, an algorithm is required to represent the soft robot with discretized sections. Each section includes an RRP (revolute-revolute-prismatic) serial manipulator architecture. The slave arm, as presented in Figure 3.6 with the exterior surface denoted with the red line, has two segments, divided by the thick dashed blue line.

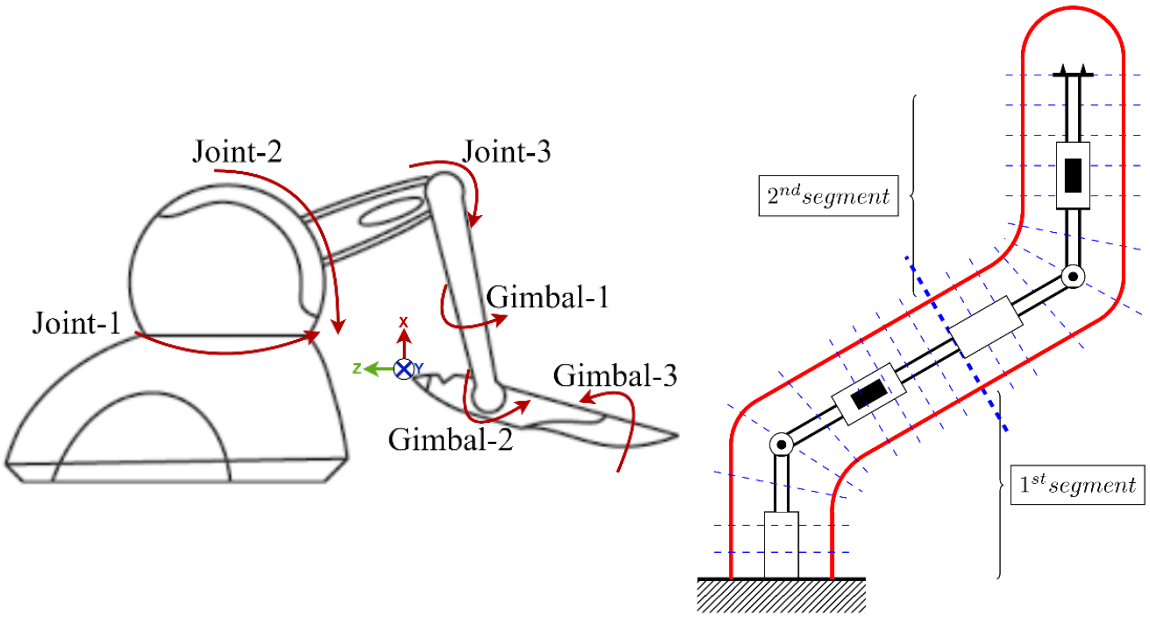

Figure 3.6 Master device - slave arm representation.

There are ten sections in each segment, illustrated in Figure 3.6 with the dashed blue lines. The master device's active joints (Joint-1, Joint-2, Joint-3) and gimbal joints (passive joints) are mapped to the slave robot arm's each segment by using various mapping strategies, which are explained in the later parts of this sub-section.

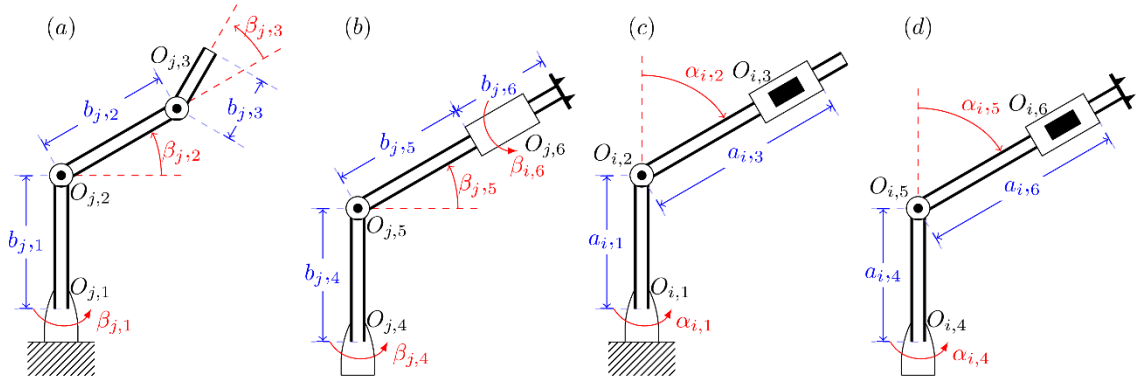

Figure 3.7 Kinematic sketches of master devices and slave arms (a) Master joints 1-2-3 (b) Master joints 4-5-6 (c) Slave first segment (d) Slave second segment.

In Figure 3.7, kinematic sketches of both the master device and the slave segment with link lengths and joint angles are presented. The slave robot arm is designed as a spherical arm with RRP joints for each segment. The master device has six revolute joints, and while the first three joint motions can be mapped to one of the segments of the slave arm, the last three joints can be mapped to the second segment of the slave arm. The $\bar{\alpha}$, $\bar{\beta}$, $\bar{a}$, and $\bar{b}$ parameters are defined as follows:

$$\bar{\beta} = \begin{bmatrix} \bar{\beta}_{m\#1} \\ \bar{\beta}_{m\#2} \end{bmatrix}, \bar{b} = \begin{bmatrix} \bar{b}_{m\#1} \\ \bar{b}_{m\#2} \end{bmatrix}, \bar{\alpha} = \begin{bmatrix} \bar{\alpha}_g \\ \bar{\alpha}_p \\ \bar{\alpha}_c \\ \bar{\alpha}_l \end{bmatrix}, \bar{a} = \begin{bmatrix} \bar{a}_g \\ \bar{a}_p \\ \bar{a}_c \\ \bar{a}_l \end{bmatrix}$$

Where, $\bar{\beta} = [\beta_{j,1} \quad \beta_{j,2} \quad \beta_{j,3} \quad \beta_{j,4} \quad \beta_{j,5} \quad \beta_{j,6}]^T$, $\bar{b} = [b_{j,1} \quad b_{j,2} \quad b_{j,3} \quad b_{j,4} \quad b_{j,5} \quad b_{j,6}]^T$, $\bar{\alpha} = [\alpha_{i,1} \quad \alpha_{i,2} \quad \alpha_{i,3} \quad \alpha_{i,4} \quad \alpha_{i,5} \quad \alpha_{i,6}]^T$, $\bar{a} = [a_{i,1} \quad a_{i,2} \quad a_{i,3} \quad a_{i,4} \quad a_{i,5} \quad a_{i,6}]^T$ and, $j = m\#1, m\#2$ which indicates Touch-1 and Touch-2 master devices, and $i = g, p, c, l,$ which indicates grasper, palpation, camera, and light arms of the slave robot.

Any system developed should allow a human operator to perform several vital tasks successfully. However, it is troublesome to match the movements of the dissimilar master-slave systems, with operator confusion being the key obstacle.

A series of mappings from rigid-link arms to continuum robots, at both position and velocity levels, which provide intuitive options for dissimilar master-slave systems, are investigated. These mappings are implemented from a 6-DoF rigid-link manipulator as a master device to a slave soft robot arm that is modeled with 30-DoF segments as a consequence of having ten 3-DoF sections for each segment. Mapping types are discussed based on task and joint space mapping options and position and velocity level information exchanges.

Frazelle et al. (2016) used joint space mapping with different matchings of the master device's joint motion to slave section motion for the OctArm soft slave robot. In the first set of tests, one-by-one respective mapping of master joints to slave sections is implemented, while in the second set, the links of each segment are mapped to the respective master device joints with respect to their proximity to their bases. An adaptation of these mapping types for this thesis is shown in Table 3.2. The mappings in Table 3.2 are selected to have a sequential order such that the first three DoFs of the master system are mapped to one segment's motion. It is foreseen that this type of mapping strategy would preserve the intuitiveness of the teleoperation and thus, ease the teleoperation of a relatively complex soft robot arm with multiple segments.

Table 3.2 Adapted mappings.

Variable Mappings in Joint Space		
Type / Slave Joint#	Full use of DoFs	Partial use of DoFs
Segment-1 #1	Joint #1	Joint #1
Segment-1 #2	Joint #2	Joint #2
Segment-1 #3	Joint #3	Joint #3
Segment-2 #1	Joint #4	Joint #1
Segment-2 #2	Joint #5	Joint #2
Segment-2 #3	Joint #6	Joint #3

Csencsits et al. (2005) investigated position-to-position, position-to-velocity, and velocity-to-velocity based joystick mappings on various continuum robots. Position-to-position mapping converts rectangular coordinates to polar (or spherical in the 3D case)

from the configuration space of the joystick to the configuration space of the manipulator section. The acquired configuration of one section is then replicated and applied to multiple sections. This mapping causes the manipulator section to curve in the direction that the joystick is pushed, with the amount of curvature defined by how far away the joystick is moved away from the center. The initial condition sent from the joystick to the slave robot causes rapid dislocations and jeopardizes the stability of the system. In multi-slave systems operated by the same master device, the switch between a slave robot arm to another yield a sudden dislocation caused by the last position of the first arm data being sent as an initial position input to the second arm.

According to the study of Csencsits et al. (2005), the position-to-velocity and velocity-to-velocity mappings provided higher precision and the ability to directly alter the speed. The position-to-velocity mappings prevented the rapid dislocation encountered. When position-to-velocity mapping is concerned, master systems with spring-based mechanical home positioning (i.e., joysticks) that move to the center position (neutral position) when left free provide ease of use when required to send a command to stop the motion of the slave device. When the master device lacks a mechanical home positioning mechanism, in order to stop the motion of the slave arm, the operator should locate the handle of the master system to the zero position on each x, y, and z-axis. The task is overly demanding, and it is almost impossible to perform during the operation. In order to eliminate this problem, the home positioning mechanism can be imitated. Any master device that allows force/haptic feedback, like Geomagic Touch, is capable of mimicking the nature of a mechanical spring. In order to provide tolerance in moving back to the home position, a dead band can be integrated. When the handle is positioned inside this dead band, the master device can be programmed to send zero-velocity commands to the slave.

The velocity-to-velocity mappings eliminate the necessity of a mechanical home position and allow the user to perform more intuitively. While the operator on board might achieve more precise movements, the workspace of the master devices, whether joystick or haptic, severely restricts the workspace of the slave robot. When the master approaches the limits of its workspace, the operator's movement on the area is similarly confined to only the opposite direction, albeit a switch that pauses steering on the workspace limits might eliminate this problem yet requires higher steering abilities.

Table 3.3 Mappings of Modes 1, 2, 3, and 4.

Master to Slave Arms Mappings on Position and Velocity Levels				
Operation& Mapping Type / Slave Joint#	Position-to-Position			Position-to-Velocity
	Mode 1 (Simultaneously)	Mode 2 (Respectively)	Mode 3 (Respectively)	Mode 4 (Respectively)
Segment-1 #1	Joint #1	Joint #1	Joint #1	Joint #1
Segment-1 #2	Joint #2	Joint #2	Joint #2	Joint #2
Segment-1 #3	Joint #3	Joint #3	Joint #3	Joint #3
Segment-2 #1	Joint #4	Joint #4	Joint #1	Joint #1
Segment-2 #2	Joint #5	Joint #5	Joint #2	Joint #2
Segment-2 #3	Joint #6	Joint #6	Joint #3	Joint #3

Adapted mappings for Modes 1, 2, 3, and 4 of teleoperation are presented in Table 3.3. In the first three modes, position-to-position mapping is used, as explained in sub-section 3.2.1.1, while in the last mode, position-to-velocity mapping is used, which is explained in sub-section 3.2.1.2.

3.2.1.1. Position to Position Mapping in Task Space and Joint Space

Modes 1, 2, and 3 of the teleoperation system are designed with a hybrid approach of task and also joint space position to position mappings simultaneously using spherical coordinates. In Modes 1 and 2, the first segment of the slave arms is driven by the first three joints on the master devices with task space mapping, while the last three joints drive the second with joint space mapping. However, in Mode 3, both segments are driven using the motion data acquired from the first three joints. The segment architecture is created as an RRP manipulator with a zero offset for $a_{i,1}$ and $a_{i,4}$; hence this architecture represents the spherical coordinates with variables $\{\alpha_{i,1}, \alpha_{i,2}, a_{i,3}\}$ for segment 1 and $\{\alpha_{i,4}, \alpha_{i,5}, a_{i,6}\}$ for segment 2. The first and second joints of the master device are mapped directly to the first and second variables of the segments because of the similarity of joint types. This mapping is shown in Equations 3.1 and 3.2. The first joints of master and slave arms operate similarly, though their second joints operate in the opposite directions and under different initial conditions, as indicated in Figure 3.7.

$$\alpha_{i,1} = \beta_{j,1} \tag{3.1}$$

$$\alpha_{i,2} = -\beta_{j,2} - \frac{\pi}{2} \tag{3.2}$$

$$a_{i,3} = \frac{b_{j,2}\cos\left(\beta_{j,2}\right) + b_{j,3}\cos\left(\beta_{j,2} + \beta_{j,3}\right)}{\sin\left(\alpha_{i,2}\right)} \tag{3.3}$$

$$\alpha_{i,4} = \beta_{j,4} \tag{3.4}$$

$$\alpha_{i,5} = -\beta_{j,5} - \frac{\pi}{2} \tag{3.5}$$

$$a_{i,6} = \beta_{j,6} \tag{3.6}$$

The third and prismatic joint of the slave segment's position is computed with Equation 3.3 presented as $a_{i,3}$. In order to derive the $a_{i,3}$ parameter, the length from the second joint of the master device ($O_{j,2}$) to the tip point of the third joint ($O_{j,3}$) is calculated and equalized to the $a_{i,3}$ parameter. The fourth, fifth, and sixth joint positions of the master device are mapped to the joint space to the slave arm's second segment in Equations 3.4, 3.5, and 3.6, respectively. The fifth joint's motion is mapped considering the opposite direction of motion and initial condition matching. The last three joints of the master system constitute a spherical wrist structure; thus, a direct relation to the spherical coordinates is not possible.

3.2.1.2. Position to Velocity Mapping in Task Space

Mode 4 of the teleoperation system is designed with task space position-to-velocity mapping on spherical coordinates. Only the first three joints of the master device are utilized for both the first and second segments of the slave arms. Since there is no mechanical spring-based homing available in the master device, the actuated joints, the first three joints, must be used for control-based homing of the device. The switch between the motion control segments is performed by the buttons on the master device, while the foot switch is used to change the commanded arm type. The mentioned equations of the position-to-position mapping are converted to velocity level equations for each segment as presented in Equations 3.7, 3.8, 3.9, 3.10, 3.11, and 3.12.

$$\dot{\alpha}_{i,1} = \beta_{j,1} \tag{3.7}$$

$$\dot{\alpha}_{i,2} = -\beta_{j,2} \tag{3.8}$$

$$\dot{a}_{i,3} = \frac{b_{j,2}\cos\left(\beta_{j,2}\right) + b_{j,3}\cos\left(\beta_{j,2} + \beta_{j,3}\right)}{\sin\left(\alpha_{i,2}\right)} \tag{3.9}$$

$$\dot{\alpha}_{i,4} = \beta_{j,1} \tag{3.10}$$

$$\dot{\alpha}_{i,5} = -\beta_{j,2} \tag{3.11}$$

$$\dot{a}_{i,6} = \frac{b_{j,2}\cos\left(\beta_{j,2}\right) + b_{j,3}\cos\left(\beta_{j,2} + \beta_{j,3}\right)}{\sin\left(\alpha_{i,5}\right)} \tag{3.12}$$

The $-\frac{\pi}{2}$ on Equations 3.2 and 3.5, is not transferred to Equations 3.8 and 3.11 to keep the initial velocity command zero. As aforementioned, the β and b parameters are defined as the joint variables and link lengths of master devices, respectively, while the $\dot{\alpha}$ and $\dot{a}$ parameters are the joint velocity commands calculated for the slave motion.

The gravity compensation of the master systems is achieved by actuating their active joints. The calculation of required actuation torque for gravity compensation for each joint, the elements of $\bar{G}\left(\bar{\beta}_j\right) = [G_{j,3} \quad G_{j,3} \quad G_{j,3}]^T$ is formulated in Equations 3.13, 3.14, and 3.15. In (Sansanayuth et al., 2012), k_1, k_2, and k_3 parameters are defined as the coefficients calculated by using the mass, gravitational acceleration, and link lengths. These parameters are reported as follows, $k_1 = 164.158 \times 10^{-3}\ \mathrm{kg\,m^2}/s^2$, $k_2 = 94.05 \times 10^{-3}\ \mathrm{kg\,m^2}/s^2$, and $k_3 = 117.294 \times 10^{-3}\ \mathrm{kg\,m^2}/s^2$ and determined by using the physical properties of the links: $m_2 = 0.035\ \mathrm{kg}$, $m_3 = 0.1\ \mathrm{kg}$, $g = 9.81\ \mathrm{m}/s^2$, $b_{j,1} = 133.35\ mm$, $b_{j,2} = 133.35\ mm$, $b_{j,3} = 23.35\ mm$, and $b_{j,4} = 168.35\ mm$.

$$G_{j,1} = 0 \tag{3.13}$$

$$G_{j,2} = k_1 cos\beta_{j,2} + k_3(\beta_{j,2} - 0.5pi) + k_2 sin\beta_{j,3} \tag{3.14}$$

$$G_{j,3} = k_2 sin\beta_{j,3} \tag{3.15}$$

In order to imitate the home position mechanism on software, the end-effector positions of the master devices are derived by the forward kinematics of Geomagic Touch as presented in equations 3.16, 3.17, and 3.18. These equations are used for constituting the feedback to indicate the home position of the master devices.

$$r_{j,x} = -sin\beta_{j,1}(b_{j,2}sin\beta_{j,3} + b_{j,1}cos\beta_{j,2}) \quad (3.16)$$

$$r_{j,y} = -b_{j,2}cos\beta_{j,3} + b_{j,1}sin\beta_{j,2} + b_{j,3} \quad (3.17)$$

$$r_{j,z} = b_{j,2}cos\beta_{j,1}sin\beta_{j,3} + b_{j,1}cos\beta_{j,1}cos\beta_{j,2} - b_{j,4} \quad (3.18)$$

The dead-band of the Geomagic Touch is identified as a sphere with a 10 mm radius, as shown in Figure 3.8, from the initial points of $r_{j,x}$, $r_{j,y}$, and $r_{j,z}$ where $\beta_{j,1} = 0°, \beta_{j,2} = 45°$ and $\beta_{j,3} = 30°$, thus eliminates the inconveniency of the lack of natural home positioning mechanism on master devices. The feedback force applied to the user is along the direction of $\overrightarrow{OP}$ when the tip point of the stylus is located on point P.

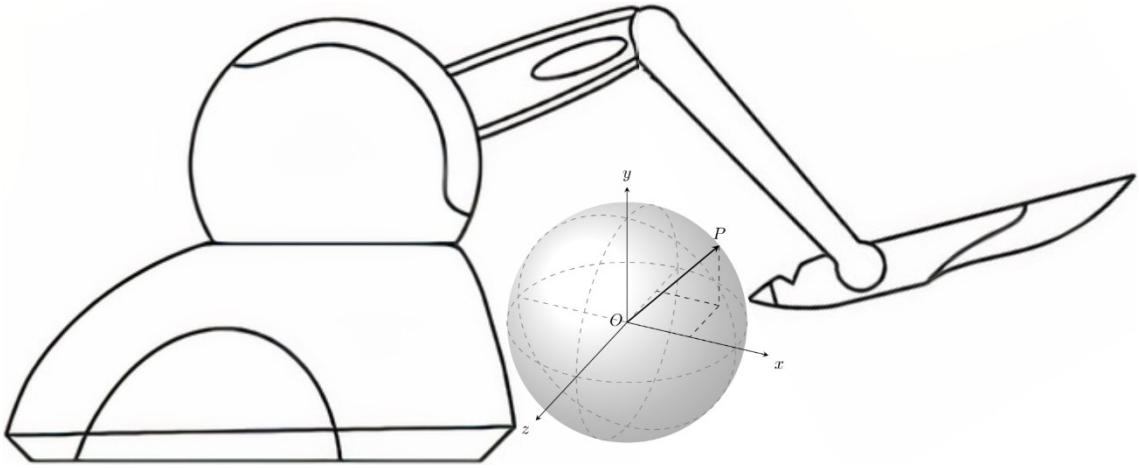

Figure 3.8 Spherical dead-band positioning.

3.2.2. Soft Arm Modelling and Piecewise Constant Curvature Approach

Mathematical modeling of infinite DoF robots' kinematics and dynamics presents challenging requirements. In order to meet the standards, set by traditional rigid robots, a soft robot model must be both computationally inexpensive and sufficiently accurate. Such a modeling framework is required for the development of soft robots' physical designs and control architectures, as well as their task-related motions and path planning.

The Piecewise Constant Curvature (PCC) modeling approach simplifies and permits closed-form kinematics and the construction of a closed-form Jacobian formulation to represent the robot as a series of mutually tangent constant-curvature

arcs. Most continuum robots are assumed to be composed of arcs. The PCC approach describes the robot as a finite set of arcs that can be simply defined by three parameters: angle of the arc (θ), angle of the plane (ϕ), and arc length (ℓ). The number of variables required significantly decreases as a result of this simplification. The concept of the PCC approach is represented in Figure 3.9.

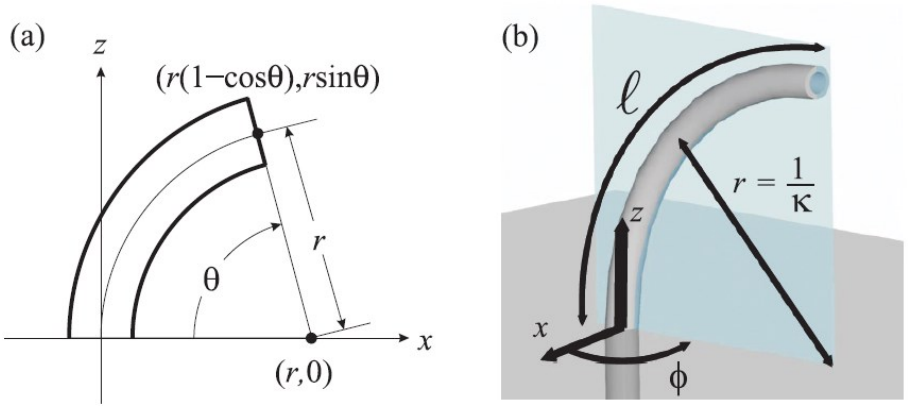

Figure 3.9 PCC, (a) $\phi = 0$, arc in the x-z plane. (b) $\phi \neq 0$.
(Source: Webster et al., 2010)

The mathematical model of the virtual slave robot arms is derived from the discretization of the PCC approach, which implies that the soft robotic arm is made up of several small discrete rigid bodies. These small-solid bodies can be freely and independently rotated from neighboring bodies. Both the orientation and the position of these bodies are in reference to the base frame, yet the bodies are connected to each other through the longitudinal axis.

Considering the discrete and equal set of rigid bodies along each of the N sections of the soft arm's segment, the continuous field is replaced with a finite set of N sections that play the role of the joint vectors of traditional rigid robots. The material abscissa is divided into N sections in the form $[(0, L_1) (L_1, L_2) \ldots (L_{N-1}, L_N)]$, illustrated in Figure 3.10 in sub-section 3.2.3, where L_N is the total length of the arm. In other words, the sections are assembled on top of each other (Renda et al., 2016).

Due to the deficiency of the curve equation obtained from the inverse kinematics model of the slave robot arms, a curve equation is assumed to be applicable to imitate the soft robotic characteristics. A quadrant equation denoted in Equations 3.19, 3.20, 3.21, and 3.22 for the first and second segment of the arms, respectively, are used to

derive the PCC parameters. The initial length of the arms without elongation is indicated as 250 mm for each segment of the arms. The relation between each discrete link is derived from the proposed equation and implemented to the angle of the arc ($\theta_{i,k,s}$) parameter on each section.

The parameters acquired from the mappings of joint variables of master devices are used in the piecewise constant curvature approach to determine the corresponding θ, ϕ, and ℓ parameters. $\bar{\alpha}_{i,2}$ and $\bar{\alpha}_{i,5}$ parameters and the initial length of each segment are placed in the quadrant equations (Equations 3.19, 3.20, 3.21, and 3.22) to obtain the tip point position of the first and second segments on the arms.

$$x_{e,1} = -r_1 \cos(\alpha_{i,2}) + r_1 \tag{3.19}$$

$$z_{e,1} = r_1 \sin(\alpha_{i,2}) \tag{3.20}$$

$$x_{e,2} = -r_2 \cos(\alpha_{i,5}) + r_2 \tag{3.21}$$

$$z_{e,2} = r_2 \sin(\alpha_{i,5}) \tag{3.22}$$

Where,

$x_{e,1}$: x-axis position of the first segment's tip point

$z_{e,1}$: z-axis position of the first segment's tip point

r_1 : Initial length of the first segment

$x_{e,2}$: x-axis position of the second segment's tip point

$z_{e,2}$: z-axis position of the second segment's tip point

r_2 : Initial length of the second segment

The acquired curve is divided into 11 points by a MatLab function called "interparc", presented in Equation 3.23, by which points are distributed at equal distances along the arc length. By using the tangent of these points, $\theta_{i,k,s}$ parameter is acquired, shown in Equation 3.24, which results as a constant curvature arc for each segment. This parameter is computed ten times in each segment for each of the ten sections. ϕ and ℓ parameters are made equal to $\bar{\alpha}_{i,1}$, $\bar{\alpha}_{i,4}$, and $\bar{\alpha}_{i,3}$, $\bar{\alpha}_{i,6}$ parameters, respectively, for segments 1 and 2.

$$(x_{k,s}, z_{k,s}) = interparc(11, x_{e,s}, z_{e,s}) \tag{3.23}$$

$$\theta_{i,k,s} = \text{atan2}\left(\frac{z_{k+1,s} - z_{k,s}}{x_{k+1,s} - x_{k,s}}\right) \tag{3.24}$$

Where,

$x_{k,s}$ = tip point position of the k[th] section and s[th] segment on the x-axis

$z_{k,s}$ = tip point position of the k[th] section and s[th] segment on the z-axis

$\theta_{i,k,s}$ = angle of the plane on the k[th] section and s[th] segment

$$k = \begin{cases} [1\ 2\ 3\ 4\ 5\ 6\ 7\ 8\ 9\ 10]\ for\ \ s = 1 \\ [11\ 12\ 13\ 14\ 15\ 16\ 17\ 18\ 19\ 20]\ for\ \ s = 2 \end{cases}$$

By means of this approach, the parameters for all arms, segments, and sections to actuate the slave arms are obtained as follows:

$$\overline{\theta}_{i,k,1} = \begin{bmatrix} \theta_{i,1,1} \\ \theta_{i,2,1} \\ \theta_{i,3,1} \\ \theta_{i,4,1} \\ \theta_{i,5,1} \\ \theta_{i,6,1} \\ \theta_{i,7,1} \\ \theta_{i,8,1} \\ \theta_{i,9,1} \\ \theta_{i,10,1} \end{bmatrix}, \overline{\Phi}_{i,1} = \begin{bmatrix} \frac{\alpha_{i,1}}{10} \\ \frac{\alpha_{i,1}}{10} \\ \frac{\alpha_{i,1}}{10} \\ \frac{\alpha_{i,1}}{10} \\ \frac{\alpha_{i,1}}{10} \\ \frac{\alpha_{i,1}}{10} \\ \frac{\alpha_{i,1}}{10} \\ \frac{\alpha_{i,1}}{10} \\ \frac{\alpha_{i,1}}{10} \\ \frac{\alpha_{i,1}}{10} \end{bmatrix}, \overline{\ell}_{i,1} = \begin{bmatrix} \frac{a_{i,3}}{10} \\ \frac{a_{i,3}}{10} \\ \frac{a_{i,3}}{10} \\ \frac{a_{i,3}}{10} \\ \frac{a_{i,3}}{10} \\ \frac{a_{i,3}}{10} \\ \frac{a_{i,3}}{10} \\ \frac{a_{i,3}}{10} \\ \frac{a_{i,3}}{10} \\ \frac{a_{i,3}}{10} \end{bmatrix}, \overline{\theta}_{i,k,2} = \begin{bmatrix} \theta_{i,11,2} \\ \theta_{i,12,2} \\ \theta_{i,13,2} \\ \theta_{i,14,2} \\ \theta_{i,15,2} \\ \theta_{i,16,2} \\ \theta_{i,17,2} \\ \theta_{i,18,2} \\ \theta_{i,19,2} \\ \theta_{i,20,2} \end{bmatrix}, \overline{\Phi}_{i,2} = \begin{bmatrix} \frac{\alpha_{i,4}}{10} \\ \frac{\alpha_{i,4}}{10} \\ \frac{\alpha_{i,4}}{10} \\ \frac{\alpha_{i,4}}{10} \\ \frac{\alpha_{i,4}}{10} \\ \frac{\alpha_{i,4}}{10} \\ \frac{\alpha_{i,4}}{10} \\ \frac{\alpha_{i,4}}{10} \\ \frac{\alpha_{i,4}}{10} \\ \frac{\alpha_{i,4}}{10} \end{bmatrix}, \overline{\ell}_{i,2} = \begin{bmatrix} \frac{a_{i,6}}{10} \\ \frac{a_{i,6}}{10} \\ \frac{a_{i,6}}{10} \\ \frac{a_{i,6}}{10} \\ \frac{a_{i,6}}{10} \\ \frac{a_{i,6}}{10} \\ \frac{a_{i,6}}{10} \\ \frac{a_{i,6}}{10} \\ \frac{a_{i,6}}{10} \\ \frac{a_{i,6}}{10} \end{bmatrix}$$

3.2.3. Kinematic Model of the Slave Arm

The geometrical representation of the robot is illustrated in Figure 3.10. The architecture of the virtual arms is designed as RRP manipulators on top of each other as ten discrete sections for 1-segment arms and twenty for 2-segment arms, and end-effectors are not included.

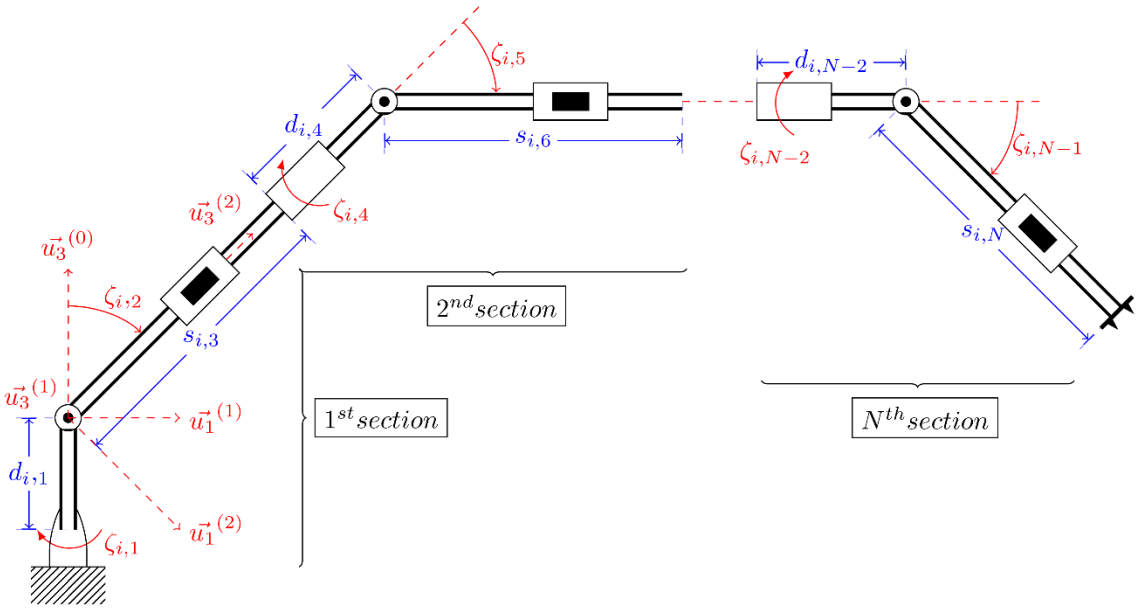

Figure 3.10 Architecture of the slave robot arm.

As a result of the design presented in Figure 3.10, the virtual robot mimics the motion of a soft robot. In fact, increasing the number of sections for a segment of the soft robot would enhance this mimicking behavior.

In order to manipulate and navigate the virtual slave, necessary equations for forward and inverse kinematics of the robotic arms are derived. In Table 3.3, the Denavit-Hartenberg parameters are presented, and these parameters are used to derive the kinematics of the slave robot. The end-effector position and rotation matrix are given in equations 3.25 and 3.26.

$$r_i = d_{i,1}\bar{u}_3 + s_{i,3}\bar{u}_3^{(2/0)} + d_{i,4}\bar{u}_3^{(3/0)} + s_{i,6}\bar{u}_3^{(5/0)} + \cdots + d_{i,3N-2}\bar{u}_3^{(3N-3/0)} + s_{i,3N}\bar{u}_3^{(3N-1/0)} \tag{3.25}$$

$$\hat{C}_i = e^{\tilde{u}_3\zeta_{i,1}} + e^{-\tilde{u}_1\frac{\pi}{2}} + e^{\tilde{u}_3\zeta_{i,2}} + e^{\tilde{u}_1\frac{\pi}{2}} + e^{\tilde{u}_3\zeta_{i,4}} + e^{-\tilde{u}_1\frac{\pi}{2}} + e^{\tilde{u}_3\zeta_{i,5}} + e^{\tilde{u}_1\pi/2} + \cdots + e^{\tilde{u}_3\zeta_{i,3N-1}} + e^{\tilde{u}_1\pi/2} \tag{3.26}$$

Where,

$\bar{u}_1, \bar{u}_2, \bar{u}_3$: column representation of the unit vector,

$\tilde{u}_1, \tilde{u}_2, \tilde{u}_3$: cross-product (a skew-symmetric) matrix generated from $\bar{u}_1, \bar{u}_2, \bar{u}_3$,

$\hat{C}^{(a,b)}$: non-column transformation matrix between F_a and F_b where F is the reference frame.

In order to cooperatively actuate the light arm with the camera arm, the inverse kinematic equations of the light arm are formulated and given in Equations 3.27, 3.28, and 3.29. To simplify the process, the sections of the arm are not included, and instead, the segment architecture is utilized.

$$\phi_l = atan2(r_{c,2}, r_{c,1}) \tag{3.27}$$

$$l_l = \sqrt{(r_{c,3} - d_{c,1})^2 + \sqrt{{r_{c,1}}^2 + {r_{c,2}}^2}} \tag{3.28}$$

$$\theta_l = atan2\big((r_{c,3} - d_{c,1}), \sqrt{{r_{c,1}}^2 + {r_{c,2}}^2}\big) \tag{3.29}$$

Table 3.4 Denavit-Hartenberg parameters.

Denavit-Hartenberg Parameters				
Parameters / Link#	ζ_i (°)	s_i (mm)	γ_i (°)	a_i (mm)
#1	$\alpha_{i,1}/10$	$d_{i,1}$	-π/2	-
#2	$\theta_{i,1}$	-	π/2	-
#3	-	$a_{i,3}/10$	-	-
#4	$\alpha_{i,1}/10$	$d_{i,4}$	-π/2	-
#5	$\theta_{i,2}$	-	π/2	-
#6	-	$a_{i,3}/10$	-	-
⋮	⋮	⋮	⋮	⋮
#3N-2	$\alpha_{i,4}/10$	$d_{i,3N-2}$	-π/2	-
#3N-1	$\theta_{i,N}$	-	π/2	-
#3N	-	$a_{i,6}/10$	-	-

3.2.4. Teleoperation System Implementation

The control algorithm is designed with mainly two subsystems as master and slave environment. The interface of the master devices with the MatLab simulation environment is created by using the Quarc block “Phantom” for both master devices separately. The virtual slave and its environment are created via the V-Realm Builder editor, and its interface with the MatLab simulation is created with the VR Sink block available under the Simulink 3D Animation toolbox. The implemented structure with

their relations is shown in Figure 3.11. The red parameters are used in Modes 1, 2, and 3 of the teleoperation system with position-to-position mapping, the blue parameters are used in Mode 4 with position-to-velocity mapping, and the black ones are employed in all of the mappings. The $\bar{x}_i$ and $\dot{\bar{x}}_i$ parameters denote the slave position and velocity, respectively for each arm. $\bar{r}_i$ denotes the end-effector position of each arm derived from the forward kinematics. The $\bar{\theta}_i$, $\bar{\Phi}_i$, and $\bar{\ell}_i$ are the parameters derived from the PCC approach. The impedance characteristics of the haptic interaction model between the palpation/grasper arm and the environment are the stiffness ($\hat{K}_i$) and damping ($\hat{B}_i$) coefficients. The palpation arm's limb ends, in the actual system, are equipped with pressure/force sensors to calculate the stiffness and damping coefficients by measuring the displacement with respect to the applied force. By means of this, calculated stiffness and damping coefficients can be applied for different types of obstacles intervened. However, since the actual slave system is not available, the stiffness and damping coefficients are determined by considering the desired characteristics of the response, such as the interaction force between the soft arm and a rigid object in the slave environment, to be provided to the operator. The parameters are determined by trial and error and b_g and b_p parameters are selected as 0.2 Ns/m, and the k_g and k_p parameters are selected as 2 N/m. All parameters are represented in their matrix form as follows:

$$\hat{B}_i = \begin{bmatrix} b_g & 0 \\ 0 & b_p \end{bmatrix}, \hat{K}_i = \begin{bmatrix} k_g & 0 \\ 0 & k_p \end{bmatrix}, \bar{\theta}_i = \begin{bmatrix} \bar{\theta}_g \\ \bar{\theta}_p \\ \bar{\theta}_c \\ \bar{\theta}_l \end{bmatrix}, \bar{\Phi}_i = \begin{bmatrix} \bar{\Phi}_g \\ \bar{\Phi}_p \\ \bar{\Phi}_c \\ \bar{\Phi}_l \end{bmatrix}, \bar{\ell}_i = \begin{bmatrix} \bar{\ell}_g \\ \bar{\ell}_p \\ \bar{\ell}_c \\ \bar{\ell}_l \end{bmatrix}$$

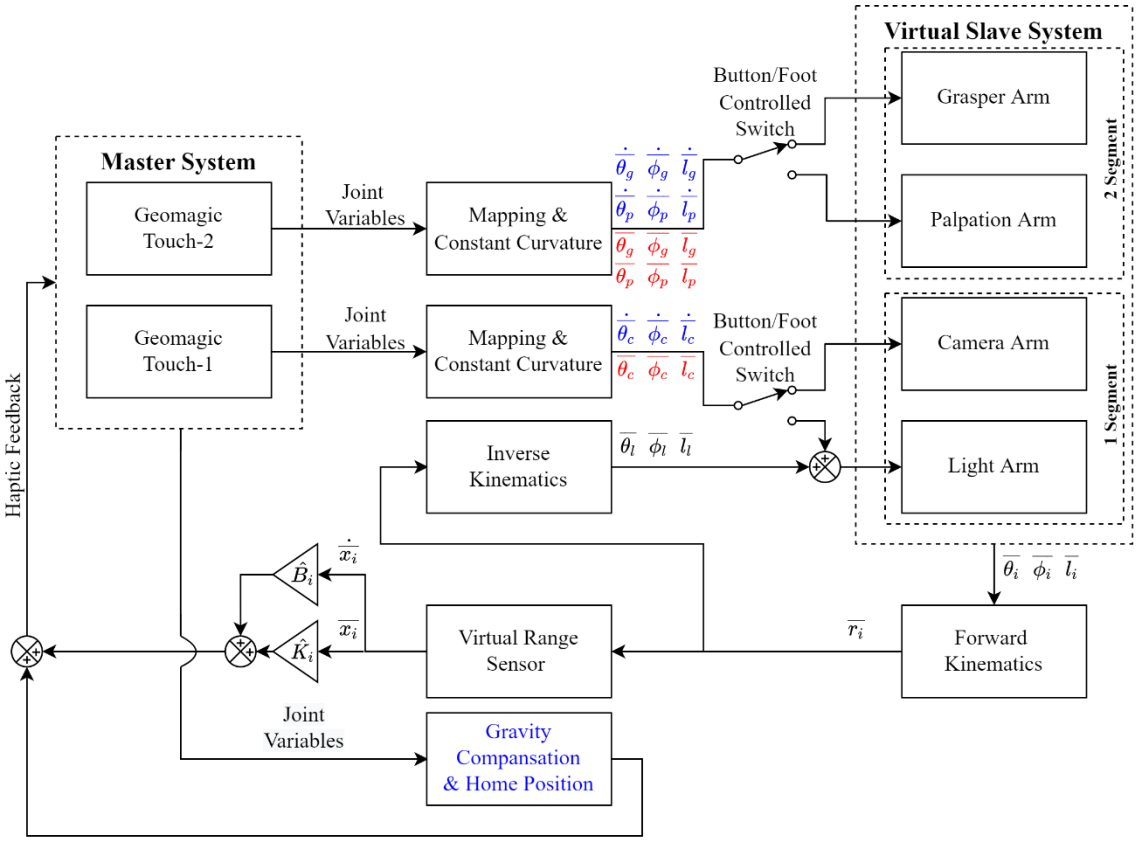

Figure 3.11 Block diagram of the control system.

The end-effector position of the camera arm, which is obtained from the forward kinematics, is used in the inverse kinematic model to calculate joint positions to be used in the manipulation of the light arm. In addition to the dependent manipulation of the light arm, depending on the mode, the buttons or a specific joint motion on the master device is used to adjust the orientation of the light arm to illuminate a specific location along the line of sight of the camera.

In order to create the haptic feedback to inform the operator about contact positions, a virtual range sensor is created by using the forward kinematics of the model and the target positions. Unlike a case with the actual system, the defined target positions are predefined and fixed at their exact positions. The abstract information acquired from the sensory data on the real system is foreseen to be disturbed, and the range information between the slave arms and the target obstacle would partially change by means of this disturbance. The performance of the system in terms of stability and transparency is not guaranteed in the presence of this disturbance. Model-mediated teleoperation is confided to overcome the effects of inevitable disturbance. Updated models of the remote environment are transferred to the master site over the delayed

communication line to generate a virtual world for the operator to directly interact. On the other hand, in the virtual range sensor, the haptic feedback is created with predefined stiffness and damping parameters, which is later translated to joint space by using the Jacobian matrix of the master device with Equation 3.30. The Jacobian matrix for Geomagic Touch haptic device is presented in Equation 3.31. The elements of the Jacobian matrix are given in Equations 3.32, 3.33, 3.34, 3.35, 3.36, 3.37, 3.38, 3.39, and 3.40.

$$\tau = J_m{}^T F \tag{3.30}$$

$$J_{\mathrm{m}} = \begin{bmatrix} J_{\mathrm{m},11} & J_{\mathrm{m},12} & J_{\mathrm{m},13} \\ J_{\mathrm{m},21} & J_{\mathrm{m},22} & J_{\mathrm{m},23} \\ J_{\mathrm{m},31} & J_{\mathrm{m},32} & J_{\mathrm{m},33} \end{bmatrix} \tag{3.31}$$

$$J_{m,11} = -\cos(\beta_{j,1})\, b_{j,2} \sin(\beta_{j,3}) + b_{j,1} \cos(\beta_{j,2}) \tag{3.32}$$

$$J_{m,12} = b_{j,2} \sin(\beta_{j,1}) \sin(\beta_{j,2}) \tag{3.33}$$

$$J_{m,13} = -b_{j,2} \sin(\beta_{j,1}) \cos(\beta_{j,3}) \tag{3.34}$$

$$J_{m,21} = 0 \tag{3.35}$$

$$J_{m,22} = b_{j,1} \cos(\beta_{j,2}) \tag{3.36}$$

$$J_{m,23} = b_{j,2} \sin(\beta_{j,3}) \tag{3.37}$$

$$J_{m,31} = -b_{j,2} \sin(\beta_{j,1}) \sin(\beta_{j,3}) - b_{j,1} \sin(\beta_{j,1}) \cos(\beta_{j,2}) \tag{3.38}$$

$$J_{m,32} = -b_{j,1} \sin(\beta_{j,2}) \cos(\beta_{j,1}) \tag{3.39}$$

$$J_{m,33} = b_{j,2} \cos(\beta_{j,1}) \cos(\beta_{j,3}) \tag{3.40}$$

The representation of the Simulink model with utilized subsystems is illustrated in Figure 3.12. The Quarc interface provides the Phantom block, indicated as “Touch-1” and “Touch-2” for both master devices, which is used to control the Geomagic Touch master devices. The virtual environment is created on the VR Sink block, denoted as “Virtual Environment”. Outputs of the Phantom blocks are used as input data of the VR Sink block after the calculations of the “Mapping & Piecewise Constant Curvature” subsystem. To inform the operator with haptic feedback, the Phantom blocks generate joint torques by the information obtained from “Forward Kinematics” and “Virtual Range Sensor” subsystems. The “Inverse Kinematics” subsystem generates the necessary information to actuate the light arm cooperatively with the camera arm.

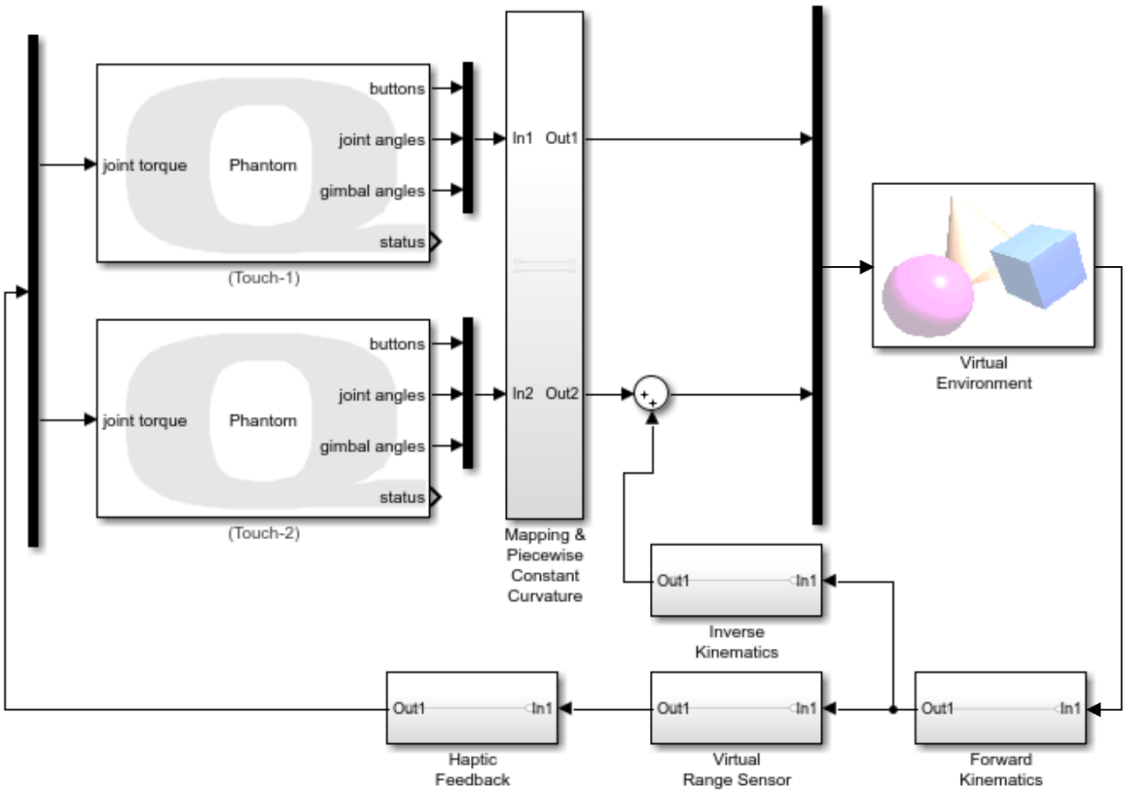

Figure 3.12 Representation of the Simulink environment.

CHAPTER 4

TELEPRESENCE AND PERFORMANCE EVALUATION TESTS AND RESULTS WITH POSITION-TO-POSITION MAPPING

The performance of the implemented control strategies and the validity of the proposed methods are investigated through a series of experiments. The efficiency and sufficiency of teleoperation and telepresence were analyzed with volunteer human test subjects. The optimized cognitive ergonomy and ease of use are researched based on user feedback acquired via teleoperation tests and questionnaires.

This section explains the methodology utilized and the evaluation of the results in terms of performance analysis. The performance of the designed teleoperation system is investigated via selected performance metrics such as task completion times and accuracy in positioning. The outcomes of the experiments and performed tests are given and discussed.

4.1. Cognitive Ergonomy

The user interface is designed considering the cognitive ergonomy for the operator. The complexity of multi-master multi-slave systems is taken into consideration to ease the work for the user. The cognitive ergonomy of the designed teleoperation system is investigated with two separate modes, as Mode 1 and Mode 2, to gain insight into how subjects interact with this system and evaluate the requirements to enhance their performances. The outcomes of the performed experiments are evaluated considering the ease of use, accuracy in positioning, and telepresence feeling passed to the user, and the results obtained through both modes are compared.

The teleoperation system consists of two master Geomagic Touch devices, denoted as Touch-1 and Touch-2, with four slave arms. Touch-1 controls the light and camera arm with Joints 1, 2, and 3, while Touch-2 controls the grasper and palpation arms with Joints 1, 2, and 3, and Gimbals 1, 2, and 3, as indicated in Figure 4.1.

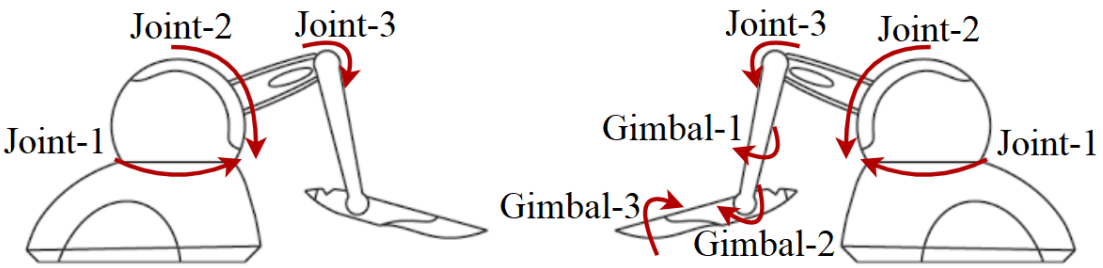

Figure 4.1 Geomagic Touch devices.

Figure 4.2 User guide of Modes 1 and 2.

A step-by-step user guide is prepared to present the operation logic designed for this study. The created user guide is also explained to subjects before and during the experiments. The proposed scheme of the user guide is shown in Figure 4.2. Color codes separate modes of operation as follows: red indicates Mode 1, blue indicates Mode 2, and black is valid for both modes.

4.2. Teleoperation Performance Tests with Modes 1 and 2

Performance evaluation tests are implemented to assess the proposed methods. Hence multi-master multi-slave systems strongly depend on the agility of the operator, and telepresence is associated with human perception; the tests are conducted with human subjects.

Ten participants took part in the experiment. Among them, nine out of ten subjects are male, while only one is female. The age distribution of the subjects is as follows; two subjects are between 18-24, and the rest are between 25-34. All subjects are mechanical engineers, five subjects are MSc students, while five are PhD students on topics related to mechanism, mechatronics, and robotics. All participants are right-handed and had no known disability. Since the performance of the operator is considered to be dependent on being accustomed to using haptic devices and video gaming experience, especially RPG and strategy games, subjects are questioned about their past experiences. Five out of ten subjects stated they had never used any haptic device; five had previous acquaintance with at least one type of haptic device. Five out of ten subjects stated they are not video game players, two play video games frequently, and three claimed themselves as experienced video gamers (Frazelle et al., 2016).

All subjects voluntarily participated in the tests and gave their written consent prior to the tests (see Appendix-A). The protocol was approved by the Scientific Research and Publication Ethics Board of Izmir Institute of Technology.

The experiments are conducted in two separate modes of teleoperation system. In each mode, subjects were evaluated by accuracy and the task completion time metrics. Before each test, users are given a limited amount of time to become accustomed to controlling the robot arms via Geomagic Touch devices. In the training phase, subjects are instructed to manipulate the robot arms, practice button usage for both arm and motion switch, and explore the workspace. During the training, subjects

are informed about the possible strategies for grasping and palping motions.

The acquired master joints' motion used for manipulating the slave segments differs for Modes 1 and 2 to compare the ease of use. In Mode 2, the operator does not receive haptic feedback, while the haptic feedback is enabled in Mode 1 to assess the effects on telepresence.

The simulation begins with the robot in its initial position as a straight arm with no bending or elongation. The user is instructed to first locate the object in the virtual environment with visual feedback through the perspective of the camera arm, then to visit each checkpoint using the grasper and palpation arms, respectively.

Ten checkpoints portrayed as circular targets on the virtual reality screen are defined before the test to regularize and automate the evaluation. These circular target locations are shown in Figure 4.3. The blue "+" signs in Figure 4.3 indicate the circular target positions. The red numbers located in the upper right of the signs are used for distributing the targets to user tests (i.e., 1, 5, 7, 8, 9 assigned to user 1 in Mode 1). Prior to tests, a randomized sequence of targets for each subject is determined.

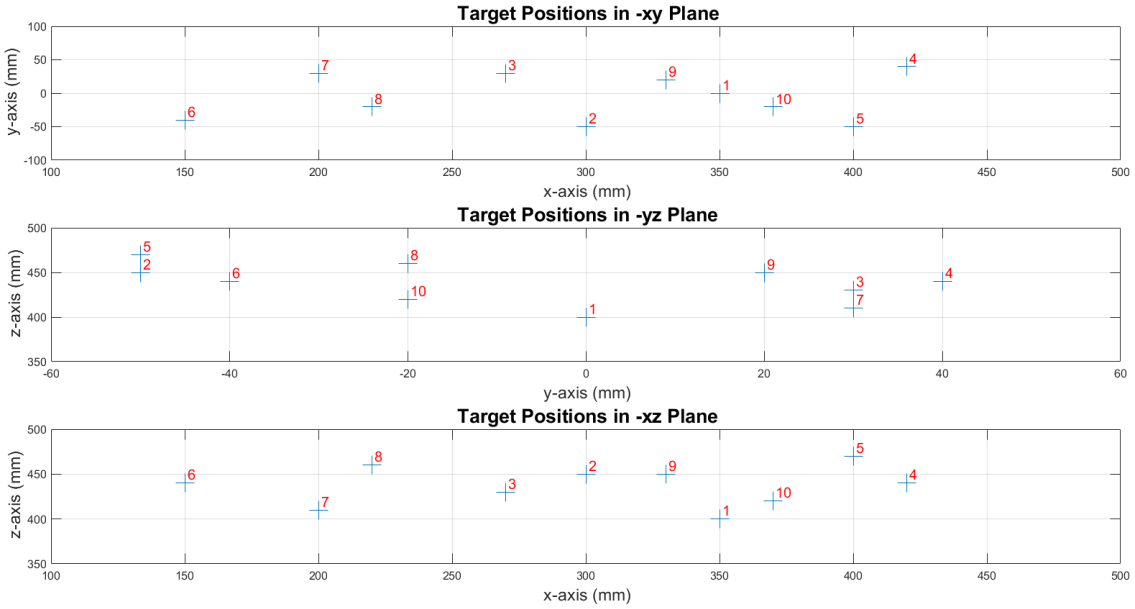

Figure 4.3 Target sequence representation in 2D planes.

The experiments aim to evaluate the performance of the teleoperation, considering task completion times and accuracy as performance metrics. In order to assess the ease of use and telepresence of the designed teleoperation system, a simulation test environment is generated in which the users are assigned tasks to reach

the targets and interact with these targets either by grasping or palping.

When the participants locate the circular target, either a cylindrical target appears if the grasper arm is used, or a rectangular prism target appears if the palpation arm is used. The target details are as follows:

i. Circular target: size 3 mm x 3 mm x 3mm. Denotes the designated location of the end-effector to grasp or palp the target.
ii. Cylindrical target: size 20 mm x 50 mm x 10 mm. Placed -25 mm on the x-axis, ±30 mm on the y-axis, and -120 mm on the z-axis away from the circular target.
iii. Rectangular prism target: size 20 mm x 20 mm x 2 mm. Placed +50 mm on the z-axis away from the circular target.

When the test subject decides that she/he has completed one task, the test conductor is informed by the test subject, and the test conductor manually initializes a new target. Each task consists of two phases as grasping and palping, carried out with the grasper arm and palpation arm, respectively. During the tests with each mode, there are five different target locations. Consequently, all subjects shall interact with ten circular targets overall to complete the 2-mode experiment. Each phase of each mode is executed sequentially without a break in the participant's control of the robot. All tests involve activities such as manipulating the arms, orienting the gripper for a proper grasp, and elongating towards the target.

In Figures 4.4, 4.5, 4.6, and 4.7, the scenario of the experiment is given step by step. However, the viewpoints on these figures are given as an example, and they are not provided to the operator during the experiments. Initially, as shown in Figure 4.4, the slave arms are in their initial conditions without any bending or elongation. Figure 4.5 shows a circular target that the operator should firstly locate in the environment with the camera arm and then approach with the grasper arm. The cylindrical target, as seen in Figure 4.6, appears after contact between the grasper arm and circular target is established, and the operator initiates the grasping motion of the arm by pressing on a button on the master system at this instant. The task continues with the palpation arm, and a similar procedure is followed. After the contact between the palpation arm and the circular target is established, the rectangular prism target appears (Figure 4.7), and the operator initiates the palping motion of the arm.

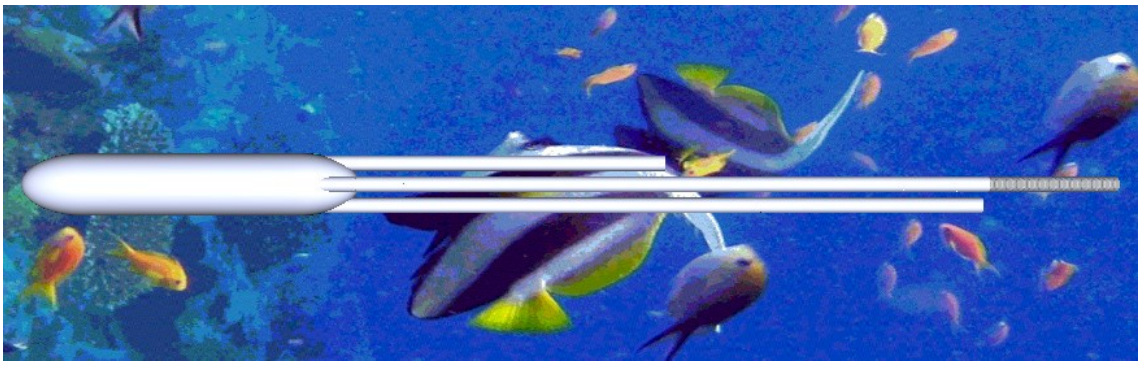

Figure 4.4 Initial condition of the robot arms.

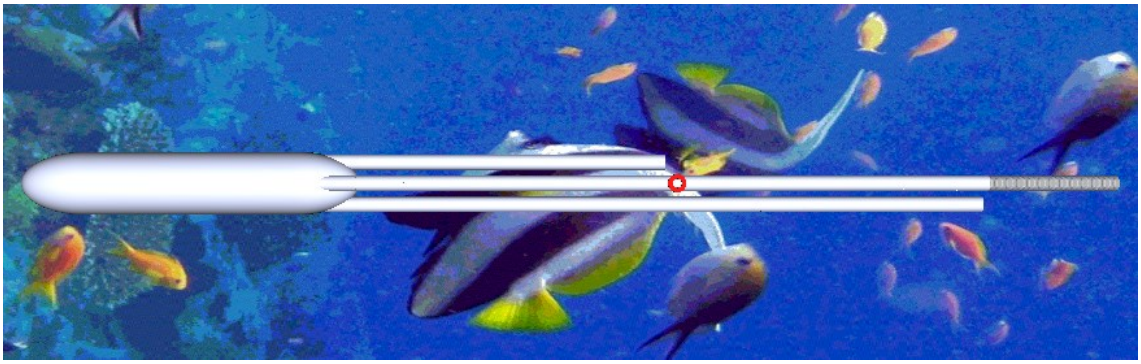

Figure 4.5 Circular target position on the environment.

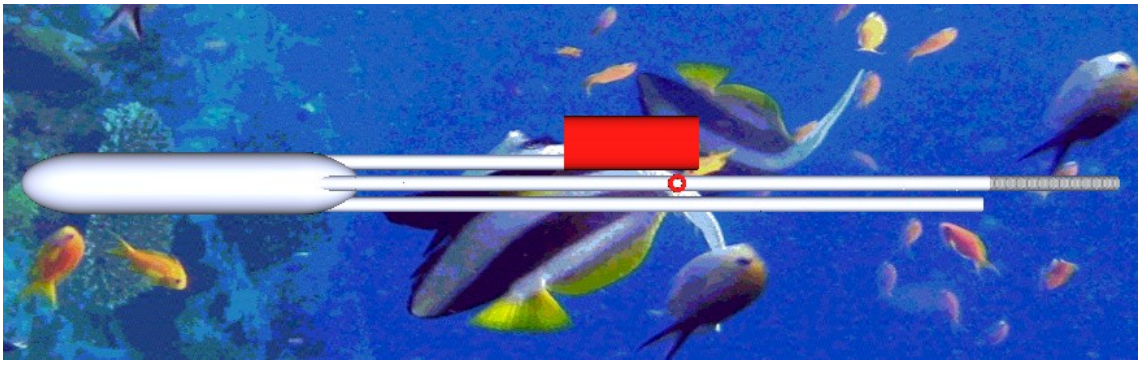

Figure 4.6 Task illustration of the grasper arm.

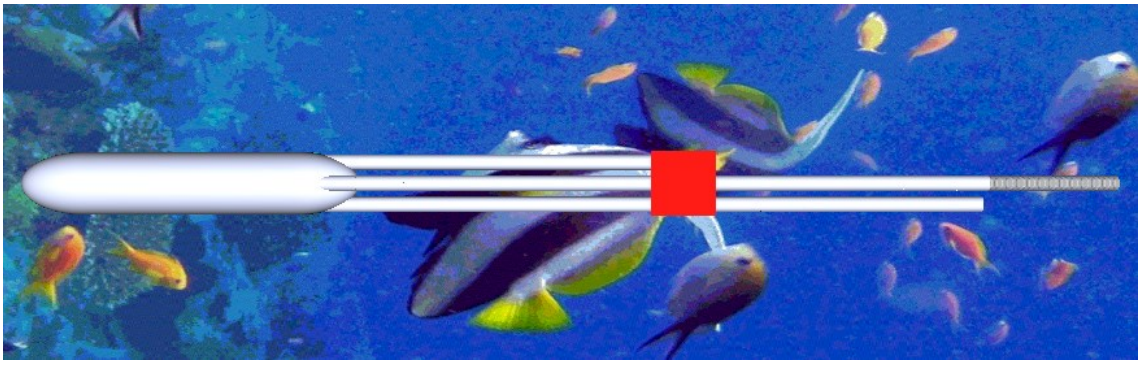

Figure 4.7 Task illustration of the palpation arm.

The first set of tests is Mode 1 of the teleoperation system in which haptic feedback is enabled, the stylus is used for adjusting the light condition with the option of locked camera position, and 2-segment robot arms are operated simultaneously. In the second set of tests with Mode 2, haptic feedback is disabled, buttons are used to adjust the light condition without the option of locked camera position, and 2-segment robot arms are operated with a switch as the first and second segments of the arms are driven respectively. In Mode 2, in order to manipulate the arm to reach the desired location, the first segment of the arm should be manipulated first to its desired shape, then the control should be switched to the second segment's manipulation, and then eventually switch back to the first segment if necessary.

The tests begin with the robot arms in their initial position. Subjects are requested to manipulate the camera arm to discover the first target. After the visual contact is established, subjects are informed to adjust the light until the perspective of the camera and light arm intersect to acquire a better view of the target (Figure 4.8). Then, subjects are asked to manipulate the grasper arm to the target position (Figure 4.9). Mode 1 provides haptic feedback when contact occurs between the arms and an obstacle, which simplifies the transition of the control from the manipulation of the arm to the end-effector grasping motion. The grasping task of the arm can be accurately performed if the end-effector of the arm remains within a range of ±15 mm from the target position and is executed right after the contact is perceived by the subject (Figure 4.10). Afterward, manipulation of the palpation arm is instructed to the subjects for the same target position to execute the palping motion (Figure 4.11), which can also be accurately performed if the range of ±15 mm from the target is not exceeded (Figure 4.12). These steps are repeated for five different targets in both modes, which adds up to ten tasks in overall.

Mode 2 does not have haptic feedback to evaluate the impact that haptic feedback has on precision of the teleoperation scenario. In Mode 2, the 2-segment robot arms and the light arm are also controlled in a different way than in Mode 1 to examine personal preferences on ease of use.

During the experiments, the subjects are informed by the test conductor on the currently controlled arm and the motion type of that arm so that the test subject can track the progress.

Figure 4.8 Visual contact with the target.

Figure 4.9 Manipulation of the grasper arm to the target position.

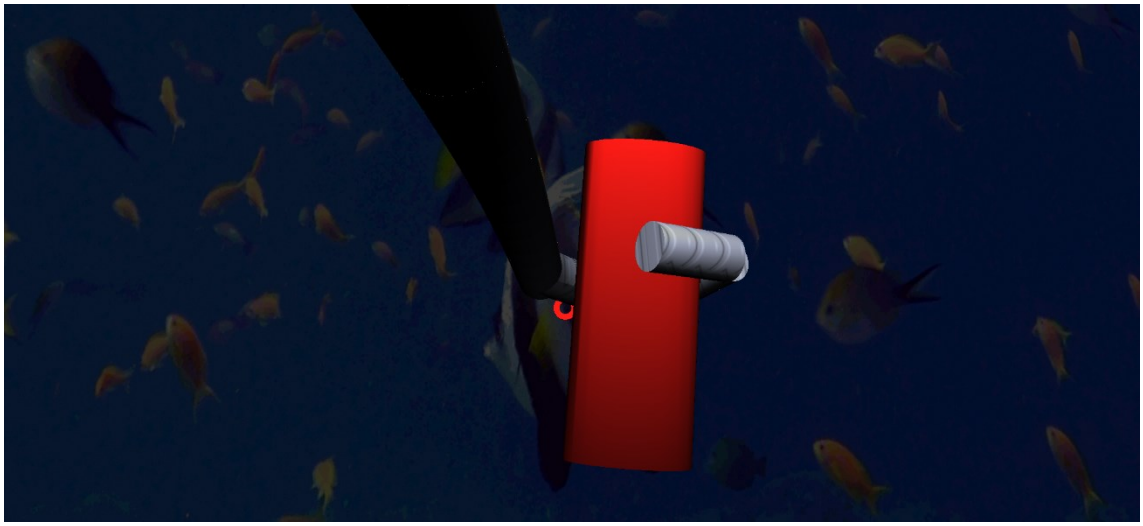

Figure 4.10 Grasping motion of the grasper arm.

Figure 4.11 Manipulation of the palpation arm to the target position.

Figure 4.12 Palping motion of the palpation arm.

Finally, after the simulation is concluded for each user, the subjects are asked to fill in a questionnaire (see Appendix-A Table-2) to evaluate their preferences and to perceive their experience. The scores are graded from 1 to 5 as 1 indicates strongly disagree, and 5 strongly agree for the first and second part of the questionnaire, which investigates the telepresence felt by the operator. In the third part of the questionnaire, the evaluation is based on the preference of modes and haptic feedback, task completion sense, and convenience of use. If the subject tends to prefer Mode 1, the given score should be on the bias of 5, and if the subject prefers Mode 2, the given score should be on the bias of 1.

4.3. Test Results with Modes 1 and 2

The outcomes of the subject test results are assessed in terms of task completion times and accuracy. Table 4.1 shows the overall task completion times. Longer task completion duration is observed on Mode 2 due to the decreased sense of task completion without haptic feedback, as expected.

Table 4.1 Task completion times.

Overall Time													
Test # / Subject #	Mode 1					Mode 2					Total		
	1	2	3	4	5	6	7	8	9	10	Mode1 Total	Mode2 Total	Total
1	242	209	112	174	201	247	174	252	71.5	94	938	838	1776
2	93.7	72.2	41.8	75.5	53.4	188	68.3	74.8	69.7	66.4	337	467	803
3	136	288	193	146	180	412	191	188	223	257	943	1272	2215
4	214	215	140	83.9	132	208	271	172	170	168	785	988	1773
5	275	121	124	119	113	227	73	156	75.4	157	752	689	1441
6	136	140	225	126	217	184	323	239	231	200	843	1178	2021
7	147	63	158	84	82.3	260	180	148	120	77.2	535	785	1320
8	224	170	270	184	95.3	395	195	147	377	229	1338	1343	2286
9	224	157	176	85.8	48.6	170	169	102	125	314	692	879	1571
10	80.6	67.5	41.8	66.8	52.9	112	96.1	51.2	137	76.6	310	473	782
mean	177	150	148	115	117	240	174	153	160	164	708	891	1599
std. Dev.	63.2	69.7	69.4	40	59.8	90.8	77.4	61.7	91.1	81.5	302	402	705

The presented task completion durations are used to form each subject's learning curve, shown in Figures 4.13 and 4.14, for Mode 1 and Mode 2, respectively. The objective of the repeated tests is to observe the learning curve. However, five repeated tests for each mode seem not to be sufficient for this observation. The expected result of the learning curve can be seen for subjects 4, 5, 7, 8, and 9 for Mode 1 and 2, 4, and 7 for Mode 2. However, in overall, the initial task completion time is more than the final test for most of the participants. This indicates that with practice, the test subjects could control the slave arms in a faster way.

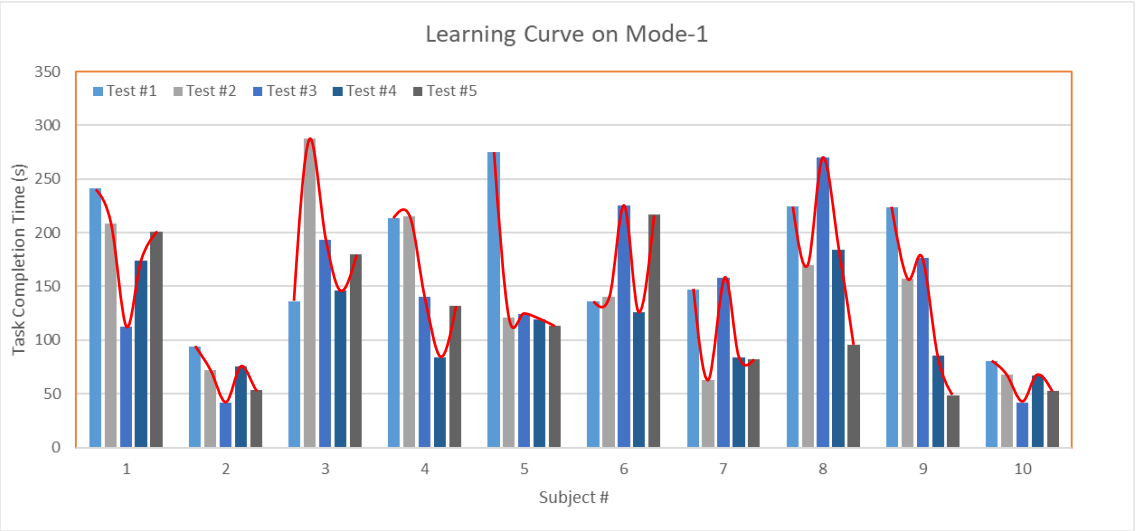

Figure 4.13 Learning curve of subjects on Mode 1.

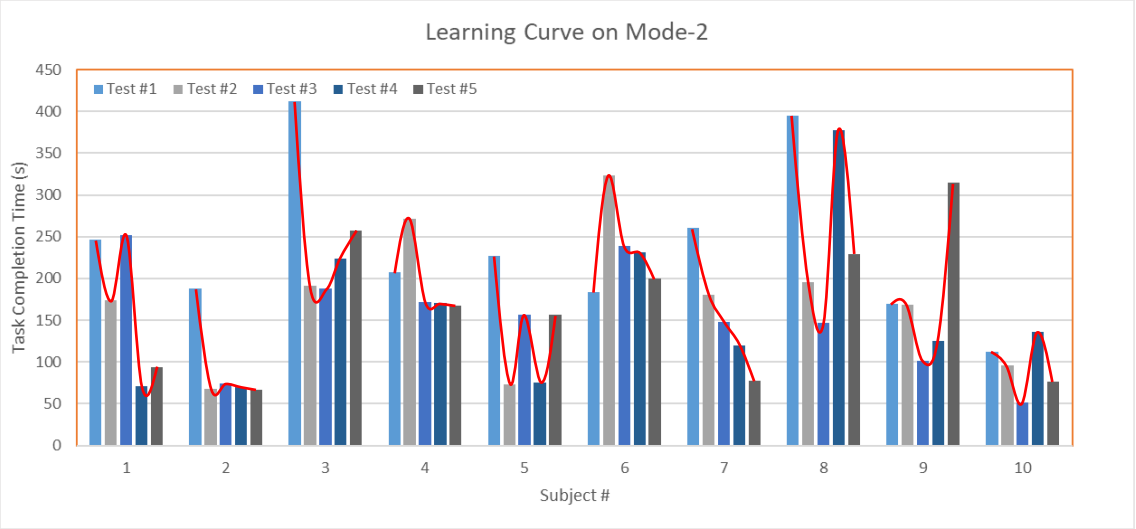

Figure 4.14 Learning curve of subjects on Mode 2.

The average total task completion time is 1599 seconds. The second and tenth subjects completed the tests in under 1000 seconds; however, the third and eighth subjects completed the tests in over 2200 seconds. The reason for this difference is the habituation level of the subjects with the Geomagic haptic devices. Although subject number 2 with the second-best result stated that she/he had never used the device before, he/she stated himself as a gamer which explains his/her agility in completing the tasks.

To understand the performance of the participants beyond the evaluation metrics, the commands to manipulate the slave for each user are evaluated.

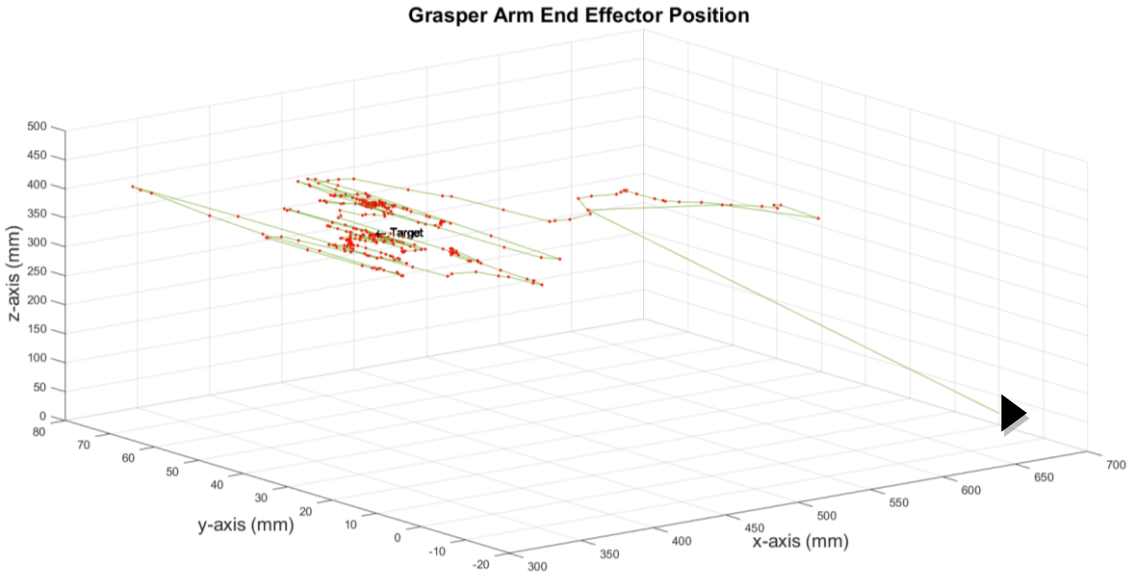

Figure 4.15 Grasper arm trajectory on Mode 1.

The paths followed by the operators, who have middling performance in terms of accuracy on target contact positions, are shown in Figures 4.15, 4,16, 4.17, and 4.18 for the grasper and palpation arms with Mode 1 and Mode 2, respectively. End-effector positions are illustrated from the initial positions (▶) to the first point of contact with the targets. The step sizes are indicated by the small red markers; as the range between markers widens, so does the end-effector's velocity.

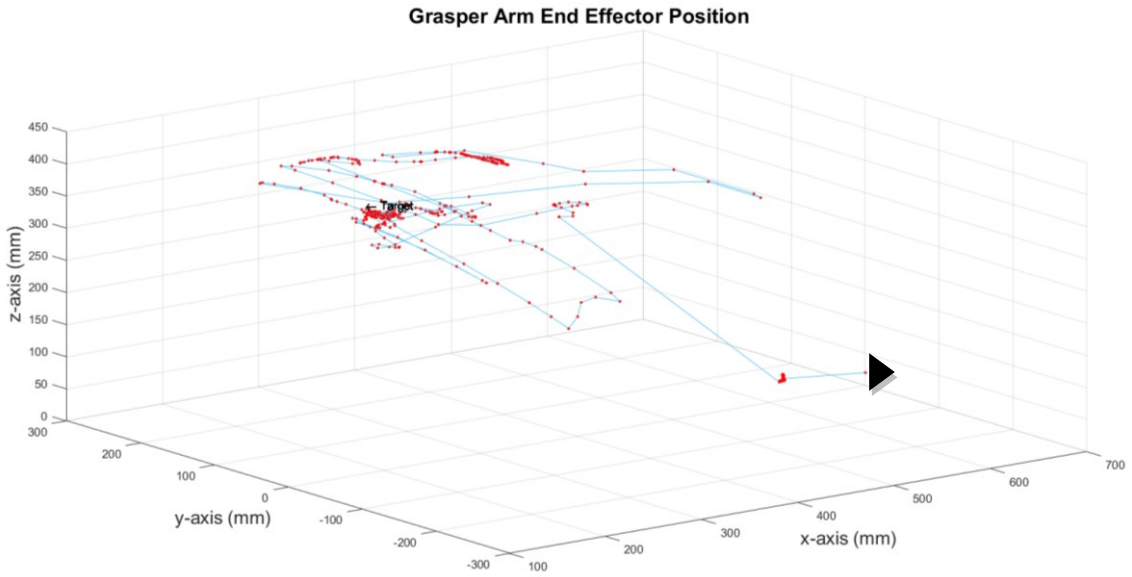

Figure 4.16 Grasper arm trajectory on Mode 2.

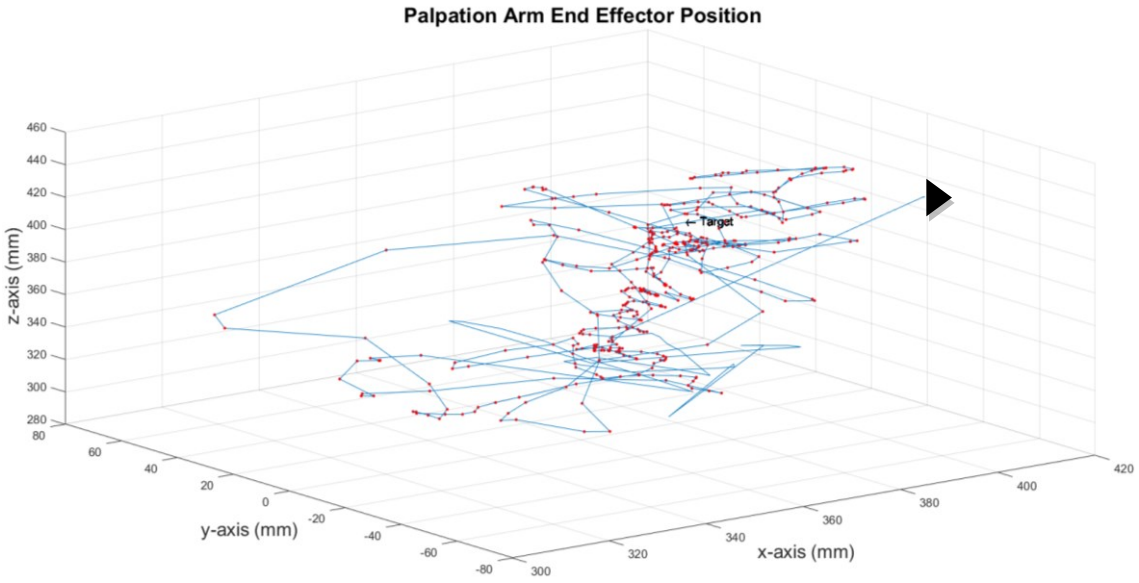

Figure 4.17 Palpation arm trajectory on Mode 1.

The straight lines between two markers on the bottom right corners of Figures 4.15, 4.16, and 4.18 and the upper right corner of Figure 4.17 represent the rapid relocation of the end-effector from its initial position to the first position command. At the beginning of the test and the next step after the switch between arms, modes, or segments, if the master device is not in the exact configuration that maps to the current configuration of the controlled arm or segment, the controlled sections of the arms jerk to the configuration currently represented by the master device.

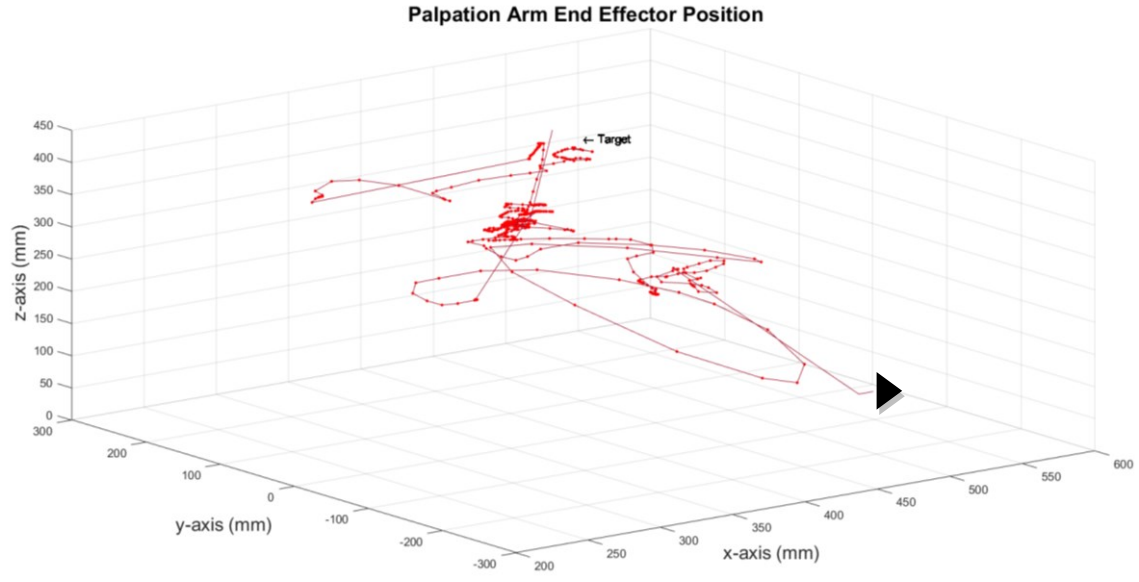

Figure 4.18 Palpation arm trajectory on Mode 2.

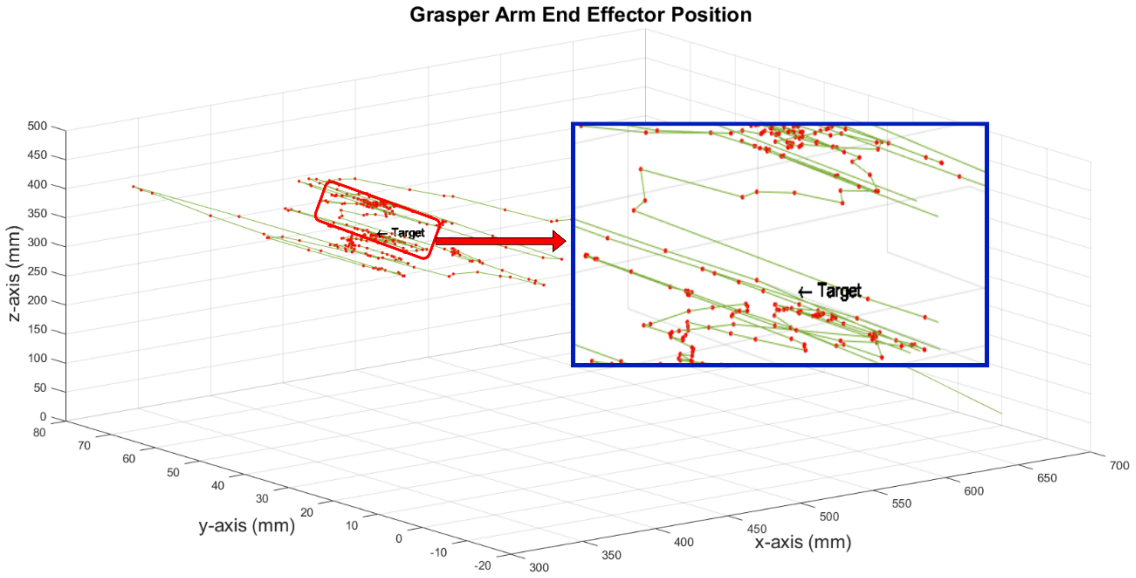

Figure 4.19 Grasper arm trajectory on Mode 1.

Figure 4.19 shows the end-effector position of the grasper arm for a middling subject working on Mode 1. The subject tends to begin the process again after a close call on the target. On subject performance analysis, this results as a two-fold increase in task completion time. The oscillating horizontal movements are performed by most of the subjects to locate the arm on the camera viewpoint. This tendency leads to sudden movements habit in subjects.

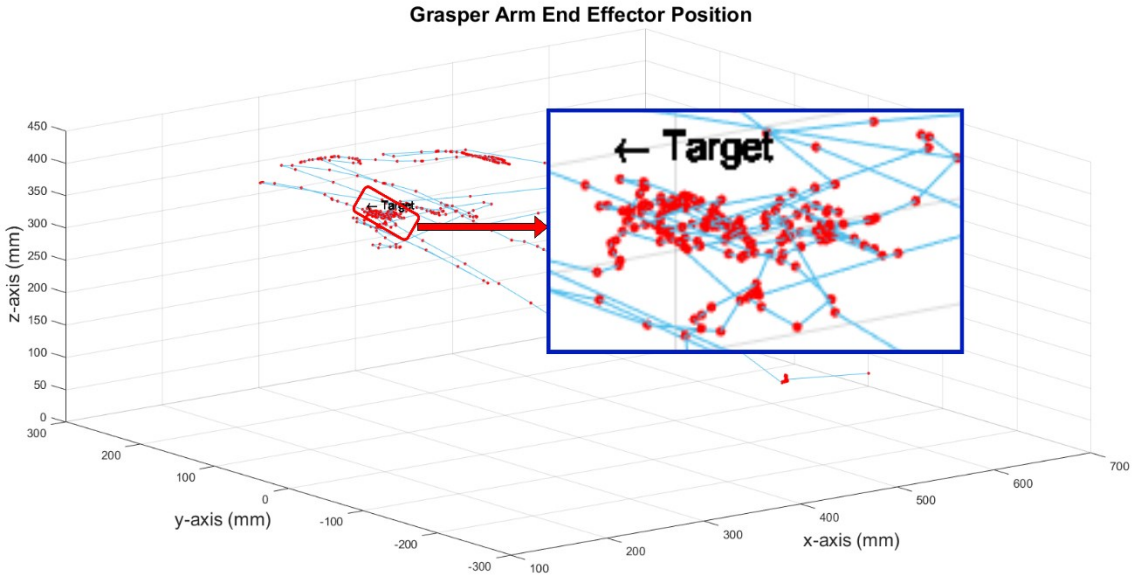

Figure 4.20 Grasper arm trajectory on Mode 2.

Figure 4.20 shows the end-effector position of the grasper arm for the middling subject on Mode 2. The subject tends to take a slight approach to the target with small step sizes since the test subject does not receive haptic feedback on this mode.

The manipulation of the palpation arm is identical to the grasper arm but differs in the palping motion. Once the subject is informed by the force feedback about the established contact, the palping motion is performed using Gimbal-2 on Geomagic Touch to palp the rectangular prism positioned ahead of the arm. Figure 4.21 illustrates the end-effector position of the palpation arm for a middling subject on Mode 1. The marked area presents the mislocating the target in the first trial and the revisiting of the target location.

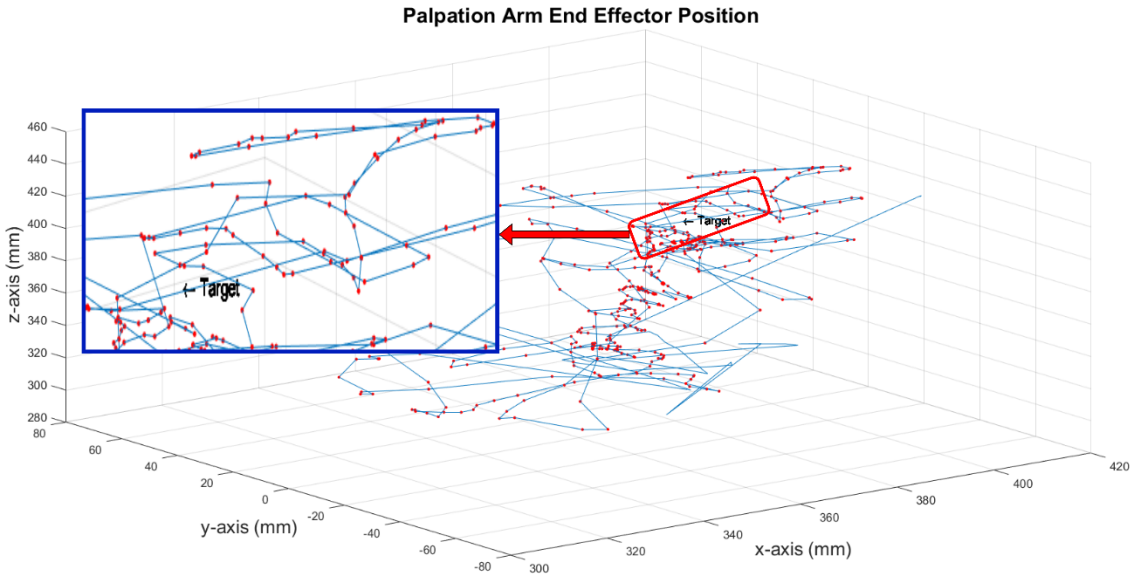

Figure 4.21 Palpation arm trajectory on Mode 1.

Figure 4.22 shows the end-effector position of the palpation arm for a middling subject on Mode 2. The highlighted area denotes a false contact prediction due to the lack of depth perception resulting in an elevated task completion duration and repeated trials. The second trial appears in the upper left corner with a broader movement. The rapid movement on the middle right side occurred due to the trial of locating the palpation arm on the camera viewpoint.

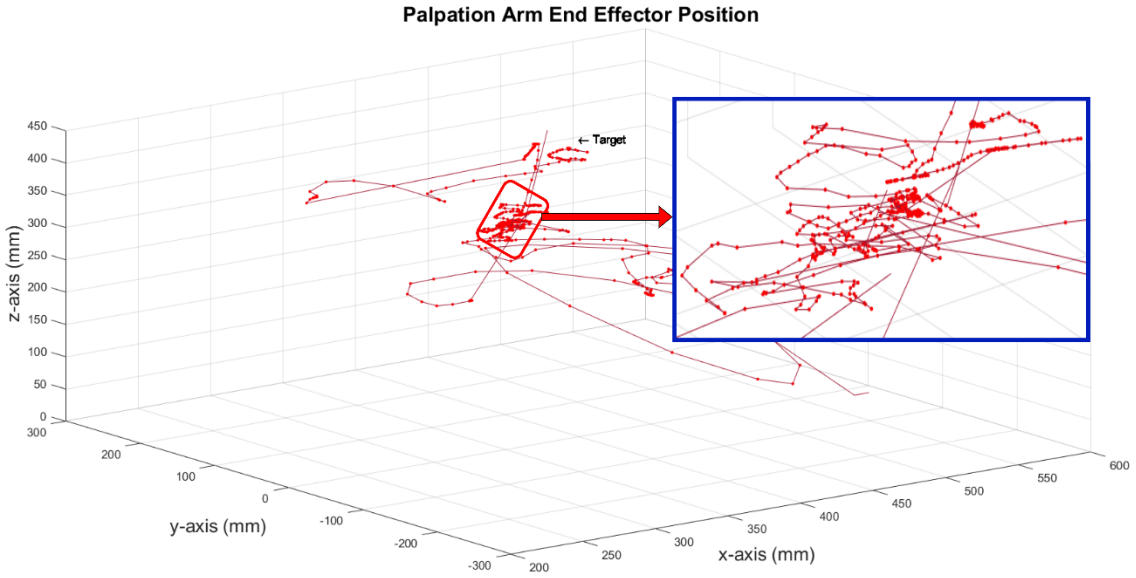

Figure 4.22 Palpation arm trajectory on Mode 2.

The mean error on the target contact positions is related to the accuracy, the freedom from error on contact positions with targets, and gives an estimation about how difficult it was to manipulate to and through the checkpoint. The end-effector positions on targets prior to the grasping and palping motions of the arms are given (see Appendix-B) for the grasper arm and palpation arm, respectively. Green markers represent Mode 1, while red markers represent Mode 2. The success and performance criteria are defined as residing in the threshold of ±15 millimeters in each axis where subjects begin to experience haptic feedback on every target in Mode 1. Figures 4.23 and 4.24 introduce the end-effector positions on contact points for targets 5 and 7 and grasper and palpation arms, respectively, to give an insight into the evaluation of accuracy.

Target 5 for both the grasper and palpation arm denotes that the subjects tend to approach the target from the same direction and show the tendency of similar errors in each plane. This target has more condensed recorded end-effector positions on contact points than others. A number of subjects abnormally vary from the others and reduce precision, the closeness and recursiveness of results to each other, in targets 3 and 7 for the grasper arm and 6 and 8 for the palpation arm with spread-out positions. Similar positioning errors on green markers are considered to depend on the excessive haptic feedback in Mode 1 that leads to challenging navigation. The difference in positioning errors reveals that the accuracy of the model depends on the skills of the operator.

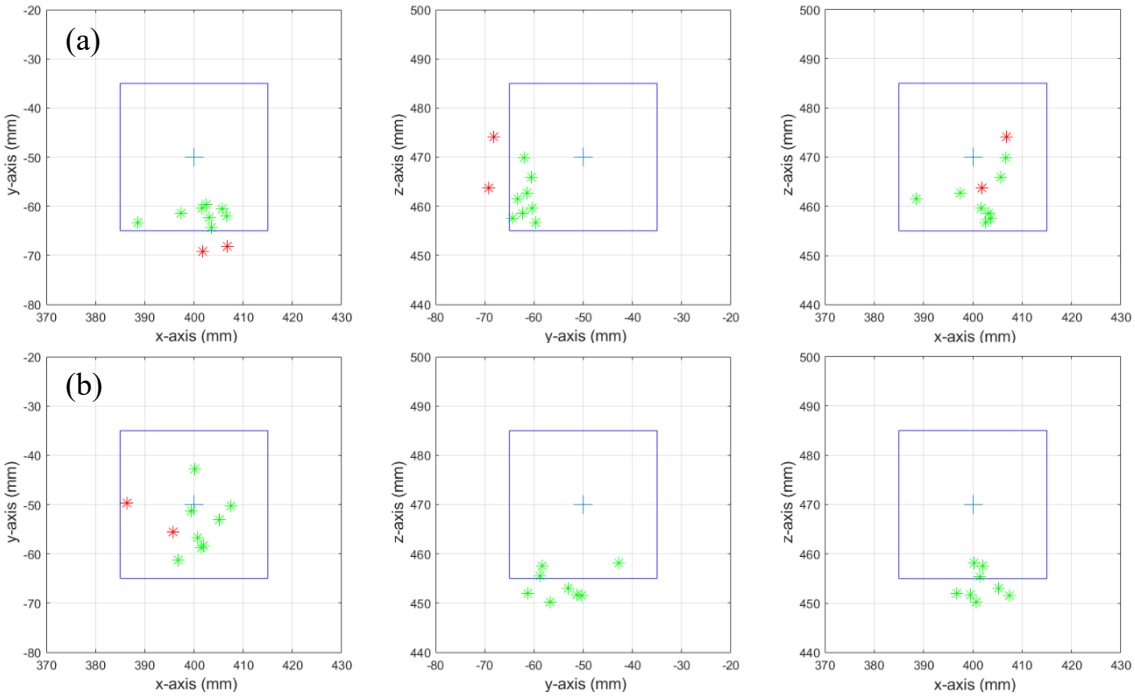

Figure 4.23 End-effector positions on target #5 (a) Grasper arm (b) Palpation arm.

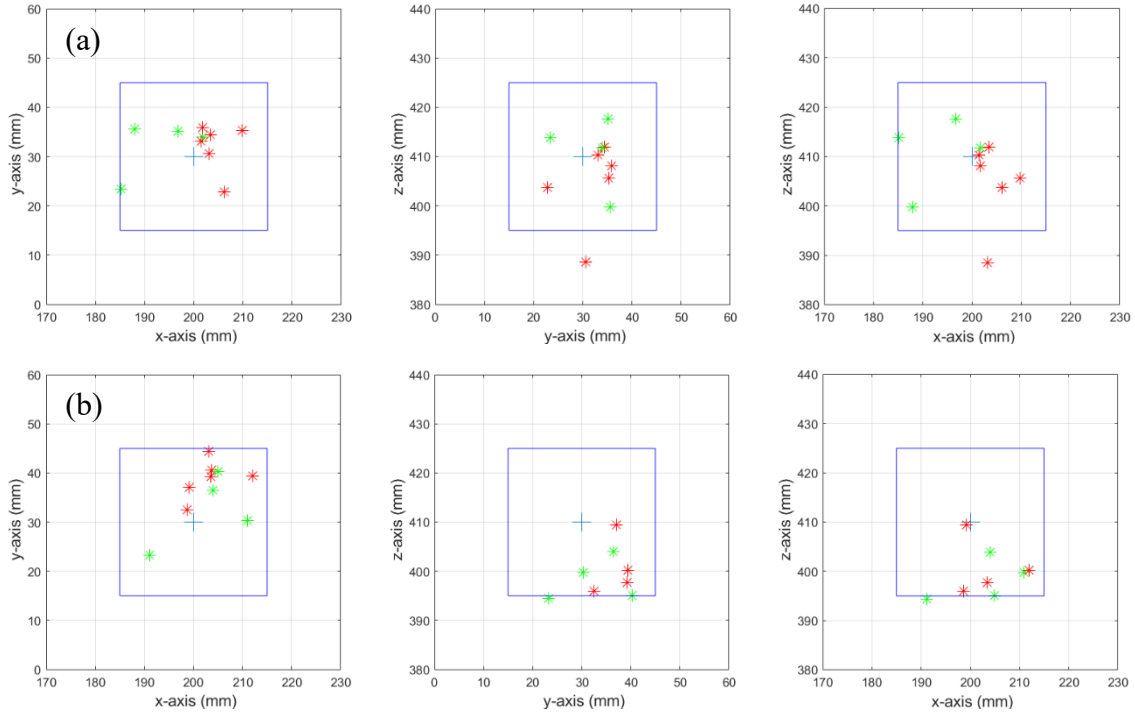

Figure 4.24 End-effector positions on target #7 (a) Grasper arm (b) Palpation arm.

Enhanced telepresence with real-time haptic force feedback improved the accuracy on contact status. An example of such a case is target 7 with the grasper and palpation arm, which resulted in better accuracy with Mode 1 (green stars) as compared to the results with Mode 2 (red stars). Among the results with other targets, target seven results are the most accurate ones.

Table 4.2 Success rate on target positions in Mode 1 and Mode 2.

Accuracy on Target Contact												
	Grasper				**Palpation**				**Total Success Rate**			
	Successful		Unsuccessful		Successful		Unsuccessful		**Grasper**		**Palpation**	
Target#	M.#1	M.#2	M.#1	M.#2	M.#1	M.#2	M.#1	M.#2	M.#1	M.#2	M.#1	M.#2
#1	4	4	0	2	2	1	2	5	100%	67%	50%	17%
#2	6	2	0	2	4	1	2	3	100%	50%	67%	25%
#3	6	4	0	0	3	2	3	2	100%	100%	50%	50%
#4	6	3	0	1	1	1	5	3	100%	75%	17%	25%
#5	8	0	0	2	3	0	5	2	100%	0%	38%	0%
#6	4	4	1	1	3	0	2	5	80%	80%	60%	0%
#7	4	5	0	1	3	4	1	2	100%	83%	75%	67%
#8	3	6	0	1	0	3	3	4	100%	86%	0%	43%
#9	5	5	0	0	4	1	1	4	100%	100%	80%	20%
#10	2	3	1	4	3	1	0	6	67%	43%	100%	14%

The success rates with each arm and for each target using both modes are given in Table 4.2. The failed tests are those that stayed outside of the ±15 mm threshold in at least one of the x, y, and z axes. The overall failure rate recorded throughout the experiments is 38%, with 76 trials unsuccessful versus 124 successful performances. Since only Mode 1 has haptic feedback, the failure rate differs significantly amongst the two modes. The failure rate is calculated to be 26,53% for Mode 1 and 49,02% for Mode 2. The failure rate of the grasper and palpation arms is expected to be similar since they are assigned with similar tasks. However, the failure rate observed with the grasper arm is 16%, while it is 60% with the palpation arm. The reason for this disparity is considered to be the subjects' habit of taking different paths with different arms. Despite being instructed to contact the circular target before moving on to the palping phase, the participants tend to activate the rectangular prism before they reach the circular target and thus, cannot achieve the palping operation. When only Mode 1 results of the grasper arm are considered, the failure rate drops to 4,17%, indicating that the task was challenging but not overly demanding.

Tables 4.3 and 4.4 indicate the positional errors in the x, y, and z axes for each subject and target. When the distance between the end-effector and target positions is below ±15 millimeters on each axis, it is considered an accurate positioning. The mean values of these positioning errors are illustrated in Figures 4.25 and 4.26 for the grasper and palpation arm, respectively. The bar graphs display the mean of the overall error, while the lines indicate the standard deviation of error. The standard deviation of the error evaluation reveals the difference between subjects on that specific target, as well as the complexity of the task.

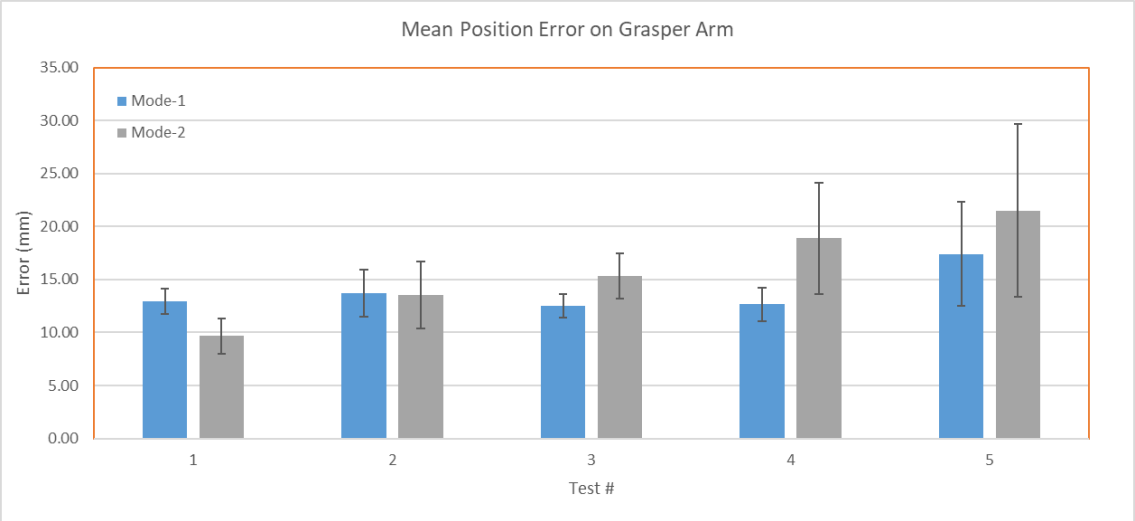

Figure 4.25 Mean positioning error on reaching the circular target for grasper arm.

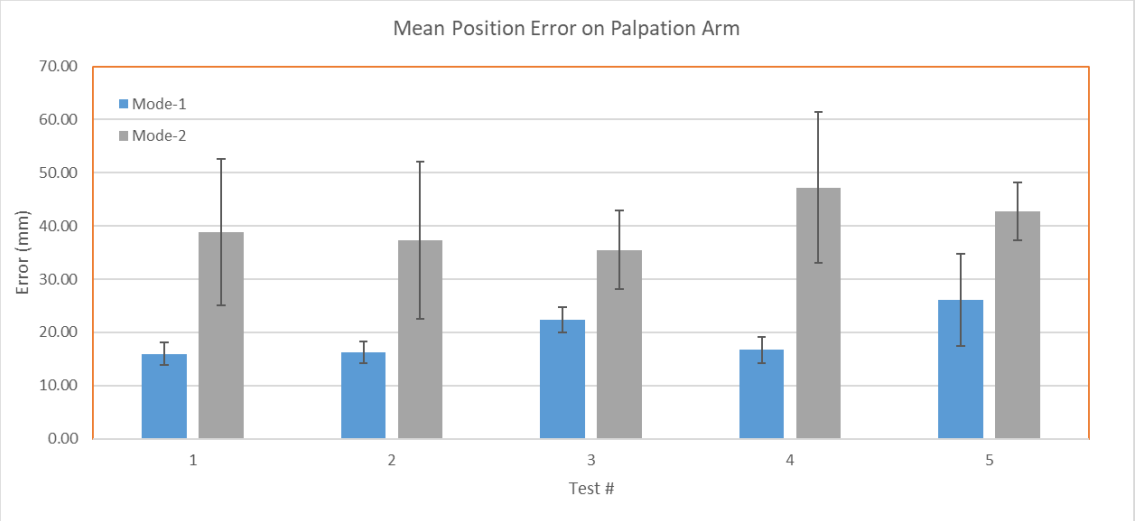

Figure 4.26 Mean positioning error on reaching the circular target for palpation arm.

Table 4.3 Overall positioning errors with the grasper arm.

Overall Error in -x, -y, -z Directions															
	Mode 1														
	Test-1			Test-2			Test-3			Test-4			Test-5		
S.#	Δx	Δy	Δz	Δx	Δy	Δz	Δx	Δy	Δz	Δx	Δy	Δz	Δx	Δy	Δz
#1	4.59	6.28	-10.18	1.74	3.93	1.75	5.68	-3.85	11.33	3.53	-14.39	-12.47	6.53	-12.78	-0.60
#2	-3.26	5.11	7.66	-0.84	-12.53	-13.45	7.38	-8.35	-8.33	0.96	-14.23	-3.57	-3.12	1.60	-7.98
#3	3.24	-2.02	-10.97	5.89	-1.98	-5.03	4.80	-0.39	-1.60	6.53	3.96	2.49	6.66	-11.99	-0.18
#4	7.84	5.50	7.13	8.09	-2.32	-0.22	5.00	-6.55	-9.57	3.29	3.99	-4.19	5.68	-10.60	-4.16
#5	2.54	-9.74	-13.34	3.13	-10.52	-11.26	2.16	6.45	-7.73	2.06	7.13	-4.10	-1.05	-1.20	-7.85
#6	-0.13	4.92	-0.80	0.22	-8.67	-6.83	10.80	-13.82	-2.32	1.16	2.77	-9.32	-11.47	-13.40	-8.53
#7	8.34	3.16	-13.57	0.92	9.47	-11.89	-4.29	-11.61	-2.39	-3.33	-12.54	-9.86	-14.86	-6.54	3.74
#8	-0.99	-8.58	-11.37	-1.71	-1.28	-10.88	5.41	0.32	-11.31	1.65	-10.36	-10.45	58.55	-15.01	-1.42
#9	-2.60	-11.41	-7.28	2.09	-12.80	6.47	-5.15	6.29	6.75	-14.95	-4.91	-12.59	1.76	-5.68	6.99
#10	3.14	-12.38	-11.44	29.67	131.94	-3.05	-12.03	5.63	-10.30	-5.11	3.34	-5.43	0.05	6.82	-8.12
	Mode 2														
	Test-6			Test-7			Test-8			Test-9			Test-10		
S.#	Δx	Δy	Δz	Δx	Δy	Δz	Δx	Δy	Δz	Δx	Δy	Δz	Δx	Δy	Δz
#1	2.42	5.72	2.04	6.68	6.26	-1.13	6.50	-6.10	-16.19	25.88	-11.02	59.20	4.10	-5.07	-7.91
#2	-2.82	1.22	-11.22	-4.06	11.07	-15.08	0.79	2.19	-3.88	1.82	-19.27	-6.33	-4.39	-3.41	-18.08
#3	5.49	-8.05	-3.04	6.46	-5.30	-0.26	6.36	5.81	-2.75	-2.39	-10.21	-3.16	3.38	4.39	1.89
#4	1.44	3.10	0.35	-2.10	1.82	-17.70	1.71	-12.23	-10.93	2.67	11.66	-0.50	1.62	-8.90	-1.17
#5	4.14	-7.71	5.74	1.70	3.31	-1.36	1.02	-5.54	-8.26	9.77	5.21	-4.35	3.63	-12.60	-1.76
#6	1.72	5.83	-1.94	-1.23	-2.06	-37.07	-0.45	-8.99	-25.42	3.84	11.93	7.11	24.55	-89.92	-7.98
#7	3.06	-7.29	-10.27	3.04	2.15	-6.46	6.77	-18.24	4.12	5.71	-8.09	-10.01	6.41	-4.55	6.18
#8	-2.76	-4.27	-7.30	10.08	12.42	-10.24	1.57	-5.46	-13.68	3.80	-8.11	-13.94	3.13	0.63	-21.47
#9	4.31	0.52	-21.35	3.14	1.03	-4.78	3.24	-12.62	-17.07	6.12	-7.17	-6.32	2.29	-13.69	-8.00
#10	3.18	-2.61	-1.79	3.32	-6.32	-1.51	6.39	4.44	8.71	3.93	-9.96	-4.94	1.78	-15.86	-3.33

The mean positioning error is relatively less in Mode 1 as expected, owing to the increased telepresence due to haptic feedback. Subject 10 produced a result on Test-2 that is considered as an outlier in the analysis of the results, and this result is not used in creating Figure 4.25. Considering the mean positioning errors for both arms and modes, it is deducted that enhanced telepresence with haptic feedback improves the performance significantly.

Table 4.4 Overall positioning error with the palpation arm.

Overall Error in -x, -y, -z Directions															
	Mode 1														
	Test-1			Test-2			Test-3			Test-4			Test-5		
S.#	Δx	Δy	Δz	Δx	Δy	Δz	Δx	Δy	Δz	Δx	Δy	Δz	Δx	Δy	Δz
#1	-0.51	3.39	-30.90	3.99	6.46	-6.08	-3.87	5.10	-22.71	-0.57	-1.35	-18.36	3.90	-11.55	-13.45
#2	10.96	0.27	-10.28	5.13	-9.72	-20.56	9.36	2.63	-37.58	17.73	-3.47	-28.34	3.39	5.25	-12.74
#3	2.47	1.94	-9.42	5.97	-6.50	-3.43	8.35	9.28	-9.41	6.59	0.41	-4.99	1.92	-8.42	-12.43
#4	4.44	6.03	-9.17	9.64	-2.33	-20.07	10.50	-5.03	-11.54	1.77	2.55	-4.96	1.46	-8.74	-14.57
#5	0.21	7.14	-11.82	4.05	-7.62	-10.83	0.93	6.27	-16.84	4.00	7.99	-12.56	-1.60	7.52	-16.43
#6	4.66	2.66	-8.65	-14.49	-17.05	-12.78	5.20	-7.42	-10.23	0.65	5.32	-11.92	-3.27	-11.24	-18.02
#7	-4.19	10.15	-15.26	5.38	7.09	-16.60	9.74	-12.43	-18.73	-10.64	1.17	-10.57	-8.92	-6.80	-15.60
#8	7.21	-2.80	-6.15	0.44	-6.18	3.70	8.46	10.32	-19.97	7.42	-0.34	-18.44	81.05	19.71	-62.16
#9	0.72	-6.77	-19.80	0.12	-9.76	-11.39	-3.60	9.62	-27.86	-10.04	7.83	-16.97	1.78	-5.70	-12.14
#10	5.12	-3.10	-16.95	7.49	-4.53	-13.85	4.93	10.33	-14.94	2.27	-4.07	-15.45	5.56	7.89	-17.80
	Mode 2														
	Test-6			Test-7			Test-8			Test-9			Test-10		
S.#	Δx	Δy	Δz	Δx	Δy	Δz	Δx	Δy	Δz	Δx	Δy	Δz	Δx	Δy	Δz
#1	-0.54	10.27	-18.40	5.63	8.80	-0.60	14.86	3.28	-46.29	-3.45	0.33	-26.44	6.01	0.99	-63.05
#2	-6.76	6.55	-36.50	-3.39	11.47	-15.88	1.23	5.37	-14.46	-13.61	0.36	-49.13	-5.98	-2.11	-31.81
#3	2.48	-1.59	-3.79	3.17	-1.21	-10.26	4.40	0.98	-15.51	-0.29	4.84	-34.95	3.62	10.53	-37.89
#4	-0.82	7.02	-0.55	-0.02	6.33	-1.76	2.86	-15.38	4.46	-7.10	14.01	-14.00	5.28	4.85	34.68
#5	2.85	-2.87	-2.51	-35.80	-53.07	-148.70	0.08	0.52	-17.65	3.45	9.21	-12.32	13.80	11.09	-62.84
#6	-1.35	2.51	-14.12	-2.95	4.29	-26.40	-11.24	2.09	-76.90	-34.22	-0.38	-86.24	-12.86	-7.77	-39.21
#7	26.91	9.28	-115.90	-1.12	5.11	-42.57	-4.29	-5.52	-33.84	10.48	7.65	-35.97	-2.71	8.23	-50.71
#8	-4.37	4.62	-15.67	-5.30	5.92	-18.36	-13.18	8.44	-66.78	-0.36	12.14	-155.77	3.06	14.41	-40.46
#9	13.55	10.99	-112.63	-3.10	5.08	-59.48	-9.74	1.05	-40.44	11.98	9.32	-9.79	15.57	6.38	-46.21
#10	-5.77	2.31	-47.85	3.78	8.69	-10.52	6.35	10.83	-13.16	0.56	0.40	-17.10	2.98	-4.59	-2.06

4.4. Test Subjects' Questionnaire Results with Modes 1 and 2

Tests are concluded with the questionnaire that was presented to all the test subjects after the simulation. All terminology is explained to the participants to avoid any possible misunderstandings. The result of the questionnaire is presented in Table 4.5.

Table 4.5 User questionnaire results.

1st part of the questionnaire										
Questions \ Subjects	1	2	3	4	5	6	7	8	9	10
1	2	4	4	4	5	3	2	5	5	3
2	3	3	2	4	5	5	3	5	5	1
3	2	2	1	3	5	3	2	4	5	1
4	3	2	2	3	5	4	2	3	5	2
5	2	2	4	5	4	5	1	3	5	2
2nd part of the questionnaire										
Questions \ Subjects	1	2	3	4	5	6	7	8	9	10
6	1	4	2	4	1	3	1	5	5	1
7	2	3	2	4	1	5	2	4	5	1
8	1	1	3	3	2	5	1	3	5	1
9	2	1	3	3	1	5	1	3	4	1
10	1	1	3	5	1	5	1	3	5	1
3rd part of the questionnaire										
Questions \ Subjects	1	2	3	4	5	6	7	8	9	10
11	5	4	5	2	5	5	5	5	5	4
12	5	5	5	2	5	5	5	5	5	5
13	5	4	4	2	5	5	5	5	5	5
14	3	5	4	5	5	4	5	5	5	5
15	5	5	3	5	5	2	5	5	5	5
16	3	5	5	1	4	5	4	5	5	5
17	5	4	4	1	5	3	4	5	5	5
18	5	5	5	2	5	5	5	5	5	5
19	5	4	5	5	5	4	5	2	5	5
20	5	5	2	1	4	5	4	3	5	4

In terms of telepresence, the first and second parts of the questionnaire are for comparing telepresence with Mode 1 (first part) and Mode 2 (second part). 8 out of 10 subjects preferred Mode 1; one subject indicated that Mode 2 provides better telepresence and one subject stated there is no difference between the modes in terms of telepresence. However, overall, the telepresence level on both modes is found to be below average by 5 out of 10 subjects.

The third part of the questionnaire investigates user preferences between the two modes in terms of task completion, haptic feedback, and convenience of use. 9 out of 10 subjects believe that the sense of task completion, sense of safety, and telepresence when contact occurs are better in Mode 1.

9 out of 10 subjects stated that initially, it was easier to control 2-segment arms with Mode 1. In contrast, one subject stated that there was no difference, and Mode 1 becomes easier to manage after a certain number of repetitions. 8 out of 10 subjects chose Mode 1 for the ease of use of 2-segment robot arms after a certain number of repetitions, while one subject selected Mode 2 and the other stated that there was no difference.

8 out of 10 subjects indicated that it was initially easier to control the light arm with Mode 1. One subject stated that there was no difference between the modes, and one subject selected Mode 2. 8 out of 10 subjects stated that it was easier to control the light arm after some repetitions with Mode 1.

The haptic feedback integration is preferred by 9 out of 10 subjects. The control of the 2-segment robot arms with Mode 1 is also preferred by 9 out of 10 subjects. 7 out of 10 subjects stated that they prefer to use Mode 1 for the control of the light arm, while one stated that there is no difference and two prefer to use Mode 2.

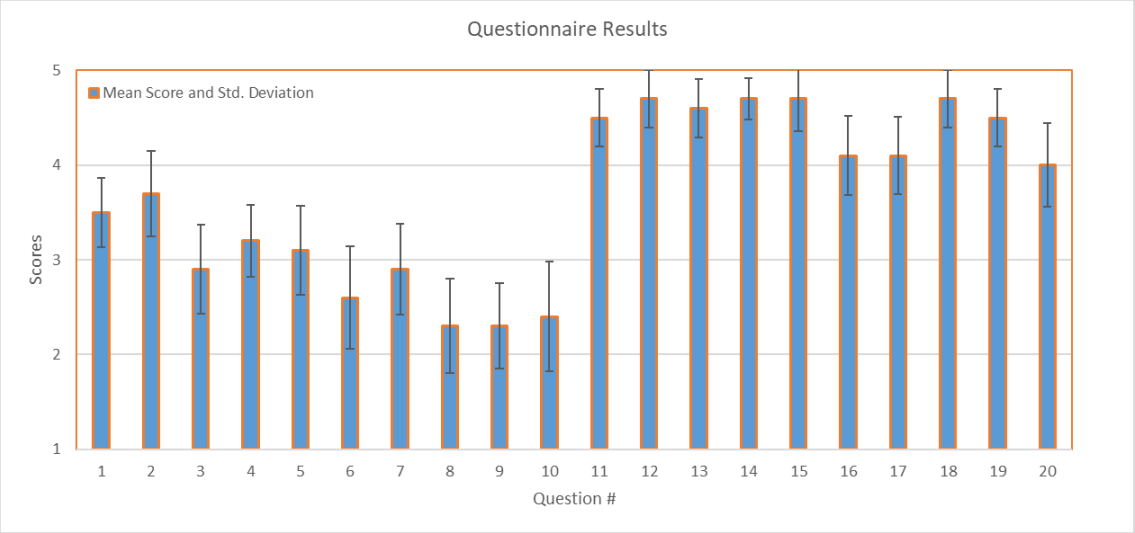

Figure 4.27 Mean of the questionnaire scores.

In Figure 4.27, bar graphs represent the mean of the questionnaire results, while lines indicate the standard deviation. The first and second parts of the questionnaire indicate that Mode 1 is preferred in terms of telepresence by a narrow margin, yet even in Mode 1, telepresence is found just above the average by participants. The third part of the questionnaire shows that Mode 1 is preferred by a majority. According to the user test results, the performance of Mode 1 and Mode 2 significantly differs in task completion time and accuracy. Taking all the feedback from the subjects into account, including the questionnaire, the proposed methods were proven as applicable and deduced that Mode 1 increases the overall performance of the teleoperation by providing enhanced telepresence.

CHAPTER 5

PERFORMANCE COMPARISION TESTS AND RESULTS WITH TWO TYPES OF MAPPINGS

The previous chapter examined the performance and efficiency of implemented teleoperation strategies and telepresence. This chapter presents the position-to-position mode which is designed based on the feedback received on the position-to-position modes that are presented in the previous chapter. Hence, this optimized version of the position-to-position mode includes haptic feedback and camera lock option. In order to compare this mode with a new position-to-velocity mode fairly, in both modes, the segments of the slave robot arm are controlled sequentially as it is the case in Mode 2.

Modes 3 and 4 are described in Chapter 3. These modes are tested on volunteer human subjects. The outcomes of the experiments are presented and discussed, including the user performance analysis and written assessments of the users.

The user interface is designed considering the ergonomy for the operator. The complexity of multi-master multi-slave systems is assessed, and feedback from subjects is used to build the user interface; the scenario is given in Figure 5.1. Unlike the previous modes, Mode 3 and 4 additionally contain a foot switch to toggle between the teleoperation of the grasper and palpation arms. Both modes provide haptic feedback to the operator on contact positions, and the segments are controlled sequentially with only acquiring the motion information of the master device's first three joints. Gravity compensation is applied to both master devices in both modes to ease the use for Mode 3 and to assist the software-based home positioning for Mode 4. The grasping motion is performed by using Gimbal-1 rather than Gimbal-2, in contrast to Modes 1 and 2, to create a more intuitive operation considering the similarity of motion of the grasper arm's end-effector and the operator's wrist motion.

To alleviate ambiguity, a display that shows the mentioned information is developed in the MatLab GUI, given in Figure 5.2. This GUI was not available during the tests with Modes 1 and 2. The lamps output red or green lights indicating whether the master device currently controls the stated part or not. The introduction of this information to the operators aims to strengthen the sense of control over the system.

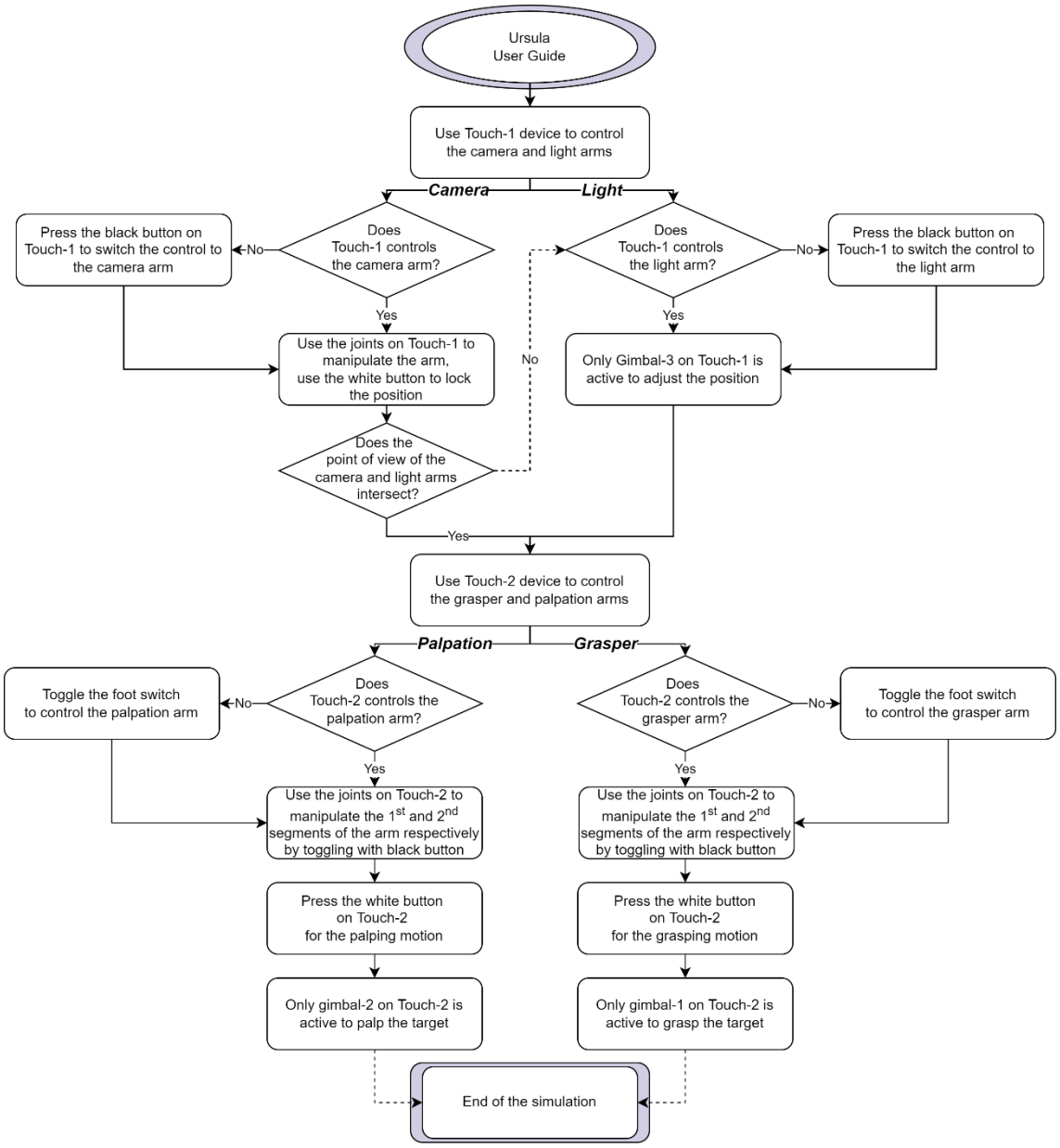

Figure 5.1 User guide of Modes 3 and 4.

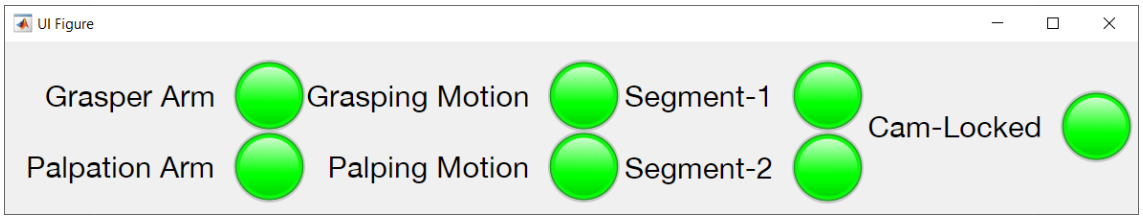

Figure 5.2 Designed display on GUI.

5.1. Teleoperation Performance Tests with Modes 3 and 4

Proposed methods are assessed using performance analysis metrics such as task completion time and accuracy. Ten participants took part in the experiments, while the majority had already participated in the first set of tests. The characteristics of the new participants in terms of age, gender, gaming/haptic device use experience, and education status are exactly the same as the ones that participated in the tests with Modes 1 and 2 and did not participate in tests with Modes 3 and 4. The procedure of the experiments is identical to the previous tests with Modes 1 and 2. After each test is concluded, the subjects are asked to complete a questionnaire (see Appendix-A Table-3) to review their experience. The scores are graded from 1 to 5 as one indicates strongly disagree, and five strongly agree. The first and second parts of the questionnaire measure their effort and users' perception of the simulation for Modes 3 and 4, respectively. The third part of the questionnaire is designed to evaluate the user preference of the modes.

5.2. Test Results with Modes 3 and 4

The outcomes of the test results are analyzed in terms of task completion times and accuracy. Table 5.1 shows the overall task completion times.

Table 5.1 Task completion times.

Overall Time													
Test # / Subject #	Mode 3					Mode 4					Total		
	1	2	3	4	5	6	7	8	9	10	Mode3 Total	Mode4 Total	Total
1	279	510	313	218	195	1269	244	518	666	160	1515	2857	4372
2	105	169	137	85	158	148	344	194	292	219	654	1197	1851
3	768	263	73	92	115	360	217	537	307	196	1310	1617	2927
4	211	196	96	118	91	430	321	367	210	355	711	1683	2395
5	230	492	84	73	114	176	245	114	186	269	992	988	1981
6	407	211	290	95	89	170	82	159	221	97	1093	729	1822
7	133	287	117	119	403	226	185	76	149	252	1059	888	1948
8	141	251	55	66	185	327	310	196	262	191	698	1285	1983
9	153	509	125	412	55	111	150	67	182	160	1254	670	1924
10	124	394	99	98	74	200	315	303	150	169	788	1137	1925
mean	255	328	139	137	148	342	241	253	262	207	1007	1305	2313
std. Dev.	191.5	128.4	84.7	100.0	95.9	323.9	80.2	163.5	144.3	68.0	600.6	779.9	1380.5

The presented durations show that in both modes, tasks are completed in longer durations than in Modes 1 and 2, even though the task is the same. Among the position-to-position mappings (Modes 1, 2, 3), the least amount of task completion durations are measured during the tests in Mode 1.

Although Mode 4 has the longest task completion time, the accuracy and questionnaire results should also be investigated to decide on the best mode. The learning curves for each subject and mode are created using the obtained results, as shown in Figures 5.3 and 5.4.

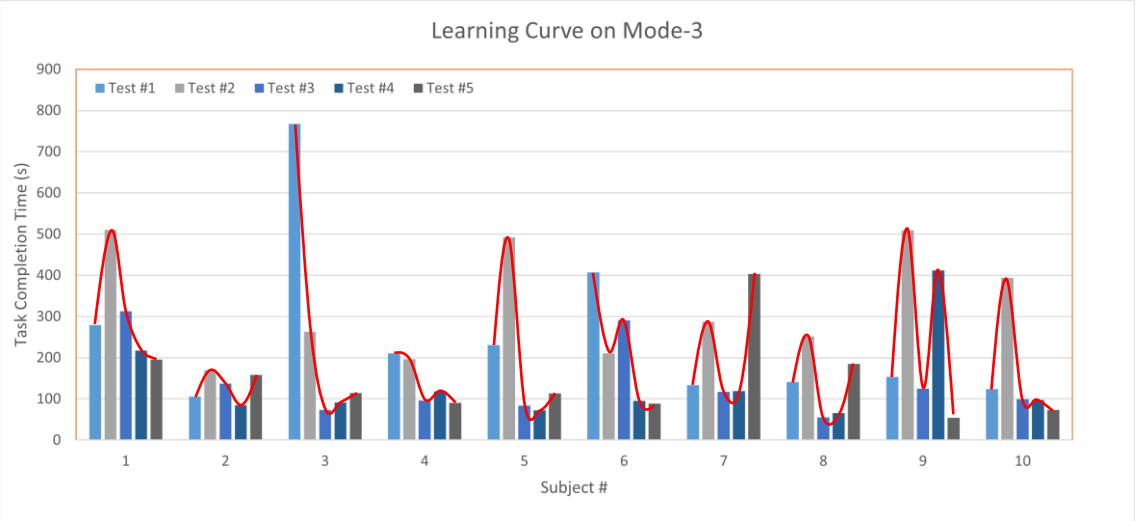

Figure 5.3 Learning curve of subjects on Mode 3.

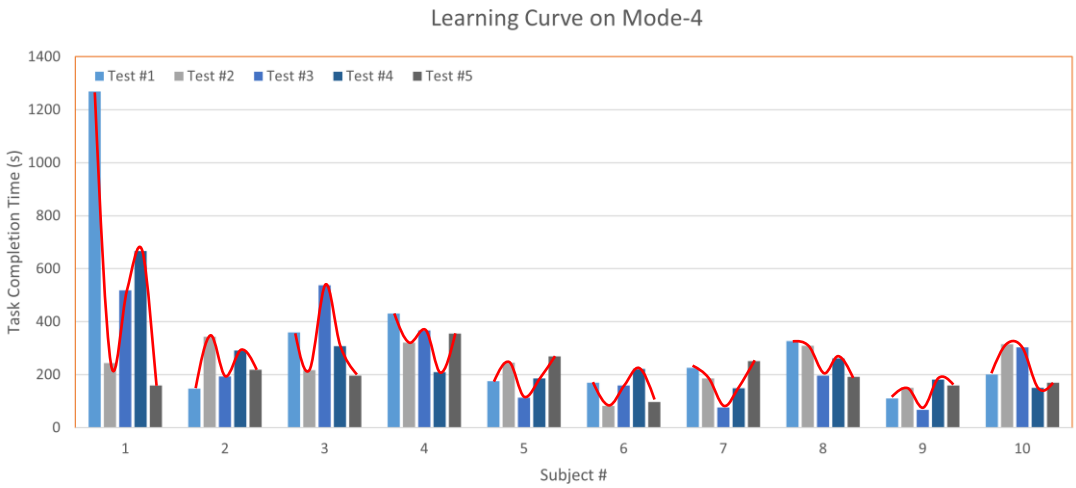

Figure 5.4 Learning curve of subjects on Mode 4.

The repeated test sequence, with five repetitions in each mode, fails to excel the curve as expected and produces inefficient results. However, particular participants, such as subjects 1, 3, 6, and 10, tend to gain acquittance with the device and teleoperation system as they lower the task completion time from the initial one to the final. The first tests of subject 3 in Mode 3 and subject 1 in Mode 4 are inconsistent with other results and are considered to be caused by not being familiar with the modes.

The paths followed by the operators to manipulate the slave arms are evaluated to create a comparison between the paths taken by different mappings. Figures 5.5 and 5.6 depict the paths of the operators who have middling performance in terms of accuracy on target contact positions for the grasper and palpation arms on Mode 4, respectively. End-effector paths are illustrated from the initial positions (▶) to the first point of contact with the circular targets. The step sizes are indicated by the small red markers; as the range between markers widens, so does the end-effector's velocity.

In all position-to-position mappings, a rapid dislocation is observed initially, as aforementioned. The advantage of the position-to-velocity mode is the elimination of this dislocation which might lead to collision with obstacles that may be present in real-world systems. The initial command in Mode 4 is zero velocity if the master device is in its home position, and after the switch between arms, segments, or modes, arms do not jerk to another configuration but continuously move by the received velocity demands.

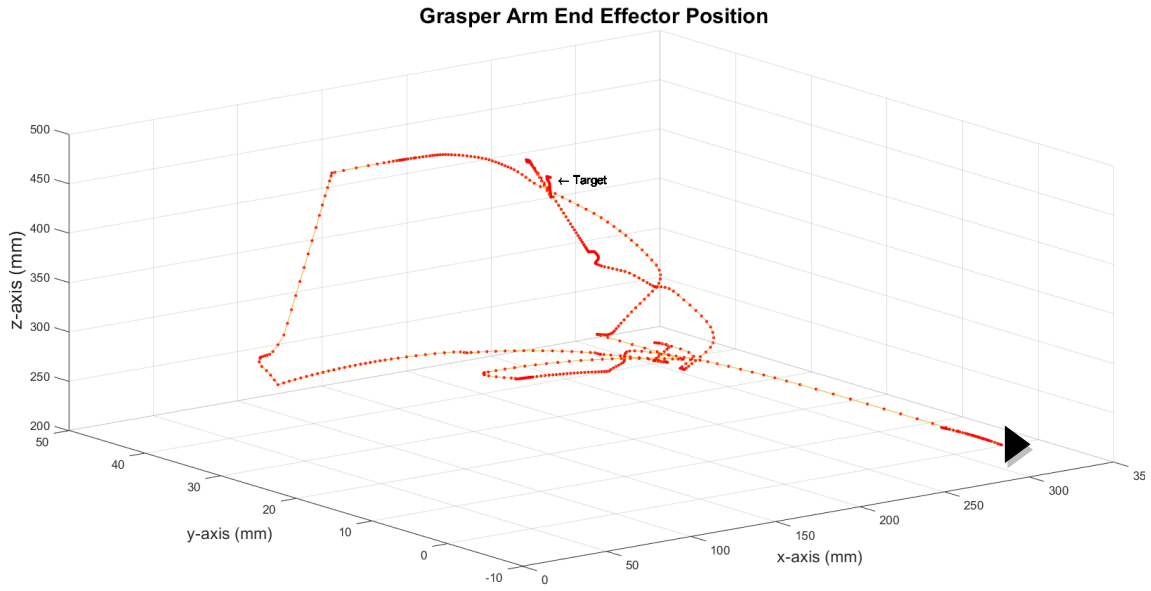

Figure 5.5 Grasper arm trajectory on Mode 4.

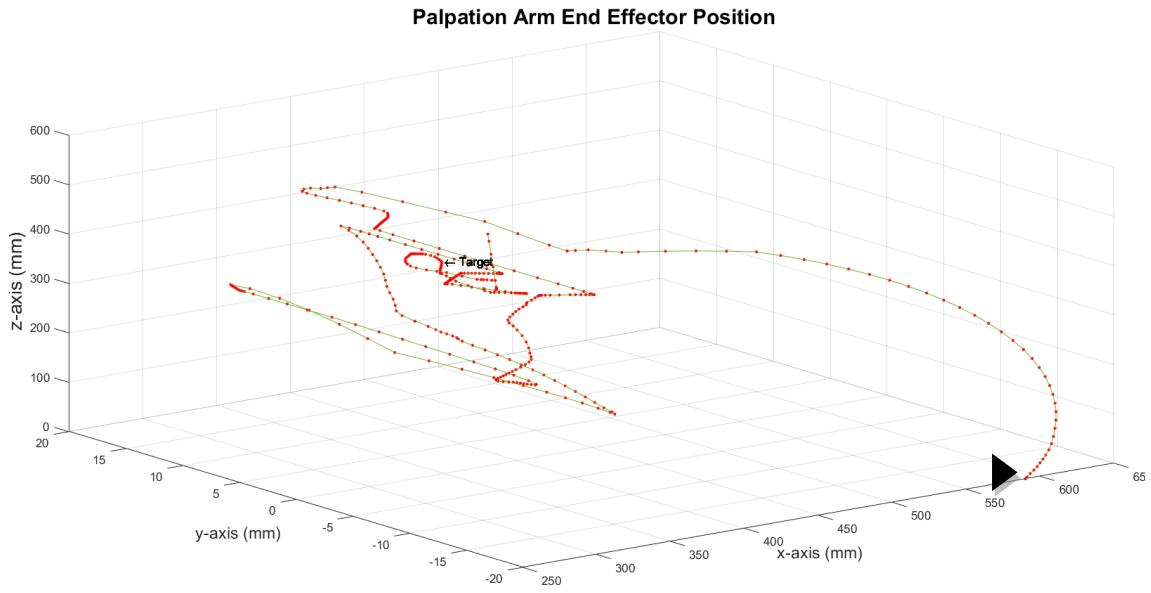

Figure 5.6 Palpation arm trajectory on Mode 4.

Another improvement achieved by implementing position-to-velocity mapping is the elimination of the habit performed by a majority of the subjects, which is locating the currently controlled arm in the point of view with navigating through almost the entire environment at high speed. The sudden movements performed by the subjects disappeared, yet most subjects had difficulty to understand the location of the arm if it was not visible at that instant.

The success criterion for each target is established as residing in the threshold region of ±15 mm for each axis which provides feedback to the operator to denote contact position. Figures 5.7 and 5.8 introduce the contact positions for grasper and palpation arms on targets 2 and 8, respectively, as green markers indicate Mode 3 and red indicate Mode 4. The rest of the graphs indicating the end-effector positions on different circular targets are given in Appendix-C.

Target 2 results show that participants tend to use the same approach strategy to the target with similar positioning errors for both arms. However, in the results obtained for some targets, it is observed that the test subjects approached the target in various directions and resulted in a graph with very distinct final positions. It is deduced that the target's position may cause this condition when the target can be reached in a relatively more complicated way. These targets are generally the ones that are closer or more distant to the base of the robot.

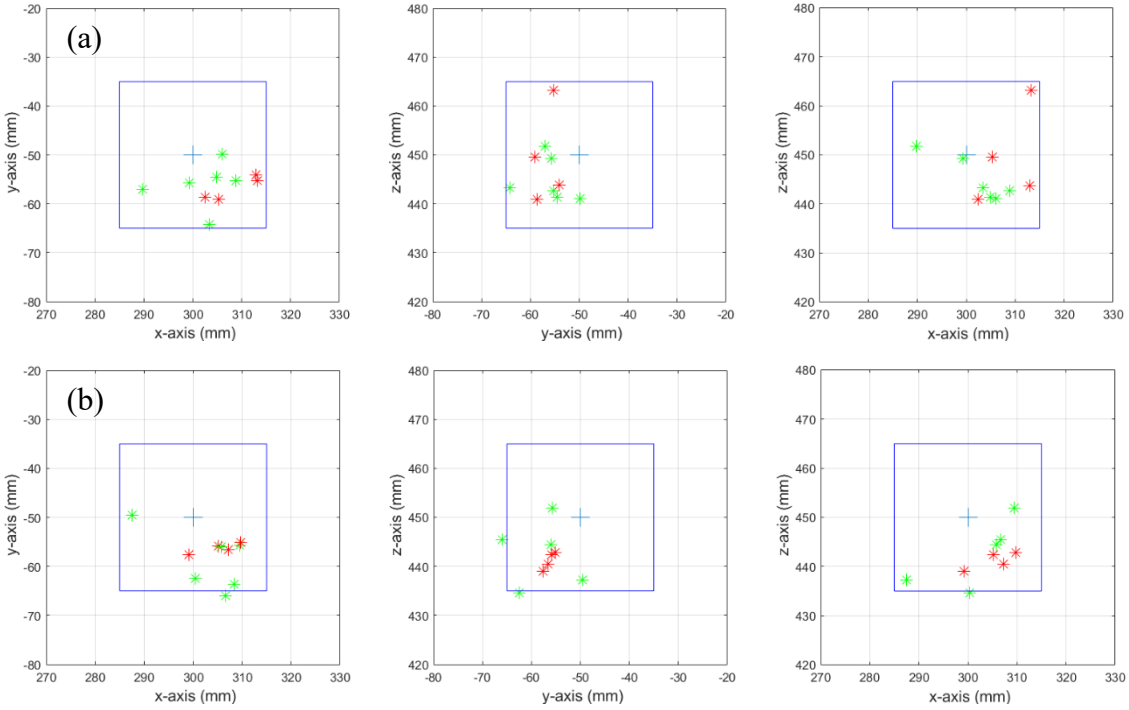

Figure 5.7 End-effector positions on target #2 (a) Grasper arm (b) Palpation arm.

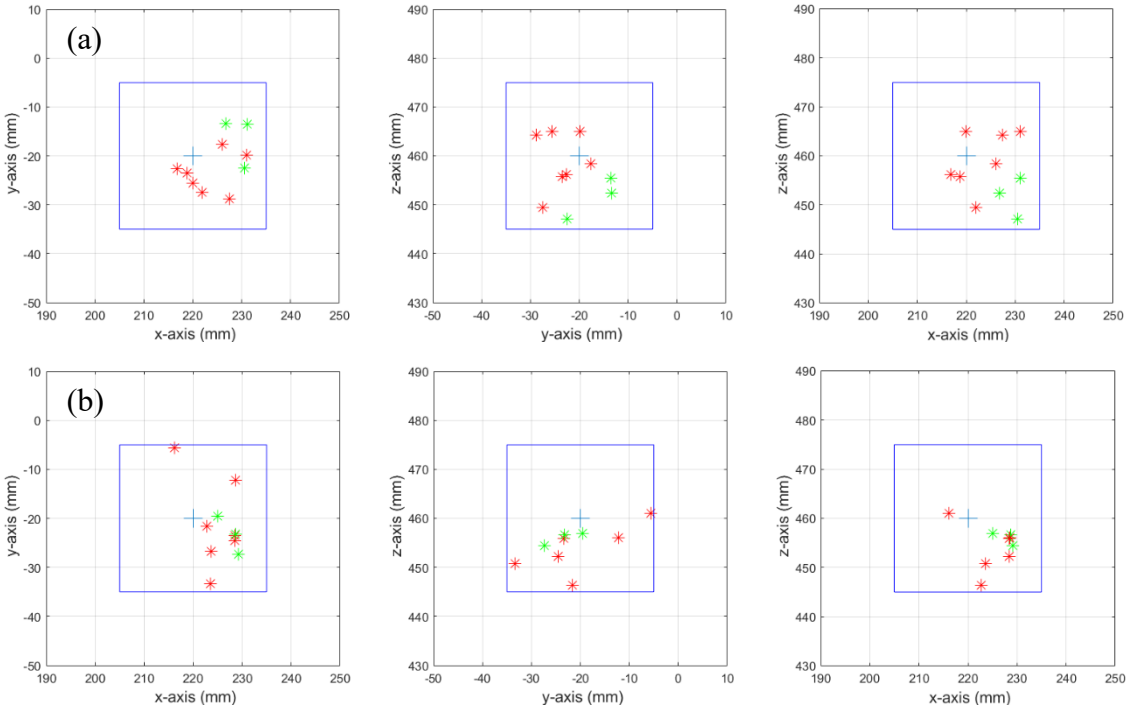

Figure 5.8 End-effector positions on target #8 (a) Grasper arm (b) Palpation arm.

Target 8 demonstrates that target locations affect the accuracy. As Target 8 is located in a relatively more straightforward position to approach, it led to higher accuracy in both Mode 3 and Mode 4. Although operating the arms with position-to-velocity mode makes it harder to stop the end-effector right on the contact positions, subjects tend to move and stop with small step sizes to preserve accuracy. Overall accuracy results are presented in Table 5.2.

Table 5.2 Success rate on target positions in Mode 3 and Mode 4.

Accuracy on Target Contact												
	Grasper				**Palpation**				**Total Success Rate**			
	Successful		Unsuccessful		Successful		Unsuccessful		**Grasper**		**Palpation**	
Target#	M.#3	M.#4	M.#3	M.#4	M.#3	M.#4	M.#3	M.#4	M.#3	M.#4	M.#3	M.#4
#1	4	6	0	0	3	5	1	1	100%	100%	75%	83%
#2	6	4	0	0	5	2	1	2	100%	100%	83%	50%
#3	6	4	0	0	4	4	2	0	100%	100%	67%	100%
#4	6	4	0	0	3	4	3	0	100%	100%	50%	100%
#5	7	2	1	0	7	2	1	0	88%	100%	88%	100%
#6	4	5	1	0	5	4	0	1	80%	100%	100%	80%
#7	3	6	1	0	2	3	2	1	75%	100%	50%	75%
#8	3	7	0	0	3	6	0	1	100%	100%	100%	86%
#9	5	5	0	0	5	2	0	3	100%	100%	100%	40%
#10	3	6	0	1	2	6	1	1	100%	86%	67%	86%

While the task completion durations are the highest on Mode 4, it produced higher accuracy. The most challenging aspect of this mode is to stop precisely at the contact point; nevertheless, with acquittance with the mode, individuals achieved to stop inside the threshold area. With 25 unsuccessful trials, the overall failure rate is 13%. The accumulated failure rate of Modes 1 and 2 is 38%, indicating that familiarity with the teleoperation system significantly increases accuracy since most of the subjects (8 out of 10) were trained on the first two modes. The failure rate calculated for Mode 3 is 14%, whereas it is 11% in Mode 4. The overall failure rate for the grasper arm in both modes is 4%, while this rate on the palpation arm is 21%. Although the task of both arms is similar, there is a difference in accuracy similar to Modes 1 and 2. The reason for this difference is considered to be the habit of taking different paths on the palpation arm and attempting to palp the target from a distance, as discussed in Chapter 4.3.

Tables 5.3 and 5.4 show the error on each axis for each subject and targets on grasper and palpation arms, respectively. The mean value of the positioning error is illustrated in Figures 5.9 and 5.10 by comparing Modes 3 and 4. The bars graphs represent the mean error while the lines show the standard deviation of the error. The mean value of the error on the palpation arm varies greatly in Mode 4, which requires higher steering skills, yet the final tests of each mode have similar outcomes. The increased standard deviation of error on Mode 4 shows that subjects had diverse results with position-to-velocity mode, as expected. The subjects that had more experience with haptic devices produced more accurate results even though the complexity of the task was increased.

Table 5.3 Overall positioning errors with the grasper arm.

Overall Error in -x, -y, -z Directions															
	Mode 3														
	Test-1			Test-2			Test-3			Test-4			Test-5		
S.#	Δx	Δy	Δz	Δx	Δy	Δz	Δx	Δy	Δz	Δx	Δy	Δz	Δx	Δy	Δz
#1	7.94	2.55	11.66	6.17	4.25	1.33	-0.60	-6.75	6.97	12.19	2.61	6.80	13.20	-5.23	13.13
#2	7.49	3.47	4.75	2.49	-8.72	-9.06	10.53	-2.52	-12.93	11.70	-5.56	-9.71	7.20	-3.40	-14.88
#3	4.30	3.98	-12.97	8.12	-2.41	-5.19	6.41	6.18	-2.50	6.10	3.57	-2.34	6.48	-3.36	-5.50
#4	4.29	3.28	8.41	11.09	6.50	-4.61	7.11	-7.46	0.55	5.13	2.31	4.68	4.76	-3.65	-3.32
#5	4.72	-14.42	-11.29	4.85	-4.56	-8.65	-0.63	-1.99	-11.77	12.53	-7.57	-7.16	14.01	-4.05	-5.21
#6	-14.08	13.26	-4.28	6.79	6.54	-7.67	11.26	-10.47	-11.10	12.06	-9.36	-9.36	12.93	-10.91	-9.72
#7	9.61	-9.22	-6.29	8.08	2.23	-4.92	6.01	0.15	-8.94	4.97	1.40	-12.96	7.98	-1.65	-25.22
#8	12.89	-4.09	-6.23	2.81	-2.39	-10.35	-1.34	6.45	-10.71	9.44	-9.21	26.22	-18.21	-13.37	-5.24
#9	14.15	-12.85	6.96	8.82	-5.28	-7.35	-6.93	4.07	-7.48	12.50	2.19	2.94	-3.33	3.30	-4.50
#10	5.22	1.12	-14.14	3.57	-0.04	-12.50	10.47	-5.59	-12.46	13.22	13.89	-9.06	9.96	4.69	-6.00
	Mode 4														
	Test-6			Test-7			Test-8			Test-9			Test-10		
S.#	Δx	Δy	Δz	Δx	Δy	Δz	Δx	Δy	Δz	Δx	Δy	Δz	Δx	Δy	Δz
#1	4.79	7.20	-1.63	3.74	6.18	-9.22	0.13	-14.58	-5.73	10.55	-8.90	7.40	-3.21	-2.71	-3.79
#2	-0.01	0.59	-3.59	1.59	3.69	2.00	5.68	5.59	10.42	6.06	-13.66	0.79	-0.86	-2.82	-4.89
#3	1.50	-4.46	-5.40	10.99	0.14	4.95	4.22	10.56	-4.36	3.37	-14.17	-6.74	1.99	14.45	1.01
#4	8.41	4.12	-4.19	-10.56	1.94	-7.69	-0.73	-5.75	-0.77	7.70	4.42	-8.12	-34.51	7.22	-27.09
#5	-1.19	-3.54	-4.24	-1.55	2.73	-9.03	-0.76	-10.35	-8.25	9.16	3.05	-7.79	10.85	-12.71	-0.40
#6	3.16	-1.42	-11.75	-8.28	-2.28	-9.38	-10.20	-7.04	1.78	12.34	8.29	-2.11	-7.88	-7.10	8.43
#7	-3.41	-6.14	1.85	-1.21	5.23	-6.24	7.80	-14.15	-11.01	7.44	-8.76	4.25	4.67	0.75	-6.71
#8	-0.71	9.48	-3.79	-2.52	-6.29	-7.27	1.94	-13.42	13.05	-0.02	-5.57	4.99	8.72	9.69	-2.64
#9	1.95	-7.44	-10.51	-3.99	8.05	-1.55	-6.49	-14.72	-4.62	2.58	-4.56	-4.81	-14.22	-2.46	10.80
#10	-1.16	3.65	3.58	6.07	2.34	-1.54	1.46	-1.00	-1.24	0.70	-11.48	3.47	5.33	-9.06	-0.40

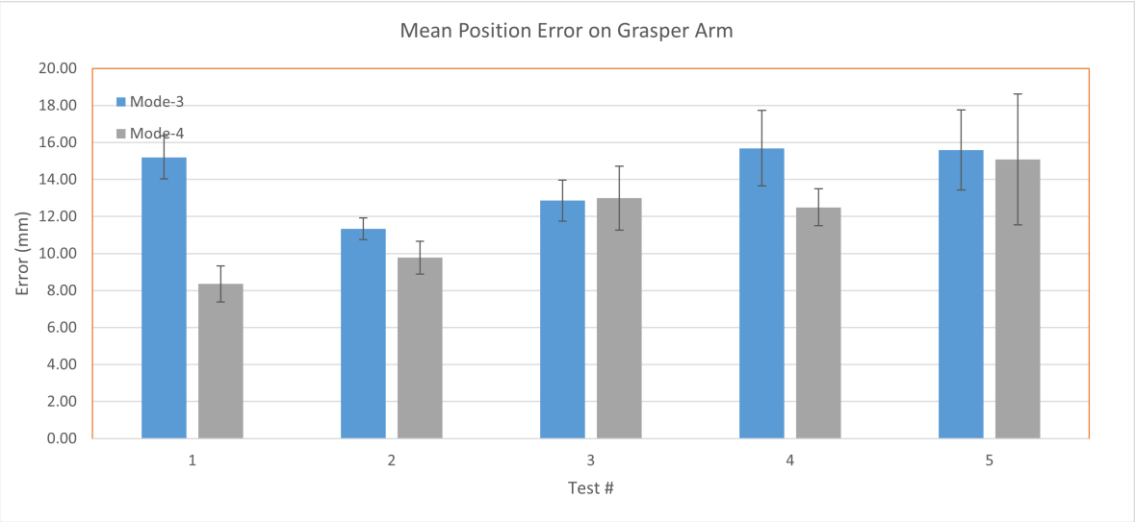

Figure 5.9 Mean positioning error on reaching the circular target for grasper arm.

Table 5.4 Overall positioning errors with palpation arm.

Overall Error in -x, -y, -z Directions															
	Mode 3														
	Test-1			Test-2			Test-3			Test-4			Test-5		
S.#	Δx	Δy	Δz	Δx	Δy	Δz	Δx	Δy	Δz	Δx	Δy	Δz	Δx	Δy	Δz
#1	10.45	0.49	0.19	8.04	1.33	-7.36	3.35	-4.87	3.72	7.10	-1.65	5.34	9.71	-5.15	-7.14
#2	8.89	4.55	-3.41	5.14	-5.87	-7.59	4.98	0.47	-3.02	8.73	2.10	1.18	7.20	5.32	-1.30
#3	9.97	-1.85	-4.34	11.43	-5.50	-6.94	6.86	4.86	-6.43	4.41	3.80	-1.04	2.78	-7.29	-2.19
#4	8.06	2.97	0.32	8.66	-3.23	-3.33	11.12	-5.55	-1.38	6.40	4.06	-0.58	14.93	-10.27	8.09
#5	10.74	-7.90	4.15	5.76	-5.95	-5.55	3.78	0.04	-11.79	13.18	1.58	-8.06	8.60	3.21	-7.99
#6	6.10	4.36	-11.22	9.20	-7.33	-5.57	8.59	-4.86	-8.55	10.38	0.91	-12.61	8.66	-3.81	-4.28
#7	5.08	1.99	-15.22	7.94	6.59	-2.81	9.51	-5.69	1.87	1.41	3.19	-1.34	12.94	1.56	-38.52
#8	-0.84	-7.56	-11.02	13.20	-8.82	18.11	4.85	9.08	4.01	2.32	-1.92	-4.29	3.38	-11.62	-5.93
#9	-3.99	-2.66	21.86	8.41	-13.71	55.43	13.35	21.95	49.82	41.28	-0.63	0.63	8.42	16.23	77.31
#10	11.73	-7.43	-8.28	6.65	-8.18	-9.35	6.12	1.13	-18.65	3.69	2.08	-18.68	10.49	2.97	-17.77
	Mode 4														
	Test-6			Test-7			Test-8			Test-9			Test-10		
S.#	Δx	Δy	Δz	Δx	Δy	Δz	Δx	Δy	Δz	Δx	Δy	Δz	Δx	Δy	Δz
#1	6.66	3.53	-5.57	-0.41	-0.76	-3.64	10.39	-11.16	-7.50	-5.02	5.41	-2.75	3.56	-13.37	-9.25
#2	2.51	3.82	-5.17	5.05	6.09	-10.80	7.00	1.33	-2.12	6.17	-2.06	-3.82	8.81	1.36	2.55
#3	1.33	1.16	-6.52	-3.87	14.40	1.07	7.35	9.75	-7.74	0.41	-12.47	-15.43	5.46	8.48	3.79
#4	-13.44	23.76	54.85	-5.14	7.23	-7.77	6.65	-15.97	-4.48	-5.49	13.75	-3.55	0.26	2.54	8.41
#5	8.45	-3.45	-4.06	-24.28	-11.76	-126.09	1.80	-5.72	-11.38	-1.71	6.35	-4.40	8.64	-7.60	-9.08
#6	-9.76	8.27	7.23	-11.87	-3.19	4.14	-12.51	0.41	-12.75	-4.44	3.17	4.98	-1.93	2.83	-3.92
#7	-1.38	-1.62	-5.94	8.21	-7.40	3.53	-1.83	-4.00	-3.33	8.48	-4.48	-7.82	6.34	7.96	-9.44
#8	10.49	12.50	3.34	6.91	5.44	5.10	-5.49	-0.53	-6.29	8.59	7.71	-4.02	16.01	9.20	-8.19
#9	3.62	-6.75	49.22	25.30	14.90	65.80	67.72	0.72	80.47	-7.38	14.98	34.87	-18.82	-17.53	66.79
#10	5.95	-3.78	-16.54	2.77	-1.64	-13.65	-10.63	12.48	-23.11	10.49	-3.72	-6.09	7.19	-6.60	-9.54

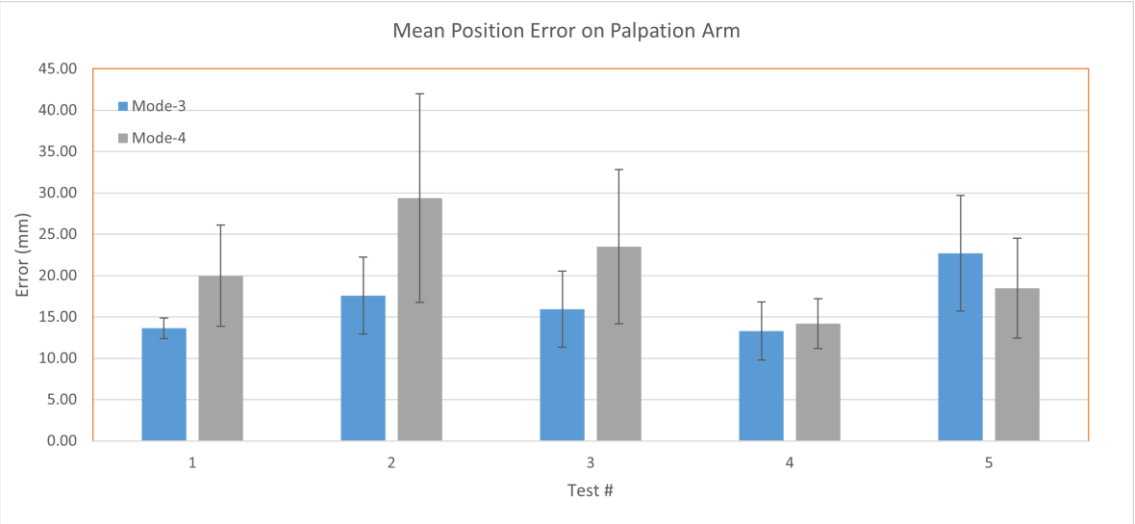

Figure 5.10 Mean positioning error on reaching the circular target for palpation arm.

5.3. Test Subjects' Questionnaire Results with Modes 3 and 4

User tests are concluded with the questionnaire presented in Appendix A Table-3. The NASA-TLX index (Hart, 1988) is used in this survey to assess the suitability of the task demand. The result of the questionnaire is presented in Table 5.5.

In terms of physical/mental effort, stress level, and difficulty, the first and second parts of the questionnaire are designed to compare Modes 3 and 4. The mean values of the results are presented as bar graphs in Figure 5.13, and lines indicate the standard deviation. It is clear that the users found Mode 3 is to be easier to operate with than Mode 4. Most subjects stated that teleoperation with Mode 3 does not require much effort to execute, even though the average task completion time is about 1000 seconds. Some users indicated that Mode 4 required especially increased mental effort.

The third part of the questionnaire investigates the preference between the modes. As stated, Mode 3 is found to be easier to operate with by the users. On the contrary, 5 out of 10 subjects preferred to use Mode 4 rather than Mode 3 even though they stated that Mode 3 is generally found to be better in terms of spent excess effort and felt pressure. The majority of the subjects that prefer Mode 4 stated that it was initially easier to use Mode 3, though after certain repetitions and becoming acquainted with Mode 4, position-to-velocity mapping becomes easier to use. The results show that position-to-position mapping has a higher intuitive approach which eases the job for the operator. Position-to-velocity mapping can be preferred by more experienced users due

to its nature, that eliminates the handicaps of position-to-position mapping as rapid dislocations, increased collision potential, and decreased accuracy.

Table 5.5 User questionnaire results.

1st part of the questionnaire										
Subjects / Questions	**1**	**2**	**3**	**4**	**5**	**6**	**7**	**8**	**9**	**10**
1	2	2	3	2	3	5	1	4	3	4
2	1	1	2	1	4	3	1	2	2	2
3	2	1	3	1	2	2	1	2	2	3
4	1	2	3	1	2	2	2	2	2	4
5	2	2	3	1	3	4	3	3	2	1
6	1	1	2	1	1	2	2	1	2	3
2nd part of the questionnaire										
Subjects / Questions	**1**	**2**	**3**	**4**	**5**	**6**	**7**	**8**	**9**	**10**
7	5	4	4	3	4	5	2	5	4	3
8	3	3	2	4	4	4	2	4	2	2
9	4	4	2	3	2	3	2	2	2	4
10	4	5	3	2	1	2	2	2	2	4
11	2	4	3	3	3	5	3	5	3	1
12	5	2	2	3	2	2	3	1	3	3
3rd part of the questionnaire										
Subjects / Questions	**1**	**2**	**3**	**4**	**5**	**6**	**7**	**8**	**9**	**10**
13	5	5	4	4	3	4	4	5	2	2
14	3	5	2	2	2	4	2	5	4	3
15	5	5	2	4	2	2	2	5	4	2

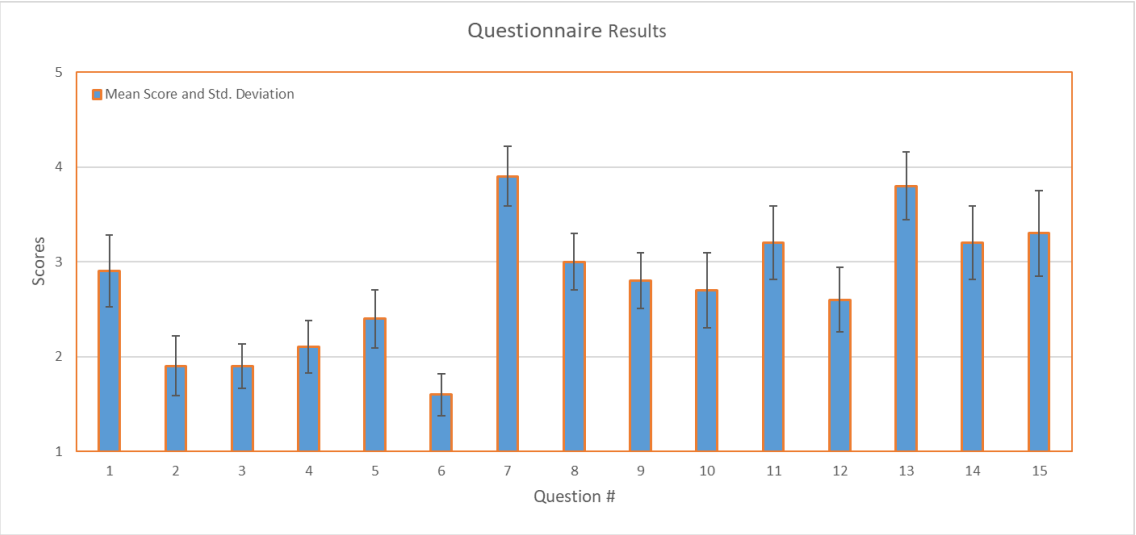

Figure 5.11 Mean of the questionnaire scores.

Considering the test results, the performance of Modes 3 and 4 differ in task completion time and accuracy in contradiction. While the accuracy is greater on Mode 4 and is likely to improve with experience, the task completion time is also longer. Taking all feedback from the subjects into consideration, including the questionnaire, both methods are acknowledged as possible candidates to be implemented on the actual teleoperation system, though Mode 4 is only suggested for proficient users.

CHAPTER 6

CONCLUSIONS

A teleoperation architecture is developed as an initial step toward formulating model-mediated teleoperation to manipulate the soft robot arms of an underwater biomimetic squid robot. This work presents a user interface for multi-master multi-slave systems with dissimilar master-slave kinematics. The virtual slave and its surroundings are created in the simulation environment. The robot arms are modeled with discretized links to form and imitate the curved motion of soft robotic arms. Taking into account the complexity of multi-master multi-slave systems, user ergonomics are studied, and four different modes of mappings are formed. Voluntarily participated human subjects took part in the experiments to validate and assess proposed methods.

The first set of experiments is conducted to evaluate the telepresence feeling passed to the users in teleoperation with and without haptics feedback. In addition, the positioning accuracy and task completion durations are recorded to evaluate the effect of Modes 1 and 2 on user performance. After each test, each test subject filled in the questionnaire asking about their preferences, ease of use, and felt telepresence. The results indicate that Mode 1 with haptic feedback is preferred by the users in terms (1) the sense of task completion passed to the user (2) control of one- and two-segment soft arms.

The second set of experiments is used for comparing the performance of the users when teleoperation mode is set to the position-to-position mapping (Mode 3) and position-to-velocity mapping (Mode 4). A software-based homing procedure was developed for Mode 4 since the haptic devices did not include a hardware-based homing mechanism. Similar to the first set of tests, positioning accuracy and task completion durations are measured, and the test subjects filled in a different set of questionnaires. The results indicate that there is no shared opinion on which one of the modes is preferred. However, subjects with experience in haptic devices or gaming got accustomed to Mode 4. They produced the most accurate results yet longer task completion times.

The results have shown that, among all modes of position-to-position mapping,

participants preferred Mode 1, in which the shortest task completion durations are obtained. Proficient or skilled users managed to teleoperate by using Mode 4 with the highest accuracy yet having a longer task completion duration. Both Mode 1 and 4 are considered applicable for the designed task in this thesis, and they can be employed on different tasks having different performance expectations.

As future work, the methods devised in this study can be employed in the teleoperation of the actual squid robot when it will be manufactured. In this case, the abstract data received from the slave robot must be used for regenerating the slave system's environment on the master side, and thus, a model-mediated teleoperation system can be developed.

REFERENCES

Anderson, Robert J, and Mark W Spong. "Bilateral Control of Teleoperators with Time Delay." Paper presented at the Proceedings of the 1988 IEEE International Conference on Systems, Man, and Cybernetics, 1988.

Balch, Tucker, and Ronald C Arkin. "Behavior-Based Formation Control for Multirobot Teams." *IEEE transactions on robotics and automation* 14, no. 6 (1998): 926-39.

Banthia, Vikram, Yaser Maddahi, Kourosh Zareinia, Stephen Liao, Tim Olson, Wai-Keung Fung, Subramaniam Balakrishnan, and Nariman Sepehri. "A Prototype Telerobotic Platform for Live Transmission Line Maintenance: Review of Design and Development." *Transactions of the Institute of Measurement and Control* 40, no. 11 (2018): 3273-92.

Bejczy, Antal K, Won S Kim, and Steven C Venema. "The Phantom Robot: Predictive Displays for Teleoperation with Time Delay." Paper presented at the Proceedings., IEEE International Conference on Robotics and Automation, 1990.

Bemporad, Alberto. "Predictive Control of Teleoperated Constrained Systems with Unbounded Communication Delays." Paper presented at the Proceedings of the 37th IEEE Conference on Decision and Control (Cat. No. 98CH36171), 1998.

Buttolo, Pietro, Petter Braathen, and Blake Hannaford. "Sliding Control of Force Reflecting Teleoperation: Preliminary Studies." *Presence: Teleoperators & Virtual Environments* 3, no. 2 (1994): 158-72.

Cheung, Yushing, Jae H Chung, and Norman P Coleman. "Semi-Autonomous Formation Control of a Single-Master Multi-Slave Teleoperation System." Paper presented at the 2009 IEEE Symposium on Computational Intelligence in Control and Automation, 2009.

Csencsits, Matthew, Bryan A Jones, William McMahan, Vikram Iyengar, and Ian D Walker. "User Interfaces for Continuum Robot Arms." Paper presented at the 2005 IEEE/RSJ International Conference on Intelligent Robots and Systems, 2005.

Davincisurgery.com. Accessed October 20, 2021. https://www.davincisurgery.com/.

Debbabi, Sana, Mohamed Daassi, and Serge Baile. "Effect of Online 3d Advertising on Consumer Responses: The Mediating Role of Telepresence." *Journal of Marketing Management* 26, no. 9-10 (2010): 967-92.

Desai, Jaydev P, James P Ostrowski, and Vijay Kumar. "Modeling and Control of Formations of Nonholonomic Mobile Robots." *IEEE transactions on Robotics and Automation* 17, no. 6 (2001): 905-08.

Fellmann, Carolin, Daryoush Kashi, and Jessica Burgner-Kahrs. "Evaluation of Input Devices for Teleoperation of Concentric Tube Continuum Robots for Surgical Tasks." Paper presented at the Medical Imaging 2015: Image-Guided Procedures, Robotic Interventions, and Modeling, 2015.

Ferrell, William R. "Remote Manipulation with Transmission Delay." *IEEE Transactions on Human Factors in Electronics*, no. 1 (1965): 24-32.

Ferrell, William R, and Thomas B Sheridan. "Supervisory Control of Remote Manipulation." *IEEE spectrum* 4, no. 10 (1967): 81-88.

Frazelle, Chase G, Apoorva D Kapadia, Katelyn E Fry, and Ian D Walker. "Teleoperation Mappings from Rigid Link Robots to Their Extensible Continuum Counterparts." Paper presented at the 2016 IEEE International Conference on Robotics and Automation (ICRA), 2016.

Furuta, Katsuhisa, Kazuhiro Kosuge, Yoshinori Shiote, and Hiromu Hatano. "Master-Slave Manipulator Based on Virtual Internal Model Following Control Concept." Paper presented at the Proceedings. 1987 IEEE International Conference on Robotics and Automation, 1987.

Goertz, Ray C. *Master-Slave Manipulator.* Vol. 2635: Argonne National Laboratory, 1949.

Hannaford, Blake, and Paolo Fiorini. "A Detailed Model of Bi-Lateral Teleoperation." Paper presented at the Proceedings of the IEEE international conference on systems, man and cybernetics, 1988.

Hart, Sandra G, and Lowell E Staveland. "Development of Nasa-Tlx (Task Load Index): Results of Empirical and Theoretical Research." In *Advances in Psychology*, 139-83: Elsevier, 1988.

Hirche, Sandra, and Martin Buss. "Insights on Human Adapted Control of Networked Telepresence and Teleaction Systems." *International Journal of Assistive Robotics and Mechatronics* 7, no. 1 (2006): 20-31.

Hokayem, Peter F, and Mark W Spong. "Bilateral Teleoperation: An Historical Survey." *Automatica* 42, no. 12 (2006): 2035-57.

Hwang, Gilgueng, Peter Tamas Szemes, Noriaki Ando, and Hideki Hashimoto. "Development of a Single-Master Multi-Slave Tele-Micromanipulation System." *Advanced Robotics* 21, no. 3-4 (2007): 329-49.

Khademian, Behzad, Jacob Apkarian, and Keyvan Hashtrudi-Zaad. "Assessment of Environmental Effects on Collaborative Haptic Guidance." *Presence* 20, no. 3 (2011): 191-206.

Kirişci, Nihat Çaghan. "Augmented Reality-Based Model-Mediated Teleoperation: A Mobile Telerobot Case Study." Izmir Institute of Technology (Turkey), 2019.

L3harris™ Fast. Forward. Accessed October 20, 2021. https://www.l3harris.com/.

Lalish, Emmett, Kristi A Morgansen, and Takashi Tsukamaki. "Formation Tracking Control Using Virtual Structures and Deconfliction." Paper presented at the Proceedings of the 45th IEEE Conference on Decision and Control, 2006.

Leung, Gary MH, and Bruce A Francis. "Robust Nonlinear Control of Bilateral Teleoperators." Paper presented at the Proceedings of 1994 American Control Conference-ACC'94, 1994.

Lichiardopol, S. "A Survey on Teleoperation." *Technische Universitat Eindhoven, DCT report* 20 (2007): 40-60.

Liu, Chao, Jing Guo, and Philippe Poignet. "Nonlinear Model-Mediated Teleoperation for Surgical Applications under Time Variant Communication Delay." *IFAC-PapersOnLine* 51, no. 22 (2018): 493-99.

Matsuhira, Nobuto, Makoto Asakura, and Hiroyuki Bamba. "Manoeuvrability of a Master-Slave Manipulator with Different Configurations and Its Evaluation Tests." *Advanced Robotics* 8, no. 2 (1993): 185-202.

Mitra, Probal, and Günter Niemeyer. "Model-Mediated Telemanipulation." *The International Journal of Robotics Research* 27, no. 2 (2008): 253-62.

Moghimi, Saba, Shahin Sirouspour, and Pawel Malysz. "Haptic-Enabled Collaborative Training with Generalized Force and Position Mappings." Paper presented at the 2008 Symposium on Haptic Interfaces for Virtual Environment and Teleoperator Systems, 2008.

National Aeronautics and Space Administration. NASA. NASA. Accessed March 23, 2022. https://www.nasa.gov/.

Niemeyer, Günter, and J-JE Slotine. "Stable Adaptive Teleoperation." *IEEE Journal of oceanic engineering* 16, no. 1 (1991): 152-62.

Oceaneering "Connecting What's Needed with What's Next.", Accessed February 25, 2022. https://www.oceaneering.com/.

Otsuka, Manabu, Naoki Matsumoto, Takaharu Idogaki, Kazuhiro Kosuge, and Tomotaka Itoh. "Bilateral Telemanipulator System with Communication Time Delay Based on Force-Sum-Driven Virtual Internal Models." Paper presented at the Proceedings of 1995 IEEE international conference on robotics and automation, 1995.

Park, Jong Hyeon, and Hyun Chul Cho. "Sliding-Mode Controller for Bilateral Teleoperation with Varying Time Delay." Paper presented at the 1999 IEEE/ASME International Conference on Advanced Intelligent Mechatronics (Cat. No. 99TH8399), 1999.

Passenberg, Carolina, Angelika Peer, and Martin Buss. "Model-Mediated Teleoperation for Multi-Operator Multi-Robot Systems." Paper presented at the 2010 IEEE/RSJ International Conference on Intelligent Robots and Systems, 2010.

Passenberg, Carolina, Angelika Peer, and Martin Buss. "A Survey of Environment-, Operator-, and Task-Adapted Controllers for Teleoperation Systems." *Mechatronics* 20, no. 7 (2010): 787-801.

Renda, Federico, Frédéric Boyer, Jorge Dias, and Lakmal Seneviratne. "Discrete Cosserat Approach for Multisection Soft Manipulator Dynamics." *IEEE Transactions on Robotics* 34, no. 6 (2018): 1518-33.

Renda, Federico, Vito Cacucciolo, Jorge Dias, and Lakmal Seneviratne. "Discrete Cosserat Approach for Soft Robot Dynamics: A New Piece-Wise Constant Strain Model with Torsion and Shears." Paper presented at the 2016 IEEE/RSJ International Conference on Intelligent Robots and Systems (IROS), 2016.

Renda, Federico, Matteo Cianchetti, Michele Giorelli, Andrea Arienti, and Cecilia Laschi. "A 3d Steady-State Model of a Tendon-Driven Continuum Soft Manipulator Inspired by the Octopus Arm." *Bioinspiration & biomimetics* 7, no. 2 (2012): 025006.

Sansanayuth, Thitipong, Itthisek Nilkhamhang, and Kanokvate Tungpimolrat. "Teleoperation with Inverse Dynamics Control for Phantom Omni Haptic Device." Paper presented at the 2012 Proceedings of SICE Annual Conference (SICE), 2012.

Shahbazi, Mahya, Seyed Farokh Atashzar, Heidar A Talebi, and Rajni V Patel. "Novel Cooperative Teleoperation Framework: Multi-Master/Single-Slave System." *IEEE/ASME Transactions on Mechatronics* 20, no. 4 (2014): 1668-79.

Shahbazi, Mahya, Heidar Ali Talebi, Seyed Farokh Atashzar, Farzad Towhidkhah, Rajni V Patel, and Siamak Shojaei. "A Novel Shared Structure for Dual User Systems with Unknown Time-Delay Utilizing Adaptive Impedance Control." Paper presented at the 2011 IEEE International Conference on Robotics and Automation, 2011.

Sheng, J, and MW Spong. "Model Predictive Control for Bilateral Teleoperation Systems with Time Delays." Paper presented at the Canadian Conference on Electrical and Computer Engineering 2004 (IEEE Cat. No. 04CH37513), 2004.

Sheridan, Thomas B. "Teleoperation, Telerobotics and Telepresence: A Progress Report." *Control Engineering Practice* 3, no. 2 (1995): 205-14.

Sheridan "Telerobotics." *Automatica* 25, no. 4 (1989): 487-507.

Stroppa, Fabio, Ming Luo, Kyle Yoshida, Margaret M Coad, Laura H Blumenschein, and Allison M Okamura. "Human Interface for Teleoperated Object Manipulation with a Soft Growing Robot." Paper presented at the 2020 IEEE International Conference on Robotics and Automation (ICRA), 2020.

Storm and Mammal Monitoring with the Slocum G3 Glider. Marine Technology Products and Solutions - Teledyne Marine. Accessed March 23, 2022. http://www.teledynemarine.com/SitePages/HomePage.aspx.

Sun, Da, Andrey Kiselev, Qianfang Liao, Todor Stoyanov, and Amy Loutfi. "A New Mixed-Reality-Based Teleoperation System for Telepresence and Maneuverability Enhancement." *IEEE Transactions on Human-Machine Systems* 50, no. 1 (2020): 55-67.

Taner, Barış, Mehmet İsmet Can Dede, and Emre Uzunoğlu. "Applying Model Mediation Method to a Mobile Robot Bilateral Teleoperation System Experiencing Time Delays in Communication." Paper presented at the Proceedings of Trc-IFToMM Symposium on Theory of Machines and Mechanisms, 2015.

Uzunoğlu, Emre, and Mehmet Ismet Can Dede. "Extending Model-Mediation Method to Multi-Degree-of-Freedom Teleoperation Systems Experiencing Time Delays in Communication." *Robotica* 35, no. 5 (2017): 1121-36.

Valenzuela-Urrutia, David, Rodrigo Muñoz-Riffo, and Javier Ruiz-del-Solar. "Virtual Reality-Based Time-Delayed Haptic Teleoperation Using Point Cloud Data." *Journal of Intelligent & Robotic Systems* 96, no. 3 (2019): 387-400.

Webster III, Robert J, and Bryan A Jones. "Design and Kinematic Modeling of Constant Curvature Continuum Robots: A Review." *The International Journal of Robotics Research* 29, no. 13 (2010): 1661-83.

Willaert, Bert, Jeannette Bohg, Hendrik Van Brussel, and Günter Niemeyer. "Towards Multi-Dof Model Mediated Teleoperation: Using Vision to Augment Feedback." Paper presented at the 2012 IEEE International Workshop on Haptic Audio Visual Environments and Games (HAVE 2012) Proceedings, 2012.

Xu, Xiao, Burak Cizmeci, and Eckehard G Steinbach. "Point-Cloud-Based Model-Mediated Teleoperation." Paper presented at the HAVE, 2013.

Yun, Sungryul, Suntak Park, Bongjae Park, Seung Koo Park, Harsha Prahlad, Philip Von Guggenberg, and Ki-Uk Kyung. "Polymer-Based Flexible Visuo-Haptic Display." *IEEE/ASME Transactions on Mechatronics* 19, no. 4 (2013): 1463-69.

Zhou, MA, and Pinhas Ben-Tzvi. "Rml Glove—an Exoskeleton Glove Mechanism with Haptics Feedback." *IEEE/Asme Transactions on mechatronics* 20, no. 2 (2014): 641-52.

APPENDICES

Appendix-A Table-1 Geomagic Touch Specifications

Table A.1 Technical specifications of Geomagic Touch devices.

SPESIFICATIONS	**GEOMAGIC TOUCH™**
Workspace	~6.4 W x 4.8 H x 2.8 D in > 160 W x 120 H x 70 D mm
Footprint (physical area the base of the device occupies on a surface)	~6 5/8 W x 8 D in ~168 W x 203 D mm
Weight	3 lbs 15 oz (~1.42 kg)
Range of motion	Hand movement pivoting at wrist
Nominal position resolution	> 450 dpi (~0.055 mm)
Backdrive Friction	<1 oz (<0.26 N)
Maximum exertable force and torque at nominal position (orthogonal arms)	0.75 lbf/3.3 N
Continuous exertable force (24 hours)	>0.2 lbf (.88 N)
Stiffness	x-axis > 7.3 lb/in (1.26 N/mm) y-axis > 13.4 lb/in (2.31 N/mm) z-axis > 5.9 lb/in (1.02 N/mm)
Inertia (apparent mass at tip)	~0.101 lbm (~45 g)
Force feedback (3 DoF)	x, y, z
Position sensing/input (6 DoF) [Stylus gimbal]	x, y, z (digital encoders) [Roll, pitch, yaw (±5% linearity potentiometers)]
Interface	USB 2.0
OpenHaptics® SDK compatibility?	Yes

Appendix-A Approval Form on Modes 1 and 2

İZMİR YÜKSEK TEKNOLOJİ ENSTİTÜSÜ
FEN VE MÜHENDİSLİK BİLİMLERİ
BİLİMSEL ARAŞTIRMA VE YAYIN ETİK KURULU

BİLGİLENDİRİLMİŞ ONAY FORMU

Sizi İzmir Yüksek Teknoloji Enstitüsü, Mühendislik Fakültesi, Makine Mühendisliği öğretim üyesi Doç. Dr. Mehmet İsmet Can Dede tarafından yürütülen, "Biomimetik Mürekkepbalığı Robotunun Kollarının Çoklu Haptik Arayüzlerle Teleoperasyonu" başlıklı araştırmaya katılmaya davet ediyoruz. Aşağıda ayrıntılı bilgileri verilen çalışmaya katılmadan önce bu formun okunması önem taşınmaktadır. Bu araştırmaya katılmak tamamen kendi iradenizle olması koşulu esasına dayanmaktadır. Araştırmaya katılmama ya da istediğiniz zaman, hiçbir sebep göstermeden ayrılma hakkına sahipsiniz. Araştırma hakkında anlamadığınız herhangi bir konuyu çekinmeden sorun. Elde edilecek kişisel bilgiler tamamen gizli tutulacak olup, anket sonuçlarından derlenecek istatistiki bilgiler proje sonuçlarının değerlendirileceği raporlarda ve bilimsel yayınlarda kullanılacaktır.

1. Çalışmanın Amacı
4 adet bağımlı robot kolun model aracılı teleoperasyon yöntemi ile kontrol sisteminin oluşturulması, bu süreçte ana kontrolcü sistemleri yöneten kullanıcının ergonomisinin göz önünde bulundurulması ve oluşturulan bu teleoperasyon sisteminin bilgisayar ortamında simüle edilmesi amaçlanmaktadır. Çalışmada 2 ana kontrolcü sistem, 1 ana bilgisayar ve simülasyon ortamında oluşturulmuş sanal bağımlı robot kolları ve bu kolların içinde çalıştığı sanal ortam bulunmaktadır. Operatörün ana kontrolcü sistemleri kullanarak sanal bağımlı robot kollarının hareketlerini yönetmesi gerekmektedir. 2 ana kontrolcü sistem kullanılarak manipüle edilecek olan 4 bağımlı robot kolun yönetiminin operatör açısından kolaylaştırılması için ergonomik kullanım yöntemi senaryoları belirlenmiş ve kontrol algoritması bu senaryolara göre oluşturulmuştur. Simülasyondaki sanal robotların ortamında belli noktalarda hedefler yaratılmıştır ve kullanıcılardan bu hedeflere bağımlı sanal robot kollarını ana kontrolcü sistemi ile yöneterek ulaşması istenmektedir. Operatör denekler ile yapılacak çalışmadan senaryoların başarı ile tamamlanıp tamamlanamadığı, ne kadar sürede tamamlandığı, kullanıcıdan farklı bir kolu kontrol etmesi istendiğinde bir kolun kontrolünden diğerine geçişte harcadığı süre, 2 farklı ergonomik kullanım yönteminin tamamlanma başarısı, süresi ve tercih edilme oranı açısından karşılaştırılması verileri toplanılacaktır. Bu sayede 216M219 numaralı Sualtında Manipülasyon için İnsansız Robot Mürekkepbalığı Geliştirilmesi ve Tasarımı projesi için uygun, ergonomik kullanım senaryosu belirlenmiş olacaktır. Testler sonunda kullanıcıdan 20 soruluk değerlendirme anketine katılması istenmektedir.
2. Çalışmanın Süresi: 7 gün
3. Planlanan Katılımcı Sayısı: 10 kişi
4. Araştırmada Yapılacak Genel İşler (Sorular hakkında genel bilgi, soru sayısı, ortalama cevaplama süresi)
Katılımcıların her biri karşılaştırmalı olarak veri işlenmesini sağlamak için bilgisayar ortamında 2 ayrı teste tabi tutulup, öğrenme eğrisinin oluşturulması için her testi 5 kez tekrarlaması istenilecektir. Her kullanıcı toplamda 10 test tamamlamış olup, testlerin her biri ortalama 1-3 dakika sürecektir. Testleri tamamlayan kullanıcıların deneyimlerini paylaştıkları 20 soruluk bir anketi cevaplandırmaları istenilecektir. Anketin ortalama

Figure A.1 Informed approval form of subjects for the 1st set of tests – page 1 of 2.

cevaplama süresi 5 dakika olup, her kullanıcı bu çalışmanın tamamına 15-35 dakika ayıracaktır.

Katılım Onayı:
Yukarıda yapılan açıklamaları okudum ve anladım. Araştırma hakkında yazılı ve sözlü açıklama tarafıma yapıldı, sorularımı sordum ve tatmin edici yanıtlar aldım. İstediğim zaman araştırmadan ayrılma hakkına sahip olduğum bilinci ile çalışmaya gönüllü olarak katılmayı onaylıyorum. Bu formun bir kopyası tarafıma verildi.

Katılımcının adı soyadı: _____ Tarih: __ /__ /_____

Katılımcının imzası:

Yürütücünün adı soyadı: Doç. Dr. Mehmet İsmet Can Dede

Yürütücünün imzası:

Figure A.2 Informed approval form of subjects for the 1st set of tests – page 2 of 2.

Appendix-A Approval Form on Modes 3 and 4

İZMİR YÜKSEK TEKNOLOJİ ENSTİTÜSÜ
FEN VE MÜHENDİSLİK BİLİMLERİ
BİLİMSEL ARAŞTIRMA VE YAYIN ETİK KURULU

BİLGİLENDİRİLMİŞ ONAY FORMU

Sizi İzmir Yüksek Teknoloji Enstitüsü, Mühendislik Fakültesi, Makine Mühendisliği öğretim üyesi Doç. Dr. Mehmet İsmet Can Dede tarafından yürütülen, "Biomimetik Mürekkepbalığı Robotunun Kollarının Çoklu Haptik Arayüzlerle Teleoperasyonu" başlıklı araştırmaya katılmaya davet ediyoruz. Aşağıda ayrıntılı bilgileri verilen çalışmaya katılmadan önce bu formun okunması önem taşınmaktadır. Bu araştırmaya katılmak tamamen kendi iradenizle olması koşulu esasına dayanmaktadır. Araştırmaya katılmama ya da istediğiniz zaman, hiçbir sebep göstermeden ayrılma hakkına sahipsiniz. Araştırma hakkında anlamadığınız herhangi bir konuyu çekinmeden sorun. Elde edilecek kişisel bilgiler tamamen gizli tutulacak olup, anket sonuçlarından derlenecek istatistiki bilgiler proje sonuçlarının değerlendirileceği raporlarda ve bilimsel yayınlarda kullanılacaktır.

1. Çalışmanın Amacı
4 adet bağımlı robot kolun model aracılı teleoperasyon yöntemi ile kontrol sisteminin oluşturulması, bu süreçte ana kontrolcü sistemleri yöneten kullanıcının ergonomisinin göz önünde bulundurulması ve oluşturulan bu teleoperasyon sisteminin bilgisayar ortamında simüle edilmesi amaçlanmaktadır. Çalışmada 2 ana kontrolcü sistem, 1 ana bilgisayar, 1 pedal, 1 Arduino Mega kontrol kartı ve simülasyon ortamında oluşturulmuş sanal bağımlı robot kolları ve bu kolların içinde çalıştığı sanal ortam bulunmaktadır. Operatörün ana kontrolcü sistemleri kullanarak sanal bağımlı robot kollarının hareketlerini yönetmesi gerekmektedir. 2 ana kontrolcü sistem kullanılarak manipüle edilecek olan 4 bağımlı robot kolun yönetiminin operatör açısından kolaylaştırılması için ergonomik kullanıcı girdisi haritalandırma yöntemi senaryoları belirlenmiş ve kontrol algoritması bu senaryolara göre oluşturulmuştur. Simülasyondaki sanal robotların ortamında belli noktalarda hedefler yaratılmıştır ve kullanıcılardan bu hedeflere bağımlı sanal robot kollarını ana kontrolcü sistemi ile yöneterek ulaşması istenmektedir. Operatör denekler ile yapılacak çalışmadan senaryoların başarı ile tamamlanıp tamamlanamadığı, ne kadar sürede tamamlandığı, kullanıcıdan farklı bir kolu kontrol etmesi istendiğinde bir kolun kontrolünden diğerine geçişte harcadığı süre, 2 farklı ergonomik kullanıcı girdisi haritalandırma yönteminin tamamlanma başarısı, süresi ve tercih edilme oranı açısından karşılaştırılması verileri toplanılacaktır. Bu sayede 216M219 numaralı Sualtında Manipülasyon için İnsansız Robot Mürekkepbalığı Geliştirilmesi ve Tasarımı projesi için uygun, ergonomik kullanım senaryosu belirlenmiş olacaktır. Testler sonunda kullanıcıdan 15 soruluk değerlendirme anketine katılması istenmektedir.
2. Çalışmanın Süresi: 7 gün
3. Planlanan Katılımcı Sayısı: 10 kişi
4. Araştırmada Yapılacak Genel İşler (Sorular hakkında genel bilgi, soru sayısı, ortalama cevaplama süresi)
Katılımcıların her biri karşılaştırmalı olarak veri işlenmesini sağlamak için bilgisayar ortamında 2 ayrı teste tabi tutulup, öğrenme eğrisinin oluşturulması için her testi 5 kez tekrarlaması istenilecektir. Her kullanıcı toplamda 10 test tamamlamış olup, testlerin her biri ortalama 1-3 dakika sürecektir. Testleri tamamlayan kullanıcıların deneyimlerini

Figure A.3 Informed approval form of subjects for the 2nd set of tests – page 1 of 2.

paylaştıkları 15 soruluk bir anketi cevaplandırmaları istenilecektir. Anketin ortalama cevaplama süresi 5 dakika olup, her kullanıcı bu çalışmanın tamamına 15-35 dakika ayıracaktır.

Katılım Onayı:
Yukarıda yapılan açıklamaları okudum ve anladım. Araştırma hakkında yazılı ve sözlü açıklama tarafıma yapıldı, sorularımı sordum ve tatmin edici yanıtlar aldım. İstediğim zaman araştırmadan ayrılma hakkına sahip olduğum bilinci ile çalışmaya gönüllü olarak katılmayı onaylıyorum. Bu formun bir kopyası tarafıma verildi.

Katılımcının adı soyadı: _____ Tarih: __ /__ /____

Katılımcının imzası:

Yürütücünün adı soyadı: Doç. Dr. Mehmet İsmet Can Dede

Yürütücünün imzası:

Figure A.4 Informed approval form of subjects for the 2nd set of tests – page 2 of 2.

Appendix-A Table-2 Questionnaire on Modes 1 and 2

Table A.2 Questionnaire of Mode 1 and Mode 2.

	1st part of the questionnaire Please answer each question in the 1st part by only considering Mode 1.					
	Scores **Questions**	**1**	**2**	**3**	**4**	**5**
1	During the exercise, I had the impression that I was immersed in the world generated on the computer screen. (Telepresence)					
2	My body was in the room, but my mind was within the computer-created world. (Telepresence)					
3	I felt like I was in the computer-created world more than the "actual world." (Telepresence)					
4	When I was navigating through the exercise, I forgot about my immediate surroundings. (Telepresence)					
5	After the exercise ended, I felt like I returned to the "real world" after a journey. (Telepresence)					
	2nd part of the questionnaire Please answer each question in the 2nd part by only considering Mode 2.					
	Scores **Questions**	**1**	**2**	**3**	**4**	**5**
6	During the exercise, I had the impression that I was immersed in the world generated on the computer screen. (Telepresence)					
7	My body was in the room, but my mind was within the computer-created world. (Telepresence)					
8	I felt like I was in the computer-created world more than the "actual world." (Telepresence)					
9	When I was navigating through the exercise, I forgot about my immediate surroundings. (Telepresence)					
10	After the exercise ended, I felt like I returned to the "real world" after a journey. (Telepresence)					

	3rd part of the questionnaire Please answer each question in the 3rd part by considering both modes.					
	Scores **Questions**	**1**	**2**	**3**	**4**	**5**
11	During the exercise, the sense of task completion is higher when the haptic model is integrated. (Sense of task completion)					
12	The haptic model increased the sense of safety considering the intervention of the slave robot with the environment. (Haptic feedback)					
13	Haptic feedback integration increased the sense of telepresence when contact occurred between the virtual slave and an object. (Haptic feedback)					
14	Initially, it was easier to control the 2-segment robot arms with Mode 1 rather than Mode 2. (Ease of use)					
15	It is easier to control the 2-segment robot arms after a certain amount of repetitions with Mode 1 rather than Mode 2. (Ease of use)					
16	Initially, it was easier to control the robot arm holding the light with Mode 1 rather than Mode 2. (Ease of use)					
17	It is easier to control the robot arm holding the light after a certain amount of repetitions with Mode 1 rather than Mode 2. (Ease of use)					
18	I prefer to use the model with haptic feedback integrated. (Preference)					
19	I prefer to use the model without the need of using buttons for 2-segment arms to change the controlled section. (Preference)					
20	I prefer to use the model with the stylus-controlled and locked-on pose version rather than the button-controlled version of the light arm. (Preference)					

Appendix-A Table-3 Questionnaire on Modes 3 and 4

Table A.3 Questionnaire of Mode 3 and Mode 4.

	1st part of the questionnaire Please answer each question in the 1st part by only considering Mode 3.					
	Scores **Questions**	**1**	**2**	**3**	**4**	**5**
1	The task required extreme mental and/or perceptual activity. (e.g., thinking, deciding, calculating, remembering, looking, searching, etc.) (Mental/ Sensory Effort)					
2	The task required extreme physical activity. (e.g., pushing, pulling, turning, controlling, activating, etc.) (Physical Effort)					
3	I felt extreme time pressure due to the rate at which the task elements occurred. (Considering the task as slow and leisurely or rapid and frantic) (Time Pressure)					
4	I think I was not successful in doing what was asked to do and not satisfied with what I have accomplished. (Performance)					
5	The task was demanding, complex and exacting. (Versus easy, simple, and forgiving) (Task difficulty)					
6	I felt anxious, worried, uptight, and harassed. (Versus calm, tranquil, placid, and relaxed) (Stress level)					
	2nd part of the questionnaire Please answer each question in the 2nd part by only considering Mode 4.					
	Scores **Questions**	**1**	**2**	**3**	**4**	**5**
7	The task required extreme mental and/or perceptual activity. (e.g., thinking, deciding, calculating, remembering, looking, searching, etc.) (Mental/ Sensory Effort)					
8	The task required extreme physical activity. (e.g., pushing, pulling, turning, controlling, activating, etc.) (Physical Effort)					
9	I felt extreme time pressure due to the rate at which the task elements occurred. (Considering the task as slow and leisurely or rapid and frantic) (Time Pressure)					

10	I think I was not successful in doing what was asked to do and not satisfied with what I have accomplished. (Performance)					
11	The task was demanding, complex and exacting. (Versus easy, simple, and forgiving) (Task difficulty)					
12	I felt anxious, worried, uptight, and harassed. (Versus calm, tranquil, placid, and relaxed) (Stress level)					
	3rd part of the questionnaire Please answer each question in the 3rd part considering both modes.					
	Scores **Questions**	**1**	**2**	**3**	**4**	**5**
13	Initially, it was easier to control the robot arms with Mode 3 rather than Mode 4. (Ease of use)					
14	It is easier to control the robot arms after a certain amount of repetitions with Mode 3 rather than Mode 4. (Ease of use)					
15	I prefer to use the model with Mode 3 rather than Mode 4. (Preference)					

Appendix-B Test Results on the 1st Set of Tests

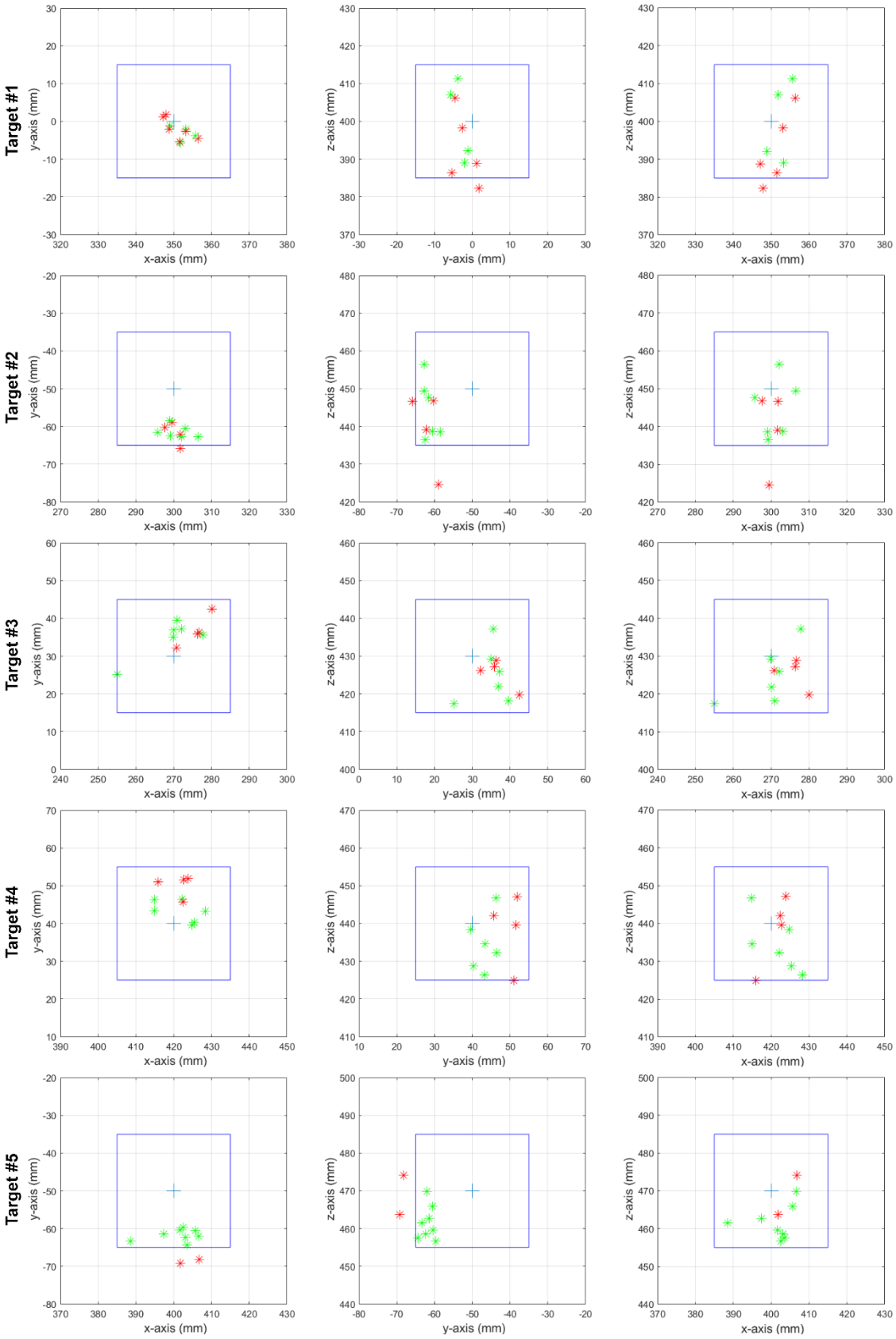

Figure B.5 Grasper arm accuracy results on targets 1-5 (Color code as, blue: threshold area, green markers: Mode 1, red markers: Mode 2)

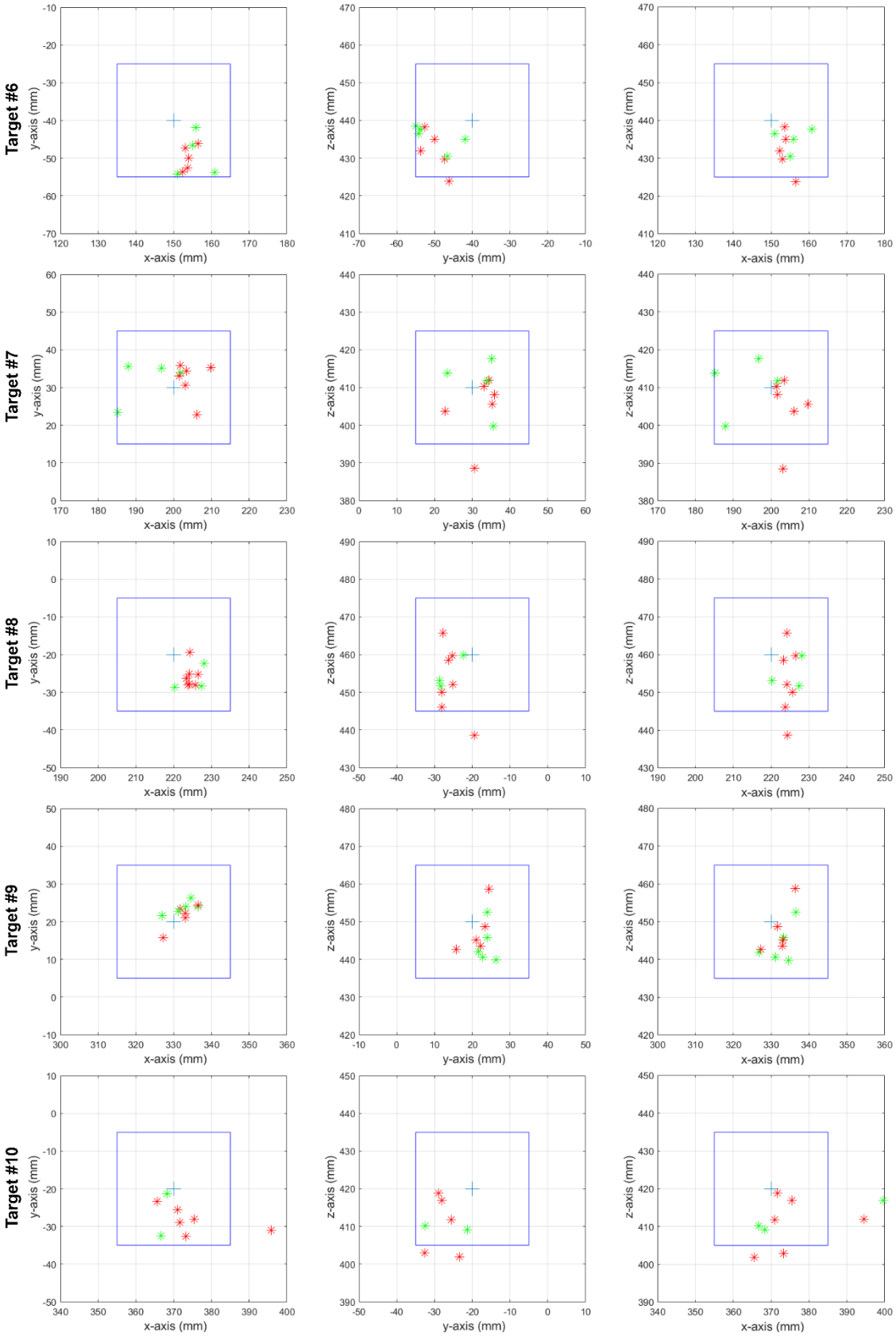

Figure B.6 Grasper arm accuracy results on targets 6-10 (Color code as, blue: threshold area, green markers: Mode 1, red markers: Mode 2)

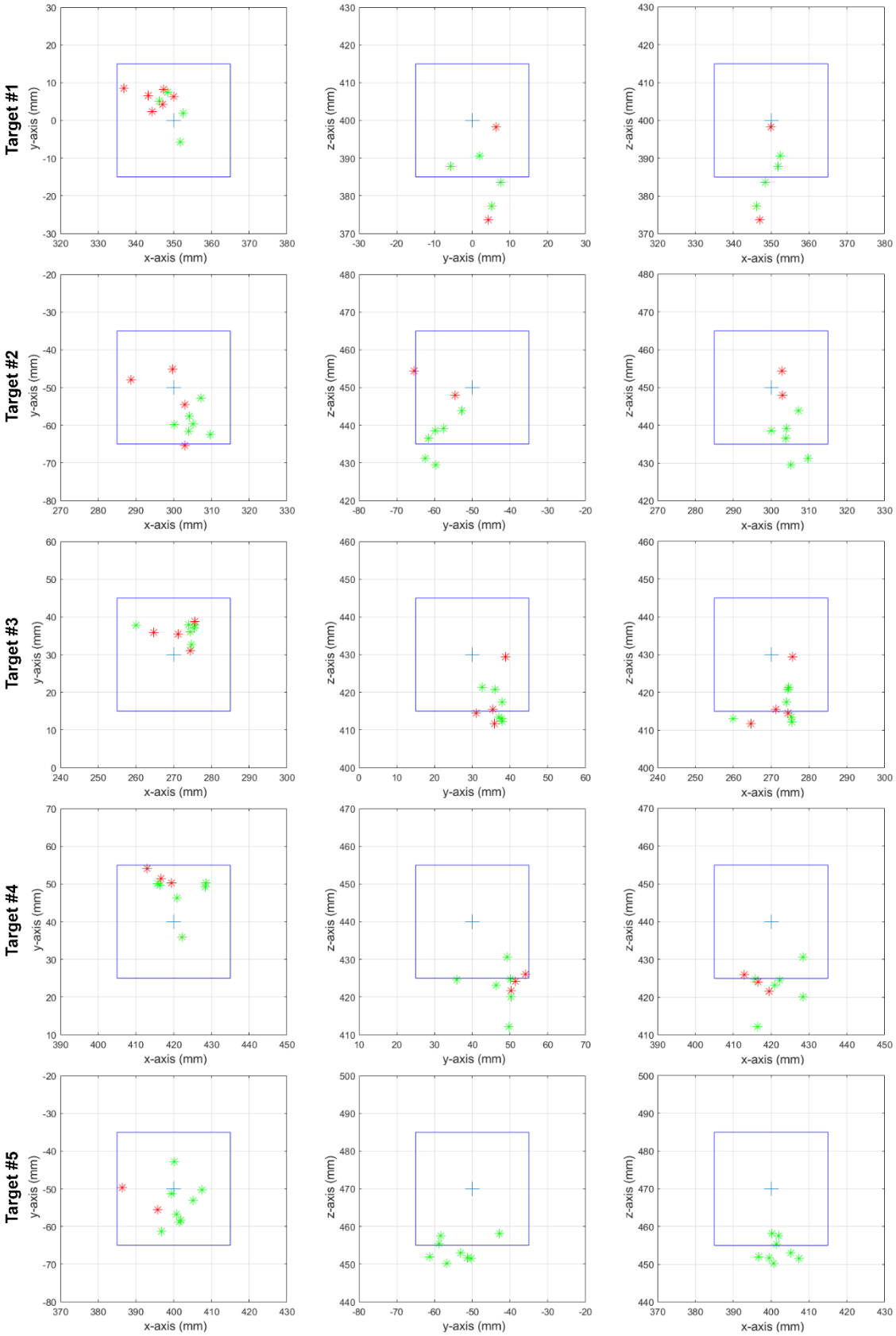

Figure B.7 Palpation arm accuracy results on targets 1-5 (Color code as, blue: threshold area, green markers: Mode 1, red markers: Mode 2).

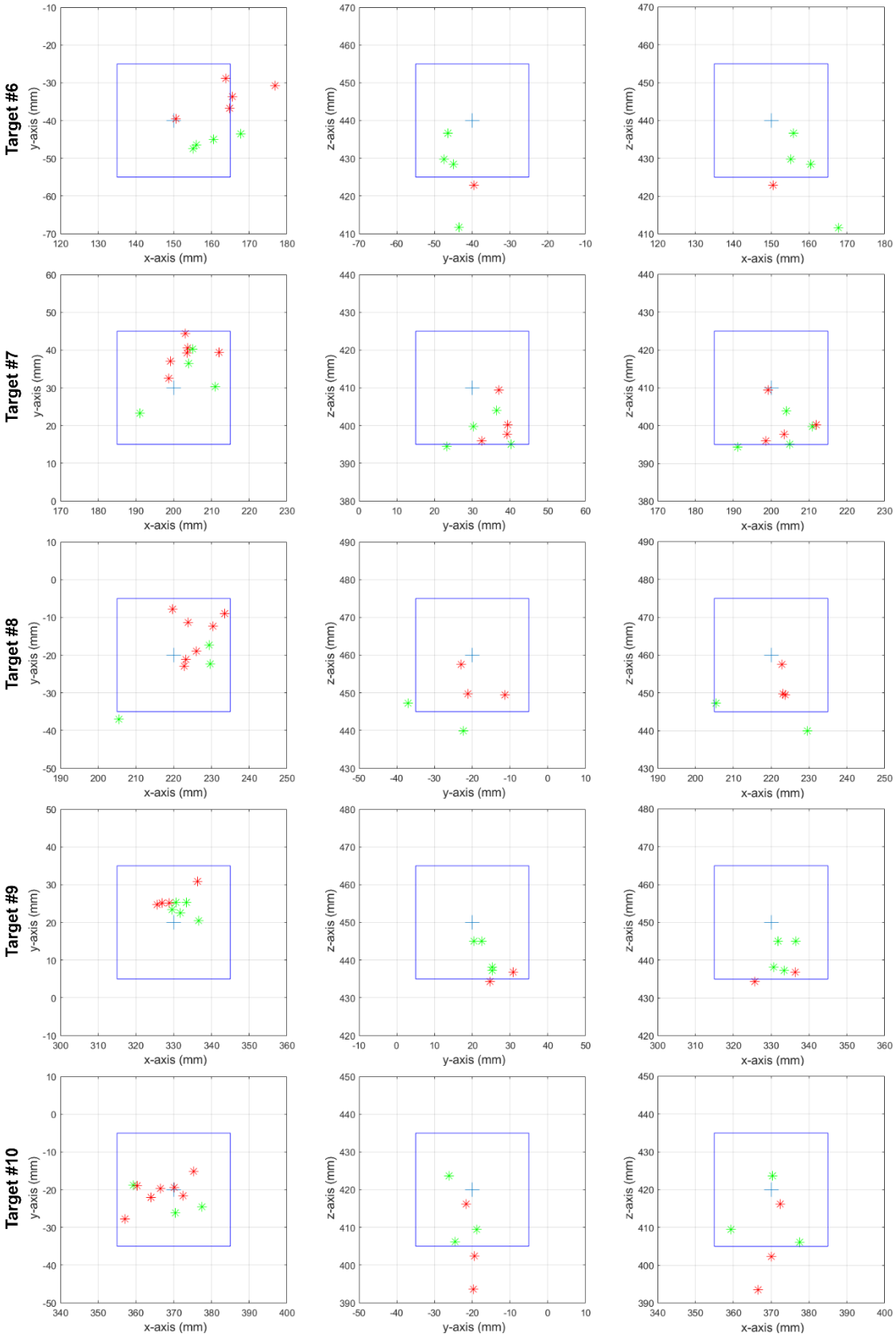

Figure B.8 Palpation arm accuracy results on targets 6-10 (Color code as, blue: threshold area, green markers: Mode 1, red markers: Mode 2).

Appendix-C Test Results on the 2nd Set of Tests

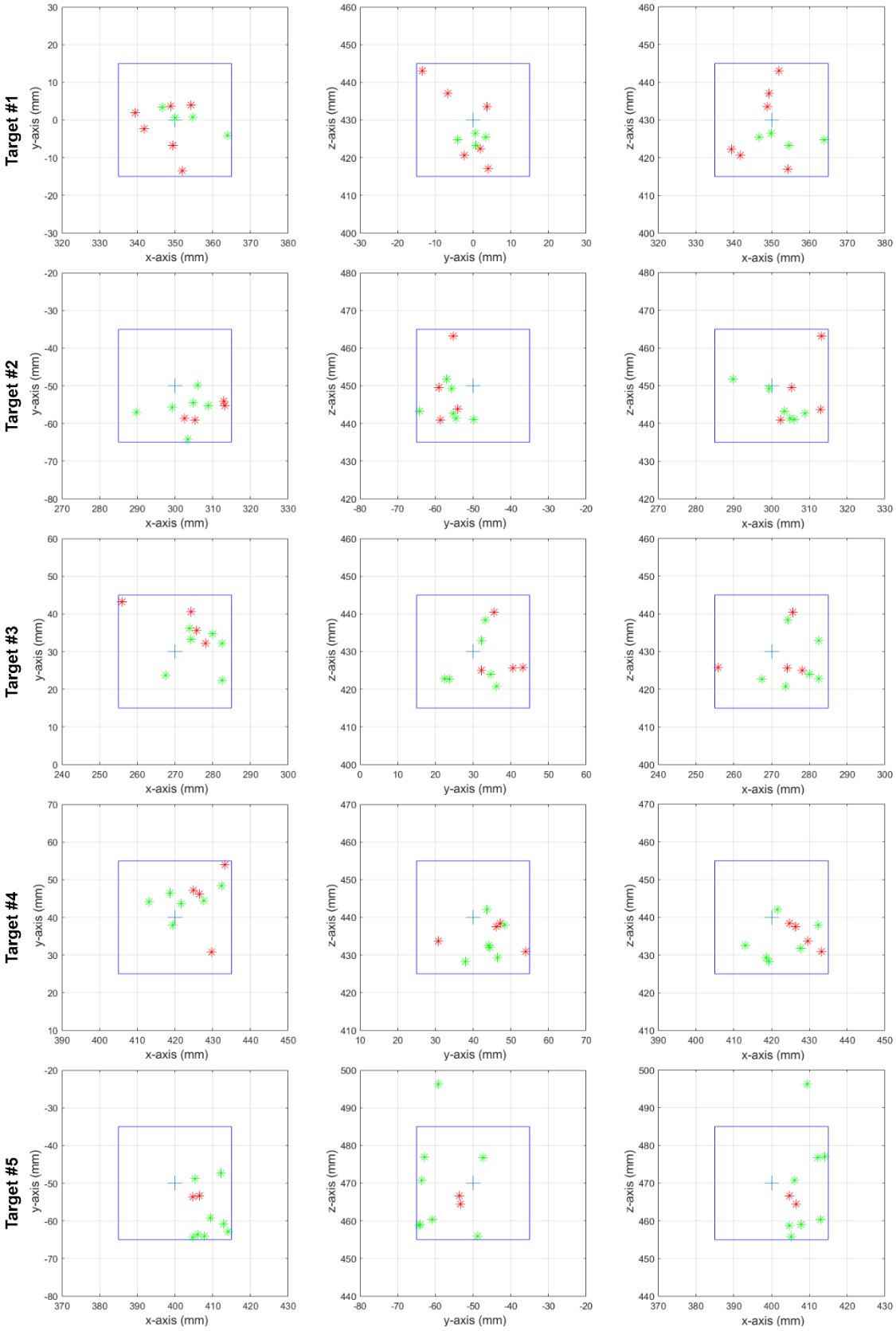

Figure C.9 Grasper arm accuracy results on targets 1-5 (Color code as, blue: threshold area, green markers: Mode 3, red markers: Mode 4)

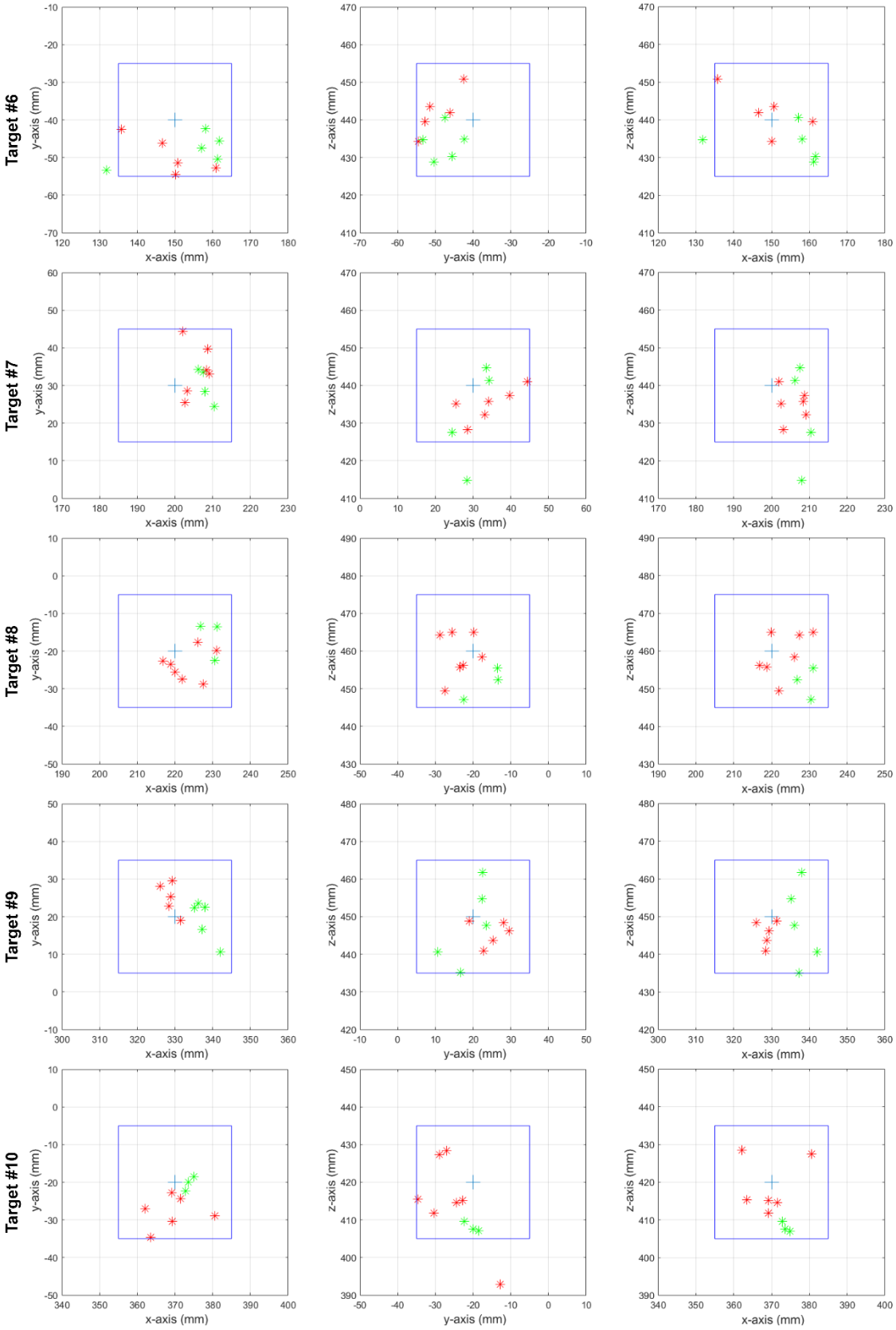

Figure C.10 Grasper arm accuracy results on targets 6-10 (Color code as, blue: threshold area, green markers: Mode 3, red markers: Mode 4)

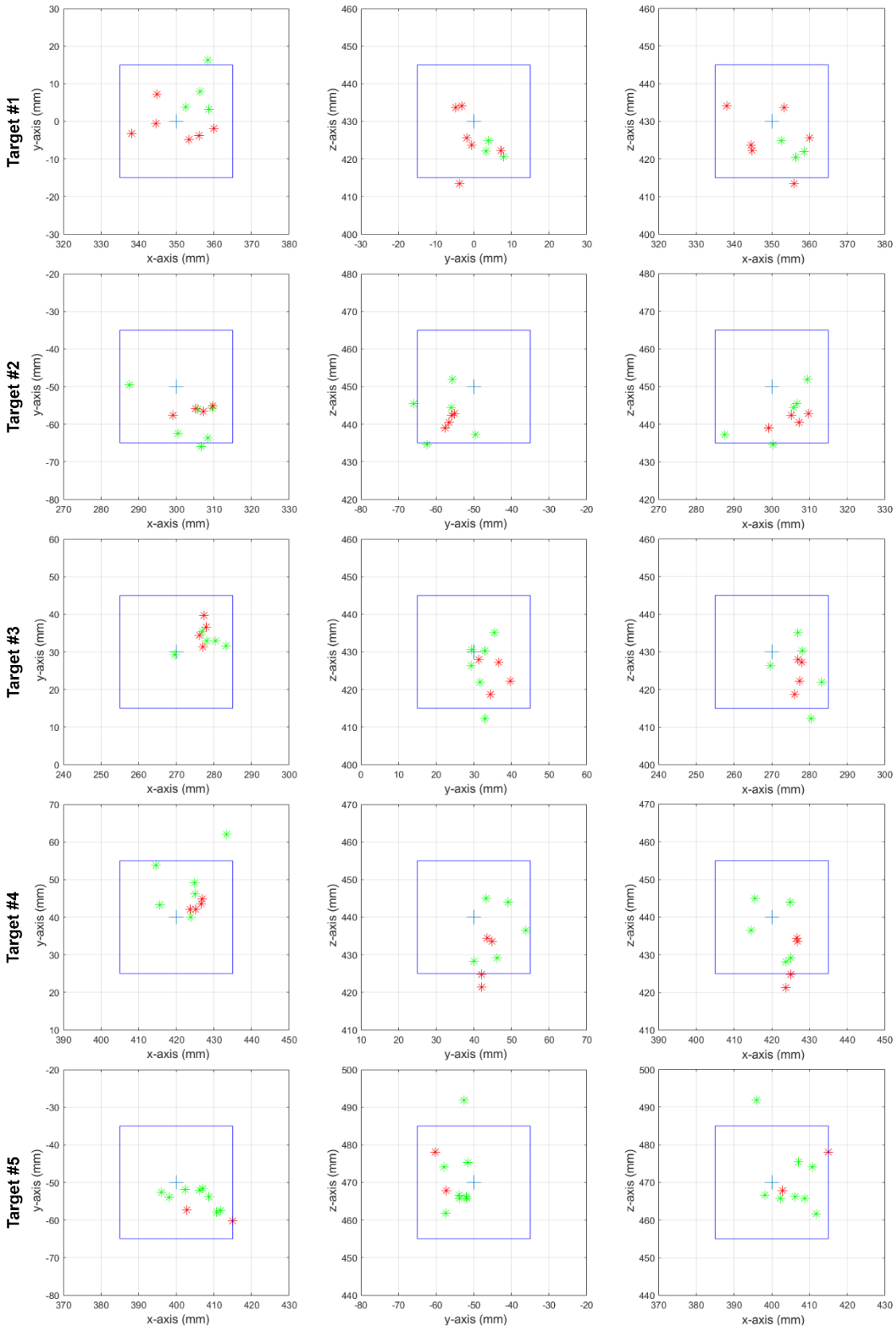

Figure C.11 Palpation arm accuracy results on targets 1-5 (Color code as, blue: threshold area, green markers: Mode 3, red markers: Mode 4).

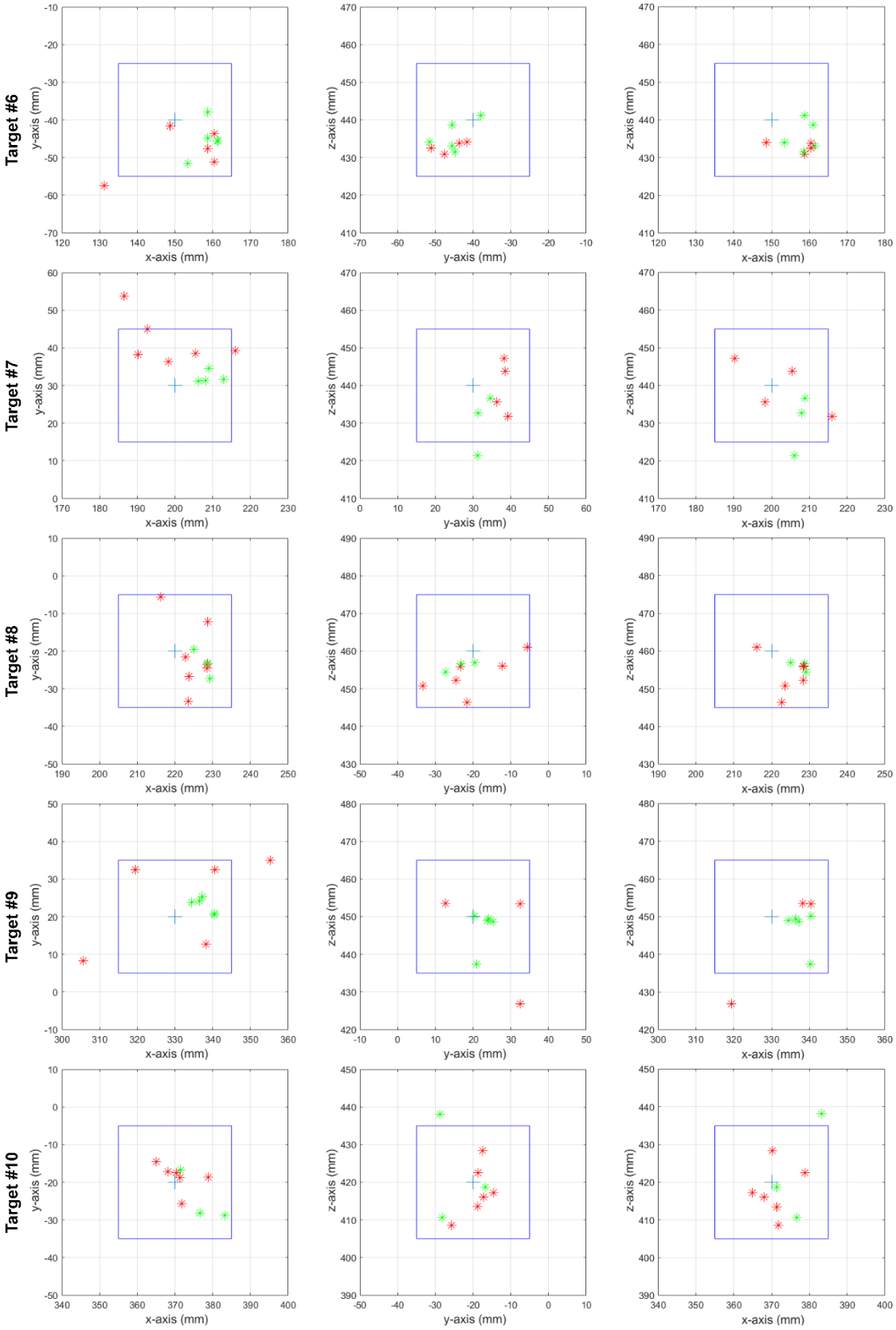

Figure C.12 Palpation arm accuracy results on targets 6-10 (Color code as, blue: threshold area, green markers: Mode 3, red markers: Mode 4).